# Characterizing the impact of genetic and environmental variation on maize utilizing phenomic approaches

A THESIS

SUBMITTED TO THE FACULTY OF THE UNIVERSITY OF MINNESOTA

BY

Sara B. Tirado Tolosa

IN PARTIAL FULFILLMENT OF THE REQUIREMENTS

FOR THE DEGREE OF

DOCTOR OF PHILOSOPHY

Advisors: Nathan M. Springer and Candice N. Hirsch

August 2020

# Acknowledgments

My journey as a graduate student and the completion of the work I have executed and present in this dissertation has been enriched and fueled by the love and support of an immense number of people. First, I would like to thank my advisors Nathan Springer and Candy Hirsch for being my primary source of knowledge, guidance, and encouragement during my time at the University of Minnesota. I could not have wished for more inspiring and supportive mentors. I would also like to thank members of the Springer Lab: Jaclyn Noshay, Erika Magnusson, Pete Hermanson, Tara Enders, Pete Crisp, and Sarah Anderson for supporting my personal and professional development and allowing every day at work to be happy and enjoyable, even under the moments of greatest pressure and challenge. I would also like to acknowledge my advisory committee: Aaron Lorenz, Joe Knight, and Volkan Isler for their valuable input and instruction throughout this process. Additionally, this work would have not been possible if not for the help of Amanda Gilbert, Susan St Dennis, Anna Deneen, Kjell Sandstrom, Shale Demuth, Danielle Sorensen and Jordan Freeman in completing field and lab activities.

My most sincere gratitude goes to my mother, Sara Tolosa Ramirez, and my brothers, David Tirado Tolosa and Jorge Tirado Tolosa, who have inspired and challenged me throughout my life to become the person I am today, and who have given me their unconditional love and invaluable support during my education. Lastly, I would

like to thank my father, David Tirado, for guiding me and helping me find my passion in agriculture during my early years of development as a researcher, and for being a source of inspiration and a motive for dedication all the way from Heaven. Lastly, I would like to thank my husband, Maximiliano Vera Juarez, who appeared in my life to provide the love and encouragement I needed to finish my academic efforts.

Lastly, I would like to thank all the agencies that provided financial support during my graduate studies to complete the research presented in this thesis.
This work was supported by a Monsanto/University of Minnesota Multifunctional Agriculture Initiative Graduate Student Fellowship, the Minnesota Corn Research and Promotion Council, the University of Minnesota Graduate Opportunity Fellowship, and the University of Minnesota APS Metric Funds Fellowship.

Dedication

*To my incredible parents,*

***Sara** and **David**,*

*and to my extraordinary brothers,*

***David** and **Jorge***

*for being my pillars of support.*

Abstract

To gain a better understanding of how genotypic elements interact with the environment, we need to develop more efficient ways of monitoring plant phenotypes so that we can gather phenotypic data through time. Remote sensing technologies provide effective means to do this. Sensor, computational, and platform technologies keep evolving and provide avenues to evaluate how plants grow and respond to environmental conditions. The goals of this thesis were to develop methods and analytical procedures to evaluate maize plant phenotypic performance under varied environmental conditions. The first set of experiments were geared towards utilizing unmanned aerial vehicles equipped with RGB cameras to assess how maize plants grow in response to various field management conditions, including various planting dates and densities, and weather events. These tools were used to assess variation for lodging responses and downstream impacts on productivity. More generally, results from this thesis demonstrate that measurements collected early in development can be useful for improving predictions of end-season traits. The second set of experiments provided insights into using hyperspectral technologies for genotypic differentiation and abiotic stress detection. There is a large amount of variation in reflectance throughout maize leaves that can be useful in distinguishing different maize genotypes at the seedling stage and for detecting and quantifying abiotic stress conditions including cold, heat, and salt stress early in

development. By documenting phenotypic differences across genotypes and environments through time in a more efficient manner by taking advantage of available remote sensing technologies, we can improve our understanding of how different environmental and genetic elements impact plant productivity and facilitate advancements in crop improvement and production.

Table of Contents

List of Tables

List of Figures

CHAPTER I

# Opportunities and Challenges in Phenotyping Row Crops from Above using Spectral Imaging

## INTRODUCTION

With current rates of population growth and climatic changes, advancements in the area of crop improvement and production are crucial. Advances in sequencing technology have allowed for the development of marker platforms that can be utilized by plant breeders to increase the pace of crop improvement through the characterization of quantitative trait loci (QTL) and the implementation of genomic selection. These have in turn aided in the elucidation of the genetic mechanisms of complex agronomic traits and enabled their selection (Yang et al., 2020). However, high-throughput acquisition of phenotypic data in field environments has become one of the major bottlenecks in crop improvement since traditional methods are labor intensive, costly, biased, and sometimes destructive (Silva-Perez et al., 2018; White et al., 2012). This lag in phenotyping advancements compared to progress in the genomics sector has driven efforts in the scientific community to develop efficient methods for acquiring, processing, and analyzing phenotypic data of crop plants in rapid, objective, and non-destructive manners by taking advantage of available technology. Advancements in sensor technology and sensing platforms have enabled the use of remote sensing to accomplish these goals (Fahlgren et al., 2015; L. Li et al., 2014). In this article, we review the major progress on

the utilization of remote sensing technology, primarily focused on the application of RGB cameras mounted on unmanned aerial vehicles (UAVs), to monitor row crops in field settings. We have focused on outdoor field phenotyping as it allows breeders to evaluate crop plants in their target production environments. Moreover, because phenotyping field settings from ground platforms can be challenging and in many cases not viable, we have focused on top-down phenotyping rather than side-scanning systems.

## ADVANTAGES AND CHALLENGES OF CURRENTLY AVAILABLE PLATFORMS AND SENSORS FOR COLLECTING TOP-DOWN FIELD PHENOTYPIC DATA

There are many platforms and sensors available for collecting top-view images of crop fields and these differ primarily in the scale and resolution of the acquired dataset as well as the efficiency and scale of application. Platforms range from ground vehicles that navigate through crop rows to aerial vehicles that navigate close to the field or farther away in space. The choice of platform impacts the amount of time it takes to image the field and also the temporal and spectral resolution that can be achieved. The sensor that is used also has a great impact on the data acquired, with a wide range of spectral and spatial resolutions available.

### *Sensing Platforms*

Ground based platforms such as tractors, carts, and sprayers are a common and simple solution for high-throughput phenotyping. Converting these ground vehicles to a phenotyping platform that can collect top-view images has been achieved by adding

imaging sensors to beams that can extend above the crop canopy or to an attached trailer (Barker et al., 2016; Busemeyer et al., 2013; Comar et al., 2012; Svensgaard et al., 2014; White & Conley, 2013). Ground-based platforms can achieve very high spatial resolutions since they operate close to the crop canopy. However, these platforms are hard to implement in large scales as these can only monitor a relatively small number of crop rows at a time. These platforms are also limited by soil and weather conditions and cannot navigate through the field under wet conditions and, in the case of tractors, are constrained by their large size and low vertical clearance hindering their application once crops achieve a certain height (Busemeyer et al., 2013; Comar et al., 2012; White et al., 2012). They can also involve substantial labor costs in operating and troubleshooting the equipment (White et al., 2012). An advancement to these platforms are unmanned ground vehicles, such as rovers or ground robots, that can navigate the field in an automated manner and acquire and upload data without the need for extensive manual labor (Ruckelshausen et al., 2009; Young et al., 2019). These include both small vehicles that tend to be outfitted with side-scanning systems to measure traits within the canopy as well as larger vehicles that can measure traits from above the canopy. These platforms are still restricted by wet soil and weather conditions and also by other common weather-induced events such as plant lodging which can block the alleys through which they navigate (Tirado et al., 2020a; Chapter 3). Their navigation is also impacted by obstructions commonly present in field grounds such as weeds or rocks. Rail-based gantry systems or fixed phenotyping towers equipped with sensors eliminate the need for manual operation, the need to navigate through unobstructed alleys, and the need for dry

field conditions. However, they are limited to the area where the system was built, which typically encompasses only a few acres, and tend to have very high initial cost (Burnette et al., 2018; Fukatsu et al., 2012). This means that the cost for large-scale experiments will linearly increase with these platforms (Yang et al., 2020).

Air-based platforms can measure crop phenotypes remotely without being confined to specific areas or soil conditions. A variety of platforms exist to measure fields from above including manned and unmanned aerial vehicles as well as satellites. The benefit of satellite images is the capability of acquiring very large-scale data from a multi-year range depending on the length of time a particular satellite has been in orbit. Moreover, satellite images are limited in both spatial and temporal scale and most available satellite data come from systems with a large visiting cycle, low spatial resolution, and poor sensitivity under cloudy conditions (Li et al., 2015; Matese et al., 2015). The WorldView-3 satellite currently provides the highest spatial resolution of approximately 31cm for shortwave infrared bands (DigitalGlobe | WorldView-3, n.d.). Although useful for assessing regions of large production fields, individual plant or plot structural elements cannot be extracted as these require higher spatial resolution. This limits the ability to use satellite imagery to extract individual plant features limiting their application in breeding programs. Manned aerial platforms can achieve higher spatial and temporal resolutions than satellites as they can fly closer to the field and are limited in time only by wind and rain, however, these are constrained by high operating costs and operational complexity (Yang et al., 2017). UAVs, on the other hand, can fly much closer to the canopy and achieve sub-centimeter spatial resolution. These UAV platforms are

easy to acquire due to their low-cost and the wide range of models available commercially. Moreover, existing open-access platforms, such as Pix4D Capture, make mission planning and data gathering from UAVs simple requiring little operational expertise (Pix4Dcapture: Free drone flight planning mobile app, n.d.). UAVs therefore provide an efficient means of gathering plant-level or plot-level information for multiple plots simultaneously making them practical for implementing at breeding scales (Araus & Cairns, 2014; Shi et al., 2016). UAV limitations include low battery life, low payload, and the inability to fly during high wind or rain conditions. Some of these challenges can be circumvented by using simple camera systems such as RGB sensors with a small payload and purchasing multiple batteries. Because of their capability to closely monitor crop fields with very high spatial and temporal capabilities, they have been widely implemented for crop phenotyping.

### *Spectral sensors utilized for measuring field phenotypes from UAVs*

Sensors that capture spectral imagery mainly differ in the number of spectral bands that they acquire, or their spectral resolution, as well as the wavelength range that they can measure. RGB sensors are the most common and image the red (564–580 nm), green (534–545 nm), and blue (420–440 nm) wavelengths which encompass the visible part of the electromagnetic spectrum corresponding to human trichromacy. These sensors are typically inexpensive, easy to acquire, and have been widely used to extract morphological traits across many crop species in both indoor and outdoor settings (Enders et al., 2019; A. Feng et al., 2019; Varela et al., 2017; Watanabe et al., 2017).

Another common sensor utilized for crop phenotyping is the near-infrared (NIR) camera, which measures a wavelength range between 750nm and 2500nm. These NIR sensors are more expensive than RGB cameras and are typically added in addition to RGB capabilities for crop sensing to extract the normalized difference vegetation index (NDVI), which has been used to monitor canopy structure, light absorption, photosynthetic ability, and drought stress in plants (Gamon et al., 1995; Jin et al., 2017; Q. Zhang et al., 2012). Because NIR sensors are typically combined with RGB cameras, they are more costly and require UAV platforms with larger payloads. Thermal sensors, similar to NIR cameras, measure emitted infrared radiation in the thermal range (8000nm to 12000nm) and have been used to monitor plant temperature which has been correlated to plant water status as well as changes in transpiration due to early pathogen infections (Jones et al. 2002; Oerke et al. 2006). Since these sensors measure canopy temperature, they can be greatly influenced by environmental conditions including wind, temperature, and sunlight making temporal and spatial standardization difficult. New multispectral (MS) or hyperspectral (HS) sensors with much higher spectral resolutions (10s to 100s of spectral bands typically extending from the ultraviolet (UV) through the NIR wavelengths) are now being used in combination with machine learning and deep learning technologies. These sensors have given researchers the ability to observe traits that are not visible to the human eye and to monitor biochemical processes occurring within plant tissues that can help identify, classify, and quantify a range of biotic and abiotic stress conditions (Alisaac et al., 2019; Blackburn, 2007; X. Feng et al., 2020; Obeidat et al., 2018; Pandey et al., 2017). Although HS and MS sensors have potential to

provide additional resolution of crop phenotypes, the data acquired by these sensors is highly sensitive to ambient light and they therefore require controlled lighting conditions or extensive use of reflective standards making them challenging to implement in field settings (Nicolas et al., 2017; Tirado et al., 2020c; Chapter 4). The sensors are also quite large and require high payload capacities which limits their application in many UAV research programs. Moreover, hyperspectral sensors can generate up to terabytes of data in a short amount of time bringing about challenges of data storage and an increased complexity in data analysis (Vadez et al., 2015).

UAVs equipped with RGB cameras can provide an economical, efficient means of collecting phenotypic data due to their high spatial and temporal resolution. Although there is still significant room for advancement, there has been major progress in the past decades in conducting RGB UAV imaging, processing the imagery, and extracting useful parameters across crop fields. In this chapter we focus on the major applications of RGB UAV imaging for monitoring plant phenotypic parameters in field settings and detail various opportunities for making additional progress in the field.

## TRAIT EXTRACTION FROM RGB FIELD IMAGES

Top-down imaging with a UAV equipped with an RGB camera allows for the estimation of many meaningful agronomic parameters used in traditional breeding programs. Traits that involve the monitoring of the upper canopy are most easily estimated with this approach. Traits linked to morphological parameters obtained from the lower canopy, such as plant silking in maize, plant stalk diameter, and plant leaf

angle, cannot be directly estimated and would require additional angles or methods of measurement. In this section we review important plant morphological and biochemical traits related to the upper canopy as well as end-season productivity that can be assessed with top-down RGB imagery. We discuss the progress that has been made in estimating these traits, including what has and has not been successful.

***Plant height***

Structure from motion (SfM) algorithms, which allow for the 3D reconstruction of a scene utilizing a set of overlapping 2D images, have revolutionized crop phenotyping. SfM algorithms work by matching features present in multiple images and reconstructing the unknown 3D scene geometry and the camera positions and orientations from those matched features (James & Robson, 2012; Snavely et al., 2008). These have allowed the 3D reconstruction of crop fields and the generation of field orthomosaics and digital surface models containing color and height information of the field from which different morphological and structural parameters including plant height can be extracted. Plant height has shown to be a useful indicator of crop nutrient stress and end-season productivity (Yin et al. 2011a; Yin et al. 2011b). It is therefore a trait extensively evaluated as it can aid in making crop selections and field management decisions.

Digital surface models (DSMs) are a 2D representation of the height element of the entire field generated from the 3D point cloud developed through SfM algorithms. Multiple programs were quick to adopt and test SfM photogrammetry methods on UAV RGB imagery for crop height extraction from DSMs in crops such as barley (Bendig et

al., 2013a) and rice (Bendig et al., 2013b). Relatively low accuracies for plant height estimates were found due to issues with the generated DSM including low GPS accuracy, low image overlaps, and the need for extending image acquisition past field borders. These studies found that the DSM-derived height values had low correlations to field measurements across multiple timepoints (r-squared values ranging from 0.22 to 0.71) and that these can sometimes extend to negative values (Bendig et al., 2013a; Bendig et al., 2013b). The DSM accuracy and quality was later found to be dependent on the positioning information (Ruiz et al., 2013). A method to overcome GPS accuracy was to use targets located in the field with high-quality GPS information, referred to as ground control points (GCPs), to transform point clouds into real-world coordinates and rectify the image positions before creating the DSM (Turner et al., 2012). Current practices now emphasize the uses of GCPs to improve the DSM accuracy and improve UAV-derived height measurement extractions.

Plant height can be extracted from the DSMs by multiple methods. One of these involves the identification of ground or soil pixels in the DSMs and their interpolation across the area to create a digital terrain model (DTM) that can then be subtracted from the DSM to obtain plant height measurements for the canopy. This has been proven useful in plant height extraction among nursery fields with bare ground areas for crops including barley (Bendig et al., 2014), wheat (Hassan et al., 2019; Holman et al., 2016; Madec et al., 2017), sorghum (Chang et al., 2017; Watanabe et al., 2017), cotton (Thompson et al., 2019), and maize (Han et al., 2019; Malambo et al., 2018; Varela et al., 2017). Although proven successful, finding ground points in a field site can be

challenging and the interpolation procedure can be computationally intensive. Moreover, height throughout a field can vary due to minor slopes present in which case identification of ground points has to be done consistently throughout the entire field site. Also, it is optimal that the parameters for terrain modeling algorithms are optimized for the field conditions to achieve the best performance since most of these have been developed for more varied terrains compared to those found in agricultural landscapes (Anderson et al., 2019).

Another method for extracting plant height from DSMs is the difference based method (DBM) which subtracts the DSM of the bare ground before crops are growing to the DSM containing the plant canopy. This approach has been applied in maize (Chu et al., 2018) and wheat (Belton et al., 2019). In this approach the two DSMs are obtained from flights on different dates and then compared. This method, however, relies on accurate flight paths and DSM registration as well as high DSM resolutions since these are typically generated by averaging elevation values for the point clouds within a pixel (Chu et al., 2018). A comparison of the DBM method to more advanced point cloud methods commonly used with lidar data for terrain modeling as well as with ground measurements found that the DBM method for plant height estimation in maize resulted in lower genetic variation and repeatability in most circumstances compared to other methods for plant height extraction (Anderson et al., 2019).

An alternate approach for plot height estimation from DSMs was presented for crop nursery fields with exposed alleys where surrounding ground points are individually identified for each plot based on the height distribution of points across the field and used

as the ground height value for the given plot to extract the plant height from the DSM of a given date (Tirado et al., 2020b; Chapter 2). Similarly, another study used an adaptive triangulated irregular network ground classifier that breaks the field into segments, extracts the lowest height value for each segment, and triangulates these points to obtain an approximate ground model (Han et al., 2019). Although successful, these methods also rely on the presence of unobstructed areas of exposed soil in the fields, which are not available in all crop species. Another study proposed a self-calibration method for sites where the ground is not visible which estimated the ground level with high accuracy by fusing the UAV data with a small number of manual ground measurements of canopy height collected while the drone was flying (Hu et al., 2018). They utilized an inverse distance weighted interpolation algorithm to predict the ground level of plots that were not hand-measured by using the estimated ground levels in the eight nearest plots that were hand-measured (Hu et al., 2018). This method proved to provide accurate height estimations compared to manual measurements by reducing error due to ground coverage. Although it requires additional labor efforts, these would not induce significant costs as they are limited and could be taken by an additional person aside from the pilot in command during the time the drone is flying as long as the person remains outside the field of view.

Plant height metrics can also be extracted directly from the SfM point clouds generated from UAV images of crop fields. Previous studies have extracted similar metrics from airborne laser scanning datasets from forests (Li et al. 2014). When implemented on a UAV crop dataset, the mean point height (R=0.86) and the 90th

percentile height metric (R=0.75) provided the best accuracy compared to the manual measurements of plant height (Li et al. 2016). Although SfM metrics extracted from point clouds can be useful, these consist of thousands of points and can exponentially increase with higher imaging resolution and overlap. Digital surface models, on the other hand, can be generated from the dense point clouds and are instead a 2D representation of the elevation of the area. These datasets are much smaller in size and easier to handle and process compared to the point clouds so they provide more efficient means for plant height extraction.

A common issue when evaluating height for a plot is determining the pixels that represent the top of plants as there will also be pixels pertaining to leaves lower in the canopy which affect the values for the different height metrics utilized. To remove outlier points caused by plant material in the lower canopy and ground pixels, a method was developed that applies a moving cuboid filter across field segments to take into account spatial information and segment the top canopy before extracting plant height (Song & Wang, 2019). Alternatively, high resolution 3D models coupled with advanced segmentation algorithms that could identify individual plants could allow for the determination of individual plant height measurements that could be used for plot height estimation. Algorithms that can take into account leaf occlusion as plants grow and leaf movement by wind still need to be developed for this approach to be utilized (Zermas et al., 2020).

The optimal SfM metrics for plant height extraction from DSMs and their accuracy varies by crop and design of study. Common SfM metrics include the median

height value (50th percentile), the 90th, 95th and 99th percentiles, and the maximum height value (100th percentile) for all pixels in a plot. Overall, the optimal SfM metric used for small grains tends to be higher percentiles, such as the 99th percentile, compared to taller grain crops such as maize and sorghum which possess morphological elements that can generate SfM artifacts and for which the optimal percentile is typically lower (ie. ~90th percentile) and varies depending on growth stage, planting density, and spatial resolution of images (Bendig et al. 2014; Watanabe et al. 2017; Madec et al. 2017). The maximum and median height metrics have been shown to be relatively inaccurate for describing plot height due to presence of ground points or outlier points due to SfM artifacts (Li et al., 2016; Madec et al., 2017; Malambo et al., 2018). Shorter crops planted at higher densities such as barley and wheat have achieved higher measurement accuracies when correlated to the ground measurements compared to taller crops with occluding leaves such as sorghum (Bendig et al., 2014; Madec et al., 2017; Watanabe et al., 2017). The canopy structure influences the UAV measurement accuracies throughout development for crops such as maize and sorghum for which the tallest vegetative parts are large leaves that move easily when exposed to the wind causing lower accuracies during the vegetative stages that increases after flowering when the tassel is exposed (Varela et al., 2017; Tirado et al., 2020b; Chapter 2). In general, a trend of underestimation of plant height values compared to ground measurements has been observed across most studies due to the presence of ground pixels in point clouds specially under low density plantings and inability to capture sparse pixels pertaining to structures in the canopy apex such as tassels (Anderson et al., 2019; Bendig et al., 2014;

Han et al., 2018; Holman et al., 2016; Madec et al., 2017; Varela et al., 2017; Watanabe et al., 2017). Overestimation of values has also been reported attributed to contamination from taller neighboring plots (Watanabe et al., 2017). An approach to extract the top leaves of the maize canopy before plot height estimation using plant segmentation followed by spatial Kriggin interpolation based on multiple neighboring maximum pixels from different plants in a plot has been explored as a way to minimize the amount of pixels not pertaining to the upper canopy (Han et al., 2018). Current best practices of plant height extraction rely on collecting images with high (more than 85%) overlap, having GCPs distributed around the area of interest, creating a DEM of the region using SfM algorithms, identifying plot boundaries, and finding optimal algorithms for adjusting the DEM height based on ground elevation to extract canopy height from individual plots. With the development of drones equipped with advanced GPS technology, such as real-time kinematic positioning information, steps such as GCP placement could be eliminated.

### *Canopy Cover*

Canopy cover is an important indicator of growth and faster canopy closure rates are associated with increased light interception, enhanced weed suppression, greater biomass accumulation, and therefore greater yield potential (Campillo et al., 2008; Jannink et al., 2001; Purcell, 2000; Xavier et al., 2017). Different methods have been used to track canopy cover changes in crop fields by using UAV imagery. One method for extracting canopy cover involves classifying orthomosaic pixels into vegetative and

non-vegetative material. This has been extensively studied and a variety of color parameters have been proven useful, including the hue and saturation values, the green vegetation index, the LAB color space, the excess green index (ExG), and the normalized green-red difference index (Ashapure et al., 2019; Han et al., 2018; Lang et al., 2019; Li et al., 2015; Purcell, 2000; Schirrmann et al., 2016; Varshney, 2017). A variety of classification methods have been successfully used as well. The most common method involves thresholding the color parameters; however, finding an optimal threshold value that is effective across different timepoints and lighting conditions requires normalization or calibration of the image color parameters prior to the analysis (Li et al., 2015; Purcell, 2000; Schirrmann et al., 2016). One study tested a variety of methods for separating maize seedling pixels from the background including K-means clustering, gaussian mixture models (GMM) , support vector machines (SVM), and fully convolutional neural networks (FCN) and found that although all methods can achieve high accuracies, K-means clustering and FCN have faster processing times and are therefore more efficient when analyzing large datasets (Varshney, 2017). A common problem with canopy cover extraction is the limited ability of different RGB indices to capture the canopy pixels that are not green or to distinguish between different vegetation classes such as crop canopy from weeds. Accuracies have been shown to be high early in the season but to then rapidly drop across crops once they develop due to the browning of vegetative tissue or the development of non-green flowers or fruits (Ashapure et al. 2019; Marcial-Pablo et al. 2019). One solution that was found to solve this problem was to perform a morphological closing operation to fill in small gaps and achieve higher canopy

extraction accuracies (Ashapure et al., 2019). This solution would not help in reducing the misclassification of weed pixels as crop canopy pixels. Weed removal or suppression is therefore important for accurate canopy cover extraction. Other image features other than spectral indices such as texture or shape information could potentially help in distinguishing and removing weed elements.

An extension to simply classifying vegetive material from the background is to distinguish pixels corresponding to various vegetation classes within the field, including the classification of different crop species, different genotypes of a single crop, or plant tissues present within a single genotype in an orthomosaic. For crop classification, color variation across orthomosaics within a maximum likelihood classifier (MLC) could effectively identify different crops growing in the cropping area including cotton, sorghum, soybean and watermelon with high accuracy (Zhang et al., 2017). Researchers have also explored the potential to use spectral information from canopy segmentation to identify which variety is growing. This can be useful when evaluating the productivity of large production fields containing mixed varieties. Planting multiple varieties has been a practice utilized among row crops in field areas with variable soil types or sub-optimal field conditions to mitigate the potential for yield loss and enhance yield in low-input agricultural systems (Barot et al. 2017). One study determined that vegetation indices derived from RGB UAV imagery, including the Excess Green Vegetation Index (ExG), the Normalized Green Red Difference Index (NGRDI), and the Visible Atmospherically Resistant Index (VARI), were able to document differences across three rice paddy varieties by capturing morphological variation across these genotypes (Afdhalia et al.,

2019). Other researchers have focused on utilizing color variation within plant canopies to find indications of crop stress. Darker green colors in the orthomosaics of wheat fields were found in a study to represent areas with denser crop canopy and higher plant vitality, while areas with lighter brown or yellow colors were associated with sparser crop canopy (Schirrmann et al., 2016). These results indicated that the distribution of the RGB colors in orthomosaics could illustrate spatial variation in plant coverage, growth stage, leaf vitality and degree of senescence (Schirrmann et al., 2016). These results would vary across development and would mainly be useful for assessing spatial variation throughout a field at a given time. Similarly, another study observed that a supervised MLC procedure was able to identify portions of maize plants that were yellow or dry which allowed them to further assess the degree of senescence of the crop canopy (Makanza et al., 2018). In this experiment, dry canopy area showed high heritabilities and moderate genetic correlations to grain yield (Makanza et al., 2018). An important thing to keep in mind when selecting the ideal metric and classification algorithm to use for the specific purpose at hand is that color calibration standards of known reflectance are sometimes necessary to adjust for differences in lighting conditions due to sunlight intensity or cloud cover. This is necessary when knowing the color intensity is required, such as when using thresholding based on color intensity, or when comparing traits that rely on color changes, such as leaf senescence through time or across plots. If classification into different classes is the only goal, different algorithms such as k-mean clustering, which subset pixels into a set number of categories based on similarity, eliminate the need for color calibration.

### *Leaf Area Index*

After identification of the crop canopy, a variety of canopy parameters can be extracted from orthomosaics. Leaf area index (LAI), defined as the total leaf area per unit ground surface area, is a key biophysical component due to its important role in crop photosynthesis, transpiration, and nutrient cycling (J. M. Chen & Black, 1992; Shibles & Weber, 1965). LAI as well as other canopy structural parameters depend not just on the growing conditions on the crop, but also on the genotype being assessed (Board & Harville, 1992). Since these parameters are extracted from the upper canopy they are a prime target for measurement from low cost UAV imagery.

A common approach for extracting biophysical parameters such as LAI utilizing spectral imagery has been to extract color or vegetation indexes and variables and correlate those to the canopy parameters of interest. One of the first studies that attempted to extract biophysical traits from UAV phenotyping tested the direct contribution of UAV image variables and spectral indices, including the excess green index (ExG), canopy cover, the individual red (R), green (G), and blue (B) color channels, as well as the ratios between the RGB channels, to phenotypes among wheat plots including LAI (Schirrmann et al., 2016). In this study all image variables except the red:blue ratio were useful in predicting wheat LAI. Similarly, another study calculated multiple color indices from UAV RGB image-derived orthomosaics, including the individual RGB channels, the L*a*b* color space and the hue (H), and utilized single regression analysis to correlate these indices to a variety of rice plant biophysical parameters (Shimojima et al., 2017). They found that the image variables were useful mainly in assessing leaf area index

(LAI) as well as grain yield, plant height, and the grain filling rate at early stage; however, these were not as useful for assessing above ground biomass, panicle length, grain filling rate, and tiller number (Shimojima et al., 2017). In a different study across four different crop species (Zhang et al., 2017), image variables were found to explain between 58.7% and 83.1% of the variability present, with the variables ExG and CIVE (CIVE = 0.441R − 0.811G + 0.385B + 18.78745) having the highest direct correlations to LAI. Another study on soybean found that the red band parameter had the strongest correlation to LAI in soybean (Maimaitijiang et al., 2017). Apart from the direct use of spectral indices to estimate LAI or other biophysical traits, a novel approach that involved first quantifying the structural complexity of the maize canopy based on methods utilized in forest studies was implemented (Li et al., 2017). The structural complexity metrics represented the different spatial patterns and heterogeneity of the crop canopy, such as the spatial distribution of leaves, in three-dimensional space. A linear regression model was then created following stepwise selection on the complexity metrics and the model showed a significant, high correlation with LAI measurements (Li et al., 2017). Another method for estimating LAI in soybean that also incorporates canopy structural information is combining uncalibrated reflectance measurements from UAV RGB imaging, a segmentation approach, and gap fraction theory to account for row interference and leaf overlap when calculating LAI into a model. This achieved high accuracies compared to manual destructive measurements of LAI (Roth et al., 2018). More recently, in winter wheat, (Hasan et al., 2019) a study found that incorporating different UAV RGB image variables including the Visible Atmospherically Resistant

Index (VARI), the Red Green Blue Vegetation Index (RGBVI), the individual B color channel, and the Green Leaf Algorithm (GLA) in a partial least squares regression (PLSR) model could achieve high prediction accuracies for LAI at the jointing stage (r2 = 0.776). Adding texture information to prediction models has also been shown to improve the estimation of biophysical parameters such as LAI in rice (Duan et al., 2019; S. Li et al., 2019). LAI has therefore been demonstrated to be accurately predicted through a range of both spectral and structural metrics. Utilizing the spectral variables requires the use of reflective standards to calibrate the images and eliminate variability due to lighting conditions, which is not required with the structural metrics.

***Biomass***

Aside from LAI, crop biomass is another biophysical trait extensively studied due to its importance in monitoring plant health and productivity and because it is a crucial parameter for calculating the nitrogen nutrition index, which is an important tool for determining the amount of N needed to maximize yield while preventing over-fertilization (P. Chen et al., 2010; G. Lemaire & Gastal, 1997). For these reasons, biomass serves as a primary indicator of yield and can be used to develop yield variation maps and aid in site-specific agricultural decision making (Jannoura et al., 2015). Traditional methods of monitoring biomass require destructive methods to weigh the plant before and after drying. Finding methods that can non-destructively estimate fresh and dry biomass has been a focus in UAV phenotyping research. Since biomass has previously been shown to be correlated to plant height, various groups have utilized plant

height values from DEMs derived through SfM algorithms from UAV imagery to develop regression equations that can predict biomass across a range of crops (Acorsi et al., 2019; Bendig et al., 2014; Brocks & Bareth, 2018; Li et al., 2016; Madec et al., 2017; Tilly et al., 2015; Varela et al., 2017; Yue et al., 2017; Zhu et al., 2019). Although the SfM plant height metrics showed overall moderate correlations to biomass across these studies, most of these correlations were primarily driven by differences across growth stages, and low prediction power was observed for any particular growth stage. These results indicate that, although plant height can be a useful metric as it explains some of the variation for biomass, it cannot by itself be used to accurately estimate biomass. Although the proportion of variation in biomass accounted by plant height is low, the plant biomass estimation utilizing plant height was found to be greatly improved by also taking into account the plant stem diameter (Varela et al., 2017). Although stem diameter cannot be accurately captured by UAVs and would require hand measurements, this still provides a non-destructive method for measuring biomass in the field. The extraction of SfM metrics also does not require the use of reflection calibration standards throughout the field as do the extraction of spectral metrics. Although height metrics themselves are poorly correlated with biomass, various studies showed that the coefficient of variation in height, which explains some of the field heterogeneity, can shed light on the spatial variation in the aboveground biomass of the maize canopy at any single growth stage (Bendig et al., 2014; Li et al., 2016; Madec et al., 2017; Tilly et al., 2015).

Various UAV spectral variables have been used to predict biomass including NDRE in peas and oats (Jannoura et al., 2015). However, it is again important to note that

spectral information requires the use of calibration standards to account for differences in lighting conditions, particularly when assessing large field areas where lighting could change throughout the flight plan or when evaluating plants through time. Studies have developed biomass prediction models that include both height and spectral information in the linear regression equations, such as the Excess Green Vegetation Index (ExG) in a specific study which achieved high prediction accuracies across five different crops (Na et al., 2018). Additional experiments have also concluded that adding spectral information from the UAV RGB images to the plant height values extracted from SfM methods improves biomass estimation compared to using only spectral or height information (Lu et al., 2019; Michez et al., 2018). On the other hand, one study found that a multivariable linear regression model based on multiple vegetation indices derived from RGB imagery was highly predictive of biomass in maize and that adding plant height information did not improve the model (Niu et al., 2019). Another study proposed a method that combines not just UAV-derived plant height, but also a variety of structural and volumetric parameters of the crop canopy together with vegetative indices into a vegetation weighted canopy volume model (CVMVI) for estimating soybean aboveground biomass (Maimaitijiang et al., 2019). The findings suggested that canopy structural metrics were more informative for biomass prediction than spectral metrics; however, combining both into an CVMVI created the best model (Maimaitijiang et al., 2019). Imaging crops at ultra high resolutions to extract image texture information and combining that with spectral vegetation indices in multivariate models can greatly improve biomass estimation in various crops compared to using either set of features by

themselves (Yue et al., 2019, Zheng et al., 2019). In general, prediction of plant dry biomass utilizing a combination of spectral and structural information, primarily plant height, gathered from UAV RGB imaging can be done with high accuracy, but there has been a lower predictive capacity for plant fresh biomass unless additional information, such as stem diameter, is included (Acorsi et al., 2019; Brocks & Bareth, 2018). New methods utilizing machine learning methodology on a range of structural and spectral parameters are being implemented to increase prediction power and minimize estimation error (Han, Yang, Dai, Xu, et al., 2019).

### *Canopy Biochemical Parameters*

Biochemical parameters of crop canopies can serve as important indicators of crop health. Two primary biochemical components studied are leaf chlorophyll and nitrogen content as these can be used to quantify foliar photosynthetic rate and primary productivity (Gitelson et al., 2006; Ripullone et al., 2003). Unlike biophysical traits, the direct use of vegetation indices and variables from RGB imagery to extract biochemical parameters such as nitrogen and chlorophyll content in crop canopies has been less successful (Schirrmann et al., 2016; Roth et al., 2018). From the different image variables and vegetation indices, the individual green band parameter provides the highest correlation to the chlorophyll a and nitrogen biochemical properties, but these correlations are somewhat weak (Maimaitijiang et al., 2017). Normalized difference red edge (NDRE) obtained from UAV imagery has also been used to estimate LAI, and LAI can then be utilized in prediction model equations together with NDRE to obtain more

accurate estimations of chlorophyll content in maize (Milas et al., 2018). This study concluded that LAI is a critical component in mapping chlorophyll content across heterogenous corn fields using UAV images (Milas et al., 2018). These findings, however, would be dependent on the crop since other experiments have found a low correlation of NDRE with LAI in crops including peas and oats (Jannoura et al., 2015). For chlorophyll detection, combining image color features with image texture features such as smoothness has been used (Lang et al., 2019). Although progress in extracting biochemical traits from RGB UAV images has been made, there is still room for improvement. Sensors with higher spectral resolution, such as multispectral or hyperspectral sensors, have the potential to provide advanced opportunities in this area (Haboudane et al. 2002).

### *Biotic and Abiotic Stress Detection*

Detecting and quantifying biotic and abiotic stresses is important for monitoring crop health and for making field management decisions to enhance crop productivity. The most common method for disease or stress detection involves scouting fields by foot and manually scoring crop stands. UAVs can increase the efficiency of the scoring process by flying large areas in a small amount of time. Algorithms have been developed and tested for detecting different stresses including root and leaf diseases as well as nutrient deficiencies from RGB imagery. These have been successful but are hampered by the limited ability of RGB sensors to distinguish between non-green pixel classes. For example, a recommendation algorithm was built to detect maize leaves among production

settings exhibiting strong symptoms of nitrogen deficiency, such as leaf choloris, and achieved strong correct-classification performance (Zermas et al. 2015). Miss-classification rates were high with yellow, non-leaf elements such as tassels constantly classified as N-deficient leaf regions (Zermas et al. 2015). Another study utilized UAV RGB images to identify the proportion of green, yellow, and brown canopy pixels and used these proportions in two modeling algorithms, random forest and neural network, to score iron deficiency chlorosis among soybean plots (Dobbels and Lorenz 2019). Misclassification errors were also seen when classifying the crop canopy since plants experiencing high chlorosis or necrotic symptoms had similar properties to the soil background (Dobbels and Lorenz 2019). A study on potato leaf blight infection that relied on the detection of chlorotic or necrotic spots also found that the distributions of RGB image features among the soil and diseased tissue overlapped (Sugiura et al. 2016). It is likely that having a sensor that captures additional spectral bands aside from RGB, such as NIR, could aid with this issue. Instead, they calculated a percentage of healthy tissue to soil and diseased tissue and used that as a metric to track differences in leaf blight infection rates between plots (Sugiura et al. 2016). Another method that was successfully used to track drought stress severity among wheat plots was to implement a machine learning model that utilizes features extracted from a square of neighboring plant pixels rather than performing individual pixel-wise classifications (Su et al. 2020). This allowed for more effective and faster classifications since spatial information was taken into account and neighboring pixels are more likely to share the same drought status. Utilizing both spectral and also color indices features were also found to achieve

higher accuracies for drought detection compared to only spectral features (Su et al. 2020). UAV RGB platforms have also been used to assess the distribution, spread, and severity of different root disease and pest infestations that cause plant death including root rot disease in alfalfa and white grub larvae damage in soybean (Mattupalli et al. 2018; Puig et al. 2015). Because the primary symptom is plant death, these rely on identifying regions of bare soil areas or low plant densities, which is easy to implement using RGB imaging if field areas are free of weeds. It is possible that with the advent of deep learning algorithms that can take into account not just spectral features but also image textural and shape information, UAV RGB imaging could become a more effective platform for scoring the severity of more complex biotic and abiotic stresses.

### *Temporal Trait Measurements*

A very attractive feature of efficient trait collection from UAVs is that the measurements can be easily acquired across many timepoints throughout the growing season and be used to track growth responses across genotypes and environments. The most common traits extracted temporally include plant height, canopy cover, and canopy color. Monitoring these parameters periodically throughout development is essential to understanding crop development and potentially nutrient and pesticide demand throughout the growing season (Dammer et al., 2009; Schirrmann et al., 2016). Moreover, extracting traits from UAV imagery provides a fast, effective, and inexpensive method to extract quantitative trait information through time that can be used in genetic studies (Xavier et al., 2017).

Different types of curves can be fit to temporal plant height measurements to represent plant growth rates including sigmoidal curves (Chang et al., 2017), linear regressions across the means of each timepoint ((Han et al., 2018), logistic functions (Anderson et al., 2019), and polynomial curves (Tirado et al., 2020b; Chapter 2). When determining which curve best fits the height data, an understanding of different elements that might impact crop growth is essential. For example, plant lodging events may not be captured by some methods of growth estimation (Tirado et al., 2020a; Chapter 3). Once developed, these growth curves can be used for many applications including genotypic differentiation. One study found that the relative increment of plant height, or growth rate, based on the final height achieved could effectively discriminate between genetic backgrounds during different growth stages (Han et al., 2018). Another study also found that clustering growth patterns using fuzzy c-means clustering analysis could help detect differences in growth across maize genotypes (Han et al., 2019). Plant height estimates derived from SfM metrics have also proven useful in the detection of quantitative trait loci (QTL) and informative when included in genomic prediction studies (Hassan et al., 2019). Similarly, the change in canopy coverage through time in soybean has been used in QTL detection through genome-wide association analysis when treated as a quantitative trait (Xavier et al., 2017). To do this, the soybean canopy coverage observations were fit to a logistic model to extract a single-trait value, referred to as the average canopy coverage, that represented the mean of the seasonal values (Xavier et al., 2017). A genomewide association analysis of the average canopy coverage detected a large QTL that led to an increase in yield. This trait was shown to be highly heritable and

strongly correlated with grain yield making it a useful trait when making genotypic selections for crop improvement.

Canopy parameters, such as LAI, are essential elements of growth and can be used to assess plant development and productivity and potentially nutrient and pesticide demands (Dammer et al., 2009; Roth et al., 2018; Schirrmann et al., 2016). These can vary drastically from one day to the next which makes temporal measurements critical and rapid collection methods such as UAVs necessary. Temporal UAV measurements of biophysical traits can lead to a better understanding of how different genotypes respond to environmental factors and stresses. In one study, tracking biophysical traits through time enabled the tracking of changes in early senescence at the individual plant level in a wheat field and the identification of soil-induced water deficit stress due to soil composition and texture variability across the field (Schirrmann et al., 2016). Similarly, another experiment showed that time sequence data analysis of crop color classes could help monitor crop vigor and senescence patterns in maize (Makanza et al., 2018). Temporal UAV measurements for plant height have also allowed researchers to track lodging responses of different maize genotypes grown across different environmental conditions to storm events and identify factors contributing to those responses (Tirado et al., 2020a; Chapter 3).

### *End-season Productivity*

The ultimate goal of crop management and research is to find methods to increase yield either by evaluating large populations and making selections of top-performing

lines, or by efficiently making farm management decisions to minimize plant stress and maximize yield. To this end, remote sensing allows researchers and farmers to evaluate larger areas per time than could be done by walking and performing personal field evaluations. Although not able to directly measure grain yield, UAV platforms can be utilized to measure and thereby select and improve traits that contribute to end of season performance including many of those mentioned in this review such as plant height, LAI, plant senescence, plant growth, and biomass. Moreover, UAVs allow for the assessment of field variability and also nutrient capacity and availability which is a primary determinant of crop yield (Kefauver et al., 2017). Different parameters have been used in regression equations to directly predict yield from in season UAV measurements. The green-red vegetation index (GRVI), which has the ability to measure crop canopy closure, together with LAI estimated from ceptometer equipment, was able to predict yield with fairly high accuracy in a maize field (Sanches et al., 2018). The advantage of UAVs is the ability to measure traits through time which can give additional insights into plant growth and development useful for yield estimation compared to single timepoint measurements. Parameters extracted from a logistic function fit to temporal plant height estimates in maize were found to achieve around a 400% improvement in grain yield predictions and a 50-150% improvement in the selection accuracy of the top 10% yielding hybrids compared to utilizing single time-point measurements of terminal plant height which are commonly used when making line advancement decisions (Anderson et al., 2019). These parameters can be predicted before plant maturity and can therefore allow for faster genotypic selection prior to flowering among breeding programs

(Anderson et al., 2019). UAV temporal measurements of plant height have also allowed for the assessment of in-season root lodging in maize which in turn was highly correlated to grain yield (Tirado et al., 2020a; Chapter 3). More recently, studies have focused on utilizing deep learning methodologies to build models that can capture important spatial features among RGB UAV imagery with respect to grain yield to aid in in-season yield forecasting (Maimaitijiang et al., 2020; Q. Yang et al., 2019). Other studies have used temporal trait measurement such as canopy closure to detect QTLs linked to increases in yield (Xavier et al. 2017). All these techniques that allow for the estimation of parameters that are correlated to end of season grain yield by utilizing UAV RGB imaging can provide researchers, breeders, and agricultural specialists the opportunity to monitor crop yield across early vegetative stages and make more effective crop selections or management decisions.

## CHALLENGES AND OPPORTUNITIES IN ACQUIRING AND ANALYSING UAV RGB DATA IN CROP FIELDS

It is clear that collecting and analyzing data using UAV technology has rapidly advanced in recent years. However, there are still numerous challenges that provide opportunities. Currently, GPS accuracy of UAV imagery continues to be an issue limiting SfM algorithm accuracy (Bendig et al., 2013b; Bendig et al., 2013a; Holman et al., 2016; Ruiz et al., 2013). The use of GCPs have greatly reduced the error of SfM models; however, accurate coordinate surveying of the GCPs is crucial and require the need of expensive GPS surveying equipment such as real-time kinematic (RTK) GPS systems.

GCPs are also hard to implement in production-like settings that lack visible alleys and where GCPs hinder the mobility of ground vehicles and can therefore not be left in the field for temporal UAV data collection. More recently, advanced drones have started to be equipped with their own RTK-GPS devices to accurately log image coordinates and eliminate the need of GCP placement, but this increases the cost of the drone substantially. Other challenges that still remain in UAV data collection involve the low payload, lack of stability under windy conditions, and low battery life (Belton et al., 2019). Sensors have been increasing in spectral and spatial resolution while decreasing in size making systems which gather additional spectral information a viable alternative for low-cost UAVs with low payloads. Moreover, although simple to operate, current US guidelines require that any person intending to fly a UAV for commercial purposes obtain a Remote Pilot Certificate from the Federal Aviation Administration which contributes to additional costs in implementing UAVs for field monitoring (FAA, n.d.).

In terms of analyzing UAV RGB imagery, the largest challenge and the one that presents the most opportunities is the need for automatic and standardized software and protocols for gathering images, processing the data, and extracting the desired traits. The biggest challenge with making progress in generating standardized protocols and software is that the needs within the scientific community in terms of traits of interest and the methods for extracting those traits will vary across platforms, sensors, field layouts, and crops of study. Interpreting raw image data is unproductive and finding the right methods to process that data can be extremely challenging. Efforts in developing protocols for uniform data collection to serve many purposes rather than different

protocols for specific aims would enable the generation of large datasets that can be used by the scientific community. This would also aid in standardizing processing software prior to data analysis. For breeding purposes, the ability to track individual crop plots through time is crucial. Currently, most techniques to detect crop plots rely on manual adjustments of individual plots after fitting a grid based on planting patterns since crop rows are rarely evenly spaced or planted in perfect grids. This is time consuming and labor intensive to do and therefore a huge limitation in making UAV image processing easy to implement in large breeding programs. Improving GPS accuracy of UAV images by utilizing GCPs and/or RTK GPS onboard the platform allows for accurate image registration and orthomosaic alignment across dates which enables the ability to reuse plot boundaries from a previous date and eliminates the need to regenerate these for each timepoint. In terms of data processing and analysis, software commonly used to generate accurate SfM models from UAV imagery, such as Pix4DCapture and Agisoft Photoscan, are proprietary, costly, and their outputs are still difficult to interpret and utilize in biological research (Agisoft & St Petersburg, 2019; Pix4D, n.d.). The outputs, primarily the orthomosaics and DEMs, can be extremely useful when analyzed properly. Many times these analyses rely on finding ways to extract traits that are normally measured by hand. However, there are many opportunities in also discovering new traits such as textural features which can only be extracted from imagery that can in turn aid in the selection of improved cultivars as described above. As we progress in finding optimal algorithms to extract desired phenotypes from crop fields, open-source software will need to become a focus in the research community for providing easy, adaptable solutions for

extracting basic traits across variable field systems and layouts so that they can start to be widely and efficiently implemented across research and breeding programs and across large scale experiments. A key component that will become important to make progress in achieving this is the generation of high quality, annotated datasets that are publicly available and can be used to develop and train new software. The development and maintenance of data and code repositories for this purpose will be necessary for these analysis pipelines to be built. Having fast and efficient pipelines for extracting agronomic traits from UAVs is crucial to advance and begin to breach that bottleneck in making progress in crop improvement and selection.

CHAPTER II

# Context Statement

## SYNOPSIS

Plant height (PH) data collected at high temporal resolutions can give insight into how genotype and environmental variation influence plant growth. However, in order to increase the temporal resolution of PH data collection, more robust, rapid and low-cost methods are needed to evaluate field plots than those currently available. Due to their low cost and high functionality, unmanned aerial vehicles (UAVs) provide an efficient means for collecting height at various stages throughout development. We have developed a procedure for utilizing structure from motion algorithms to collect PH from RGB drone imagery and have used this platform to characterize a yield trial consisting of 24 maize hybrids planted in replicate under two dates and three planting densities. Plant height data was collected using both weekly UAV flights and manual measurements. The comparisons of UAV-based and manually acquired PH measurements revealed sources of error in measuring plant height and were used to develop a robust pipeline for generating UAV-based PH estimates. This pipeline was utilized to document differences in the rate of growth between genotypes and planting dates. Our results also demonstrate that growth rates generated by PH measurements collected at multiple timepoints early in development can be useful in improving predictions of PH at the end of the season. This

method provides a low cost, high throughput method for evaluating plant growth in response to environmental stimuli on a plot basis that can be implemented at the scale of a breeding program..

## PUBLICATION

Chapter II entitled 'UAV Based Imaging Platform for Monitoring Maize Growth Throughout Development' has been adapted from work in the publication:

**Tirado, S. B.**, Hirsch, C. N., & Springer, N. M. (2020). UAV-based imaging platform for monitoring maize growth throughout development. *Plant Direct*, *4*(6). https://doi.org/10.1002/pld3.230

## CONTRIBUTIONS

During the course of this work, multiple people have made contributions. Nathan Springer and Candice Hirsch helped conceive this experiment and analyze the data and also contributed to writing this paper. Amanda Gilbert and Pete Hermanson provided field technical support. Anna Deneen, Kjell Sandstrom, Shale Demuth, Danielle Sorensen and Jordan Freeman helped me collect and process the UAV data for this experiment. Sara Tirado provided all the protocols and developed the tools for collecting, processing and analyzing this data. Author contact information and acknowledgments have been removed and formatting has been adapted to be consistent throughout this thesis.

CHAPTER II

# UAV Based Imaging Platform for Monitoring Maize Growth Throughout Development

## INTRODUCTION

Plant height (PH) serves as a major growth indicator and can be used for assessing crop productivity and making crop management decisions. PH has been shown to be linked to nitrogen (N) nutrition during vegetative development in maize (Yin et al., 2011-1; Freeman et al., 2007), making it useful for assessing spatial variability in crop response to N. PH can therefore help guide precision agriculture practices such as variable-rate N applications within the field. PH has also been linked to plant biomass in maize and barley crops (Li et al., 2016, Freeman et al., 2007, Bendig et al., 2014). Studies have found that PH measurements at early to mid-developmental stages in maize are correlated to grain yield (Yin et al., 2011-2; Katsvairo, Cox and Van Es, 2003), and can be useful for forecasting crop yields (Yin et al., 2011-1) or improving yield predictions (Sharma and Franzen, 2013). These findings suggest that tracking plant height at these earlier stages and throughout development can be useful for identifying superior cultivars in plant breeding programs and for developing management practices that account for spatial heterogeneity in production fields. However, there is still substantial variation across these studies in the level of utility of early-season PH in predicting end of season traits such as yield making this a topic that needs to be further evaluated. To maximize

the utility of PH data, and to address some of the uncertainties regarding the utility of PH, data for large-scale experiments at various stages throughout development needs to be gathered. With current methods for measuring height this can be challenging. Similar to many phenotypic traits, current practices of gathering height in field settings involve physically measuring PH with a large ruler, which is time consuming and difficult to implement on a large scale. Ruler measurements are also subject to user bias and error, decreasing the accuracy and utility of these measurements.

Remote sensing technology has been proposed as an efficient means for collecting rapid and objective measurements for PH (Araus et al., 2014, Madec et al., 2017, Yang et al., 2017). Unmanned aerial vehicles (UAVs) have proven to be a promising platform for collecting remote sensing data as they are inexpensive yet capable of achieving very high spatial and temporal resolutions. Many modern UAVs also have the functionality of flying automatically along a path specified by the user through mission planning software, increasing reproducibility through time. Commercial UAV platforms come equipped with RGB cameras that can be utilized to capture images along the field to create 3D field reconstructions using structure from motion (SfM) and multiview stereo (MVS) algorithms which rely on estimating the 3D structure of a scene utilizing a set of 2D images (James and Robson, 2012). The speed and ease with which UAVs can be flown for data acquisition provide advantages in scale and temporal resolution over other remote sensing methods utilized for creating 3D models, such as light detection and ranging (LiDAR), which involve high costs in data acquisition and processing (Díaz-Varela et al., 2015). However, there is substantial improvement that is needed in

developing tools and approaches for simple implementation of UAV technology to generating phenotypic data in field settings.

There are examples of success in using RGB sensors to extract a number of traits that, if taken through time, can give us insight into plant growth and the relative effects of genetic and environmental variables on these traits. Canopy coverage estimates have been gathered for soybeans using digital cameras and these have been found to highly correlate to canopy light interception measurements (Purcell, 2000) and grain yield (Xavier et al., 2017). Previous studies have estimated PH from UAV imagery in sorghum (Chang et al, 2017; Shi et al., 2016; Watanebe et al., 2017), wheat (Madec et al., 2017; Michalski et al., 2018; Holman et al., 2016), cotton (Feng et al., 2018), barley (Bendig et al., 2014 ) and maize (Anderson II et al., 2019; Anthony et al., 2014; Geipel, Link and Claupein (2014); Grenzdörffer, 2014; Su et al., 2019; Varela et al., 2017 ). Although these studies have reported high correlation in PH measurements for various dates pooled together to manual measurements, they lack estimates of how daily correlations of imagery-derived PH ($PH_{UAV}$) and ruler-derived PH ($PH_R$) vary throughout different growth stages and how this compares to the inherent error in $PH_R$ measurements.

Taking into account past efforts in height estimation from UAV platforms, the present work aims to implement SfM algorithms for the estimation of $PH_{UAV}$ for a maize field throughout development and compare these measurements to daily $PH_R$ measurements collected using the traditional manual ruler-based method. We tested the error in $PH_R$ measurements and assessed the correlation of $PH_{UAV}$ to $PH_R$ measurements.

We also evaluated applications in which this method could be used such as in estimating terminal height from early-season $PH_{UAV}$ data.

## MATERIALS AND METHODS

### *Experimental Design*

Two replicates of 12 maize hybrids were planted in 4-row plots at two dates (05/14/2018 and 05/21/2018) and three densities (60k, 90k and 120k plants per hectare) following a randomized complete block design blocked by planting date and replicate within planting date in St Paul, MN in the summer of 2018 (Figure 2.1). Each row was 15ft long center-to-center with 12 ft of plots and 3ft of alleys and 30in spacing between rows. There were a total of 144 four-row plots planted for this experiment. The 12 hybrid genotypes utilized were generated by crossing ex-PVP lines selected due to their past use in production settings and the availability of seed. This experiment was grown on two acres. Nine 1m x 1m ground targets were distributed around the border and internal alleys of the field for use as ground control points (GCPs) based on previously developed optimization algorithms (Gomez-Candon, De Castro and Granados, 2014).

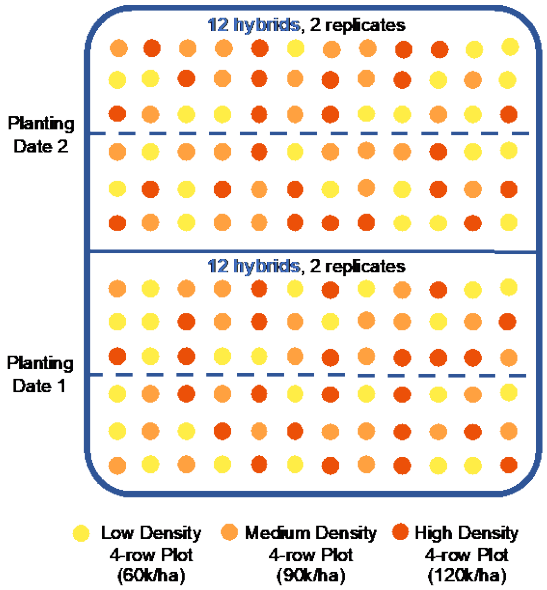


**Figure 2.1.** Field experimental layout for 2018 biological material.

### *Drone Image Data Collection*

The field was imaged approximately weekly from planting until plants reached terminal height using a DJI Phantom 4 Advanced drone flown 30m above ground to achieve a ground sampling distance (GSD), measured as the ground distance represented between the centers of two neighboring pixels, of approximately 0.82cm. SfM algorithms for 3D reconstruction of field points from 2D images rely on finding correspondences between images. Wind can cause issues by causing the object to move between two consecutive recordings. This can be reduced by using a high measuring repetition rate (Paulus, 2019). Images were collected in a grid pattern using 85% frontlap and 85% sidelap to maximize reconstruction efficiency (Figure 2.2B). A total of 615 images were

gathered per mission and a total of twelve missions were conducted throughout the season.

### *Manual Measurement Data Collection*

Manual measurements for plant height ($PH_R(2)$) were collected on the same day as eight of the drone flights by measuring two plants per row from each of the middle two rows of each four-row plot using a ruler. $PH_R$ was measured as the distance between the ground and the topmost freestanding vegetative part of the plant until plants reached reproductive growth and then to the top point of the tassel. For 18 selected plots, hand measurements of all plants in one of the middle two rows ($PH_R(All)$) were collected to get estimates of variance in height within a row. The 18 plots comprised of one replicate of all three densities in the early planting date for 6 randomly selected genotypes (DK3IIH6 x LH198, LH198 x PHN46, LH82 x PHK76, PHB47 x LH198, PHB47 x PHP02 and PHK56 x PHK76).

### *Data Processing Workflow*

Agisoft software (Agisoft Photoscan Professional Edition v1.4.4, 2018) was used to process the collected imagery and generate crop surface models (CSM) and RGB orthomosaics for each date following the developed workflow (Figure 2.2C). Processing steps implemented in Photoscan include feature matching, solving for camera intrinsic and extrinsic orientation parameters, building a dense point cloud, building a field orthomosaic, and building a digital elevation model as specified by Photoscan manual

recommendations (Agisoft LLC, 2018; Figure 2.2A). Parameters set for image alignment included: high accuracy for obtaining camera position estimates, reference pair selection so that overlapping pairs of photos are selected based on measured camera locations, a key point limit of 40,000 points, and a tie point limit of 4,000 points. Ground control points were then used to optimize camera alignment. For generating the dense point cloud, the quality value was set to High with Moderate depth filtering to optimize processing time and model quality.

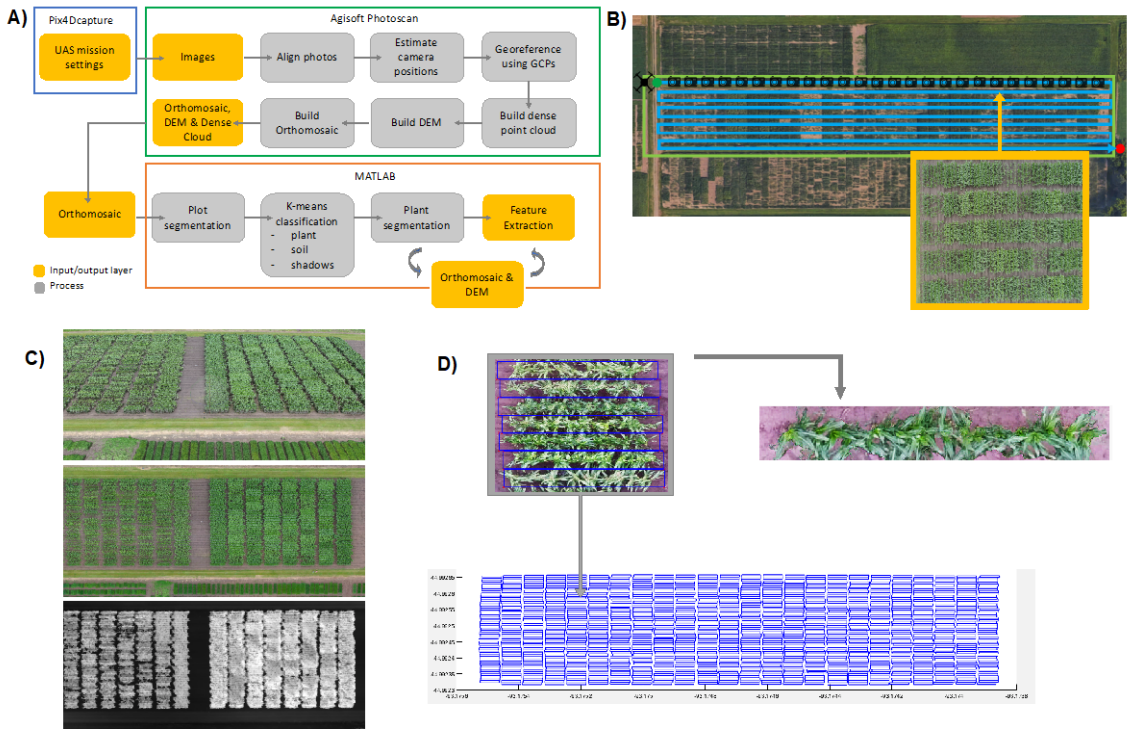


**Figure 2.2**. Procedure for feature extraction from UAV images.

***A)*** *Image generation and processing pipeline.* ***B)*** *UAS flight mission structure for gathering images.* ***C)*** *Dense cloud (top), orthomosaic(middle) and DEM (bottom) output from Agisoft Photoscan Professional Edition.* ***D)*** *Plot boundary extraction from grid shapefile for plot segmentation.*

QGIS software (QGIS v2.18.9, 2017) was utilized for plot boundary extraction by overlaying a grid based on plot size and spacing and exporting plot boundary coordinates for the middle two rows of each plot (Figure 2.2D). Custom MATLAB algorithms were developed to process the CSMs and orthomosaics to extract height estimates for individual plots. Plant height was extracted by segmenting individual plots from the CSMs, overlaying a grid with 20 bins along the plot and extracting the 3$^{rd}$ percentile and 97$^{th}$ percentile height values for each bin. To select these optimal percentiles, the

minimum 1st, 3rd and 5th percentile values from all bins were first extracted and defined as ground height estimates for a subset of plots and the resulting plot height estimates compared to each other to select the optimal ground height extraction procedure. All three methods utilizing the different percentiles represented plot ground height values in the alleys; however the 3rd percentile was selected as this value reduced the amount of error in ground height extraction compared to the 1st percentile due to outlier points present in the 3D models and the subsequent DEMs that were generated. This percentile also produced plot height estimates that had a higher correlation to ground truth measurements compared to utilizing the 5th percentile. The 97th percentile was selected following the same logic and to keep the procedure consistent. To extract the $PH_{UAV}$ value for each bin, the ground height value (minimum 3rd percentile across bins) was subtracted from the 97thpercentile height value in each bin. To calculate the mean $PH_{UAV}$ per plot, a trimmed mean function was implemented on the $PH_{UAV}$ values of the middle 12 bins of the plot trimming the two bins with the highest and lowest height values and determining the average of the remaining 10 height values (Figure 2.3). Only the middle 12 bins for the middle two rows in each plot were assessed when calculating an average PH value to prevent the average height for a given plot to be biased by the height of plants near alleys or different density treatments. A piecewise polynomial spline of order 20 was fit using the MATLAB splinefit function to better represent the continuous plant growth that occurs throughout the growing season (Lundgren, 2019). To assess how growth changes through time, we then extracted the first derivative, or slope, of the curve to get change in height through time.

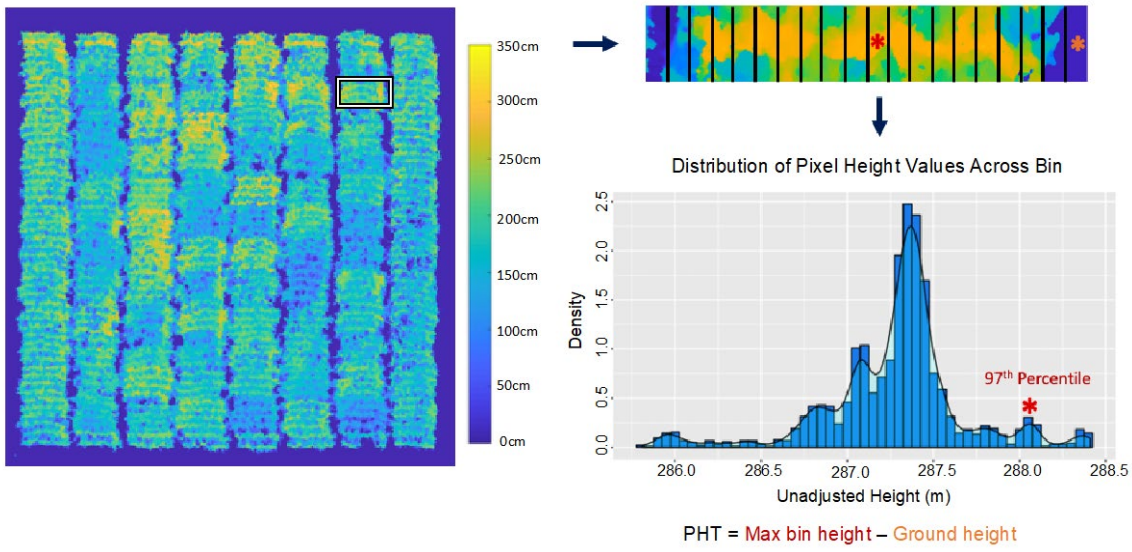


**Figure 2.3.** Method for extracting mean $PH_{UAV}$ values for a given plot.

*The plot is segmented and broken down into 20 bins. The 3rd and 97th percentiles for each bin are extracted and used to calculate the average plot height by subtracting the minimum 3rd percentile of all bins from the 97th percentile of each bin.*

### *Statistical Analyses*

A total of 1,152 mean plot $PH_{UAV}$ values were extracted across eight timepoints. Outliers were identified for each timepoint as those values that were less than or larger than the mean $PH_{UAV}$ value for that date plus or minus the standard deviation multiplied by a factor of 2½. A total of 17 outlier points across all dates were identified and removed from the dataset for subsequent analysis. It should be noted that while there was a strong wind event that caused substantial lodging in the experiment (see below), these outlier points were random and not enriched for data points collected at or shortly after the lodging event. To measure the strength of the linear relationship between different PH measurements, Pearson's correlation was utilized.

Variation in mean plot plant height values was partitioned into genotype, planting date, density, genotype-by-density interaction, genotype-by-planting date interaction and replicate all treated as fixed effects with the linear model $y_{ijkl} = u + g_i + e_j + d_k + r(e)_{l(j)} + (ge)_{i*j} + (gd)_{i*k} + e_{ijkl}$ where $y_{ijkl}$ is the phenotype value of the ith genotype in the jth planting date in the kth planting density of the lth replication; $u$ is the phenotypic mean across planting dates and planting densities; $g_i$ is the ith genotype effect; $e_j$ is the jth planting date effect, $d_k$ is the kth planting density effect; $r(e)_{l(j)}$ is the lth replication effect nested within the jth planting date; $(ge)_{i*j}$ is the interaction effect of the ith genotype by the jth planting date; $(gd)_{i*k}$ is the interaction effect of the ith genotype by the kth planting density; and $e_{ijkl}$ is the residual effect. To test the significance of the various effect variables of the linear model on plant height, we used the anova function of the R stats package (R Core Team, 2012).

***Model Development for Predicting Terminal Height***

A piecewise polynomial function of 20 degrees was fit to $PH_{UAV}$ values for each plot through time to create a smooth curve with optimal fit. The first derivative of the fitted curve was then extracted to get change in height through time (Figure 2.8B). The slope curve was then broken up into 100 equidistant timepoints for each plot. The contribution of each timepoint to the prediction of mean terminal height for each respective plot, based on hand measurements after plants had reached the reproductive stage, was tested utilizing a linear regression model. A new linear regression model was

then created to predict terminal height utilizing slope values for the timepoints that provided the largest contribution, in this case more than 40%, of the observed variation for terminal hand height. The final model contained the terminal height as the response variable and the slope at nine timepoints as the predictor variables (Figure 2.8B). This model was derived from ¼ of the data points and tested to predict the terminal height of the other ¾ of the plots.

## RESULTS AND DISCUSSION

Our goal was to implement a robust low-cost platform for efficient estimation of plant height for maize plots. High-throughput collection of plant height measurements throughout the growing season can provide a better understanding of how different environments influence maize growth and can help to dissect the underlying cause of end of season genotype x environment (GxE) interactions that are commonly observed. In order to develop a robust plant height collection pipeline and to begin to consider the factors that influence plant growth rates, we planted a set of hybrids in a design that incorporated multiple planting densities and planting dates such that plants would be exposed to similar environments but at different growth stages (Figure 2.1). To decrease the impact of neighboring plots, each plot was grown as a four-row plot and only plants in the middle two rows were measured. Manual measurements were taken using a ruler on the dates that aerial images were obtained. Analysis of variance showed significant variation in final plant height within this experimental design due to genotype, planting date, and density (Table 2.1).

**Table 2.1.** Analysis of variance of hand measured plant height for 12 hybrids across 6 environments at physiological maturity (08/09/2018).

| | Degrees of Freedom | Sum of Squares | Pr(>\|t\|) |
|---|---|---|---|
| Genotype | 11 | 40518 | < 2e-16 *** |
| Planting Date | 1 | 31241 | < 2e-16 *** |
| Density | 2 | 764 | 0.007114 ** |
| Replicate | 1 | 146 | 0.161268 |
| Genotype*PlantingDate | 11 | 7194 | 1.19e-10 *** |
| Genotype*Density | 22 | 2042 | 0.214862 |
| PlantingDate*Density | 2 | 1418 | 0.000151 *** |
| Residuals | 93 | 6810 | |

* significant at $p$ =0.05; ** significant at $p$ =0.01; *** significant at $p$ =0.001; N.S., not significant.

Aerial images of the field were collected throughout the growing season until plants reached terminal height (approximately weekly, weather permitting). The images were used to create high resolution 3D models, field orthomosaics, and DEMs using existing SfM algorithms (Figure 2.2). There are multiple methods that have been utilized for extracting plant height from UAV images. A common approach used is the difference based method (DBM) which involves subtracting a digital terrain model (DTM) of the bare ground from the DEM (Varela et al., 2017). The DTM can be generated by flying the bare ground but requires an additional day of data collection and processing and can

introduce error due to minor fluctuations in flight altitude within and across dates that are common with most commercial drone platforms. Other approaches attempt to create the DTM by identifying and extracting ground points from the pointcloud and interpolating the height of intermediate points to create a surface model of the ground and then taking the difference between the DTM and DEM, but these approaches require processing large 3D point clouds and finding optimal parameters for the interpolation algorithm which can be computationally intensive (Su et al., 2019). Different algorithms for generating a DTM including DBM and three point cloud interpolation methods were evaluated by Anderson II et al. (2019) to see which provides higher accuracy when estimating plot heights. They found that all methods had similar, consistent performance in flat, uniform fields similar to those used in breeding trials.

Rather than generating a DTM, we developed a pipeline that involves identifying ground height values individually for each plot directly from the DEMs of a given date when calculating mean plot height. For each plot the height was estimated from the DEMs derived from UAV imagery ($PH_{UAV}$) by calculating the difference between the ground height and surface height of plant material across each plot and calculating a mean plot height value (Figure 2.3, see methods). It is important to note that this method relies upon determining ground height values based on visibility of ground pixels within the alleys separating adjacent plants. This means that this method requires spaces between plots that are free of weeds. The viability of this approach would be limited in situations of high weed pressure or non-existent alleys, as would occur in production settings.

***Error within ruler height measurements***

A critical question for any application using $PH_{UAV}$ is the quality of the height estimates that are obtained through this high throughput measurement. However, there are multiple complicating factors in truly assessing the quality of $PH_{UAV}$ estimates. An important factor is that the manual measurements of plant height ($PH_R(2)$) that are used as the 'ground truth' for determining the accuracy of $PH_{UAV}$ estimates can include some level of error. In order to begin to understand the quality of the $PH_{UAV}$ estimates, we replicated hand measurements of the same plants for a subset of plots at three of the timepoints (6/13/18, 7/17/18, and 8/9/18). To do this, we measured the same two plants per row twice for 12 randomly selected plots by having personnel return to the same plots when taking manual measurements and measuring the same plants which were tagged. An assessment of the correlation and error in replicated hand measurements of the individual plants and plot mean $PH_R(2)$ revealed variation in the correlations and RMSEs (Table 2.2). In the earliest timepoint which corresponds to crop vegetative stages of V6 and V4 for the first and second planting respectively, the correlation between ruler measurement replicates showed the lowest correlation (adj. r-square value of 0.45 for individual plant measurements and 0.64 for plot mean measurements calculated using the two plants from the middle two rows). This correlation improved with later developmental stages. This improvement could be due to larger differences in height later in development due to the genotypic variation present. Similarly, the NRMSE between ruler measurement replicates was highest in the first timepoint but was consistently lower at later timepoints. The correlation at terminal plant height was high (adj. r-square value

of 0.9 for individual plant measurements and 0.64 for plot mean measurements) and had a low amount of error (NRMSE of 0.03 for individual plant measurements and 0.01 for plot mean measurements; Table 2.2).

**Table 2.2.** Adjusted r-square values, root mean square error, and normalized root mean square error by mean for the linear correlation of various PH measurements.

| | PH-R Replicates for Individual Plants | | | Plot Mean PH-UAV to PH-R(2) for Plot Subset | | | Plot Mean PH-R(2) Replicates for Plot Subset | | |
|---|---|---|---|---|---|---|---|---|---|
| | **Adj R2** | **RMSE** | **NRMSE** | **Adj R2** | **RMSE** | **NRMSE** | **Adj R2** | **RMSE** | **NRMSE** |
| 6/13/18 | 0.45 | 4.50 | 0.12 | 0.05 | 12.29 | 0.34 | 0.64 | 2.52 | 0.07 |
| 7/17/18 | 0.97 | 7.75 | 0.03 | 0.47 | 27.36 | 0.11 | 0.88 | 4.00 | 0.02 |
| 8/9/18 | 0.90 | 7.18 | 0.03 | 0.72 | 27.19 | 0.11 | 0.98 | 3.00 | 0.01 |

*From left to right: replicated hand measurements obtained for 2 plants across 12 plots, means derived from the replicated hand measurements obtained for 2 plants of the same 12 plots, and algorithm-derived plot mean height values to the respective hand-measured plot mean height of the same 12 plots.*

Another potential difference between $PH_R$ and $PH_{UAV}$ estimates of plot height is that manual measurements are often collected for a subset of plants in a row while the UAV measurements are often generated as a per plot mean height that samples a larger number of plants. To investigate the accuracy in plot mean $PH_R(2)$ obtained by measuring

only two random plants per row, we randomly sampled two individual plant $PH_R$ measurements at each timepoint twice for the 17 plots in which all plants for one of the middle two rows were measured and calculated new replicates for plot mean $PH_R(2)$ measurements with the intention of assessing the accuracy and error in traditional methods of plot mean calculation. We replicated this procedure 100 times for each plot and timepoint to get an estimate of the average amount of error in $PH_R(2)$ mean values calculated by measuring only two plants per row. Plot mean $PH_R(2)$ measurements obtained from different sets of plants within a row showed a much lower correlation and larger error across most timepoints compared to the correlations between $PH_R$ replicated measurements of the same two plants (Table 2.2). These correlations are comparable to those obtained when correlating plot mean $PH_{UAV}$ measurements to plot mean $PH_R(2)$ measurements (Figure 2.5A). This indicates that $PH_R$ measurements can have substantial variation that is impacted by the number of plants measured and the selection of plants to be measured.

***Correlation of ruler height to UAV-derived height measurements***

There are limitations in accuracy of ruler-estimated heights for specific plants as well as for estimating the height of a plot. However, these measurements can still be used to assess the quality of $PH_{UAV}$ measurements, if we accept that the quality of the correlations between $PH_{UAV}$ and $PH_R$ likely cannot be improved beyond the inherent errors in $PH_R$ measurements. Compared to our manual height estimates, analysis of variance showed significant variation in terminal $PH_{UAV}$ within this experimental design

due to genotype and planting date; however, density had a smaller effect (Table 2.3). Comparison of $PH_R(2)$ and $PH_{UAV}$ showed the overall correlation across all data collection dates was strong (adj. r-square value of 0.96 for our dataset; Figure 2.4), as has been previously shown in other studies (Varela et al., 2017). However, assessing the accuracy of all timepoints together from a biological standpoint offers little value. A more biologically relevant comparison is evaluating the correlations within individual timepoints of data collection. The correlations within a single date were much lower (Figure 2.5A). This is likely due to the fact that the level of variation for height on a single date tends to be relatively low. The root mean square error (RMSE) for mean plot $PH_{UAV}$ compared to the mean plot $PH_R(2)$ across all dates and both planting dates was 25.38cm, but varied from 14.39cm to 38.80cm across dates for the first planting date and from 10.24cm to 33.59cm across dates for the second planting date (Figure 2.5A). The root mean square error normalized by the mean plot $PH_R(2)$ measurements (NRMSE), on the other hand, showed that overall the error was higher at early developmental stages and then lowered and leveled off across later timepoints in both planting dates. The lower correlations and higher error for the first planting date was likely due to a storm that occurred on July 1st that produced strong winds. This storm caused large degrees of lodging, especially within plots in the early planting date treatment causing larger variability in height among plants within plots.

**Table 2.3.** Analysis of variance of UAV-derived plant height for 12 hybrids across 6 environments at physiological maturity (08/09/2018).

| | Degrees of Freedom | Sum of Squares | Pr(>\|t\|) |
|---|---|---|---|
| Genotype | 11 | 11246 | 0.00638 ** |
| Planting Date | 1 | 46425 | < 2e-16 *** |
| Density | 2 | 150 | 0.82635 |
| Replicate | 1 | 375 | 0.33116 |
| Genotype*PlantingDate | 11 | 4582 | 0.40237 |
| Genotype*Density | 22 | 6218 | 0.8087 |
| PlantingDate*Density | 2 | 3078 | 0.02339 * |
| Residuals | 90 | 35365 | |

* significant at $p$=0.05; ** significant at $p$=0.01; *** significant at $p$=0.001; N.S., not significant.

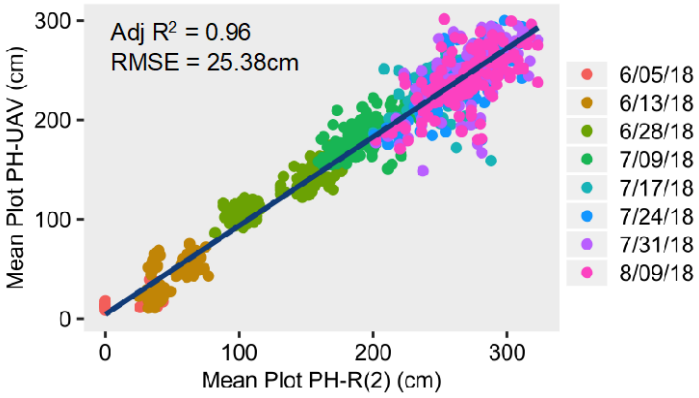


**Figure 2.4.** Pearson correlation plots of various PH measurements.

*Correlation of mean plot $PH_{UAV}$ and mean plot $PH_R(2)$ across all dates.*

| | A) PH-UAV to PH-R(2) | | B) PH-UAV to PH-R(All) | C) PH-R(2) Subsample Replicates | D) PH-95 to PH-R(2) | |
|---|---|---|---|---|---|---|
| | **Planting Date 1** | **Planting Date 2** | **Planting Date 1** | **Planting Date 1** | **Planting Date 1** | **Planting Date 2** |
| | **Adj R2** | **Adj R2** | **Adj R2** | **Adj R2** | **Adj R2** | **Adj R2** |
| 6/5/18 | 0.06 | NA | 0.21 | 0.32 | 0.05 | NA |
| 6/13/18 | -0.01 | 0.11 | 0.40 | 0.20 | 0.00 | 0.11 |
| 6/28/18 | 0.32 | 0.09 | 0.47 | 0.48 | 0.27 | 0.07 |
| 7/9/18 | 0.24 | 0.26 | 0.35 | 0.18 | 0.09 | 0.12 |
| 7/17/18 | 0.09 | 0.31 | 0.20 | 0.42 | 0.21 | 0.28 |
| 7/24/18 | 0.33 | 0.17 | 0.49 | 0.51 | 0.07 | 0.20 |
| 7/31/18 | 0.20 | 0.14 | 0.69 | 0.32 | 0.13 | 0.17 |
| 8/9/18 | 0.27 | 0.66 | 0.62 | 0.54 | 0.21 | 0.15 |
| All Dates | 0.95 | 0.98 | 0.96 | 0.97 | 0.93 | 0.96 |
| | **RMSE** | **RMSE** | **RMSE** | **RMSE** | **RMSE** | **RMSE** |
| 6/5/18 | 14.39 | NA | 14.65 | 4.65 | 18.05 | NA |
| 6/13/18 | 14.53 | 15.78 | 20.82 | 11.19 | 15.35 | 18.92 |
| 6/28/18 | 15.89 | 10.24 | 11.57 | 11.95 | 17.75 | 12.79 |
| 7/9/18 | 21.51 | 12.14 | 13.64 | 23.73 | 33.15 | 15.32 |
| 7/17/18 | 36.47 | 17.38 | 30.18 | 17.23 | 42.33 | 48.73 |
| 7/24/18 | 37.97 | 26.39 | 29.72 | 17.01 | 42.53 | 47.95 |
| 7/31/18 | 38.74 | 28.81 | 16.55 | 28.04 | 41.36 | 34.78 |
| 8/9/18 | 38.80 | 33.59 | 27.27 | 12.90 | 37.47 | 31.32 |
| All Dates | 29.31 | 21.31 | 21.74 | 17.29 | 32.96 | 31.57 |
| | **NRMSE** | **NRMSE** | **NRMSE** | **NRMSE** | **NRMSE** | **NRMSE** |
| 6/5/18 | 0.41 | NA | 0.41 | 0.13 | 0.51 | NA |
| 6/13/18 | 0.25 | 0.43 | 0.59 | 0.31 | 0.27 | 0.51 |
| 6/28/18 | 0.10 | 0.10 | 0.08 | 0.08 | 0.11 | 0.12 |
| 7/9/18 | 0.11 | 0.07 | 0.07 | 0.12 | 0.16 | 0.08 |
| 7/17/18 | 0.15 | 0.07 | 0.12 | 0.07 | 0.17 | 0.20 |
| 7/24/18 | 0.15 | 0.09 | 0.12 | 0.07 | 0.17 | 0.17 |
| 7/31/18 | 0.15 | 0.10 | 0.07 | 0.11 | 0.16 | 0.12 |
| 8/9/18 | 0.15 | 0.12 | 0.11 | 0.05 | 0.15 | 0.11 |
| All Dates | 0.16 | 0.12 | 0.12 | 0.10 | 0.18 | 0.18 |

**Figure 2.5.** Adjusted r-square values and root mean square error for the linear correlation of various PH measurements.

*A) UAV-derived ($PH_{UAV}$) plot mean height values compared to the respective hand-measured plot mean height ($PH_R(2)$) for plots where two plants per row were hand measured. B) UAV-derived ($PH_{UAV}$) plot mean height values compared to the respective hand-measured plot mean height ($PH_R(All)$) for plots where all plants for one of the middle two rows were hand measured. C) Means derived from two iterations of random sampling of hand-measured height values for two*

*plants across plots were all plants for one of the middle two rows were hand measured. D) 95th percentile of height values from entire plot compared the respective hand-measured plot mean height values ($PH_R(2)$).*

If we compare the error in $PH_{UAV}$ measurements to that in $PH_R(2)$ replicated measurements for the subset of plots where two individual plants were hand-measured twice, we see that the correlations of $PH_R(2)$ and $PH_{UAV}$ measurements for the same plots increased throughout development but were lower than the correlation between $PH_R(2)$ replicated measurements (Table 2.2). By terminal height the correlation between $PH_R(2)$ and $PH_{UAV}$ measurements was high (adj. r-square value of 0.72) but had a substantial amount of error (Table 2.2). Unlike the high correlation and low RMSE obtained from plot mean $PH_R(2)$ measurement replicates calculated by measuring the same two plants per row, plot mean $PH_R(2)$ measurements obtained by sampling different sets of plants within a row showed a much lower correlation and larger error across most timepoints (Figure 2.5C; Table 2.2). These correlations between plot mean $PH_R(2)$ calculated by measuring varying plants in a row, however, are comparable to those obtained when correlating plot mean $PH_{UAV}$ measurements to plot mean $PH_R(2)$ measurements (Figure 2.5A;1.5C). The direct comparison of the PHR(2) and $PH_{UAV}$ measurements obtained therefore yielded an error comparable to the inherent error in estimating $PH_R(2)$ across most timepoints.

Given that mean plot $PH_{UAV}$ estimates take into account variation in height throughout a plot, we can better assess their correlations to mean plot $PH_R$ measurements by looking at the subset of plots where all plants in a row were measured. Doing so, we

see that the correlations and error estimates of mean plot $PH_{UAV}$ to mean plot $PH_R$(All) greatly improve relative to those calculated by comparing mean plot $PH_{UAV}$ estimates to mean plot $PH_R$(2) measurements (Figure 2.5B). This indicates that mean plot $PH_{UAV}$ measurements better resemble the true plot mean compared to the mean calculated from measurements of just a subset of plants per row.

It is worth noting that in our approach mean plot height values are obtained using a binning procedure across the plot (see methods), whereas most current methods for calculating mean plot height from UAV imagery extract a constant value, such as the 95th percentile, from the entire plot. However, the height for maize plants throughout a row can vary and extracting a single value might not capture this variation. When performing ruler measurements, researchers typically measure plants towards the center of a row due to the border effects that might cause plants near alleys to vary in height due to lower competition for sunlight, water and nutrients. Thus, we decided to collect height across bins throughout the length of the plot and only utilize height values for bins towards the center of the plot to calculate an average plot height. To assess whether our binning approach provided a more informative framework for assessing the average height of an entire plot as would be collected through traditional hand measurements, we extracted the 95th percentile height value ($PH_{95}$) from entire plots without binning, subtracted the 3rd percentile ground height values for each plot same as in our binning approach, and compared their correlations to $PH_R$(2) measurements. $PH_{95}$ showed low correlation to $PH_R$(2) and high error rate throughout most individual timepoints with an RMSE ranging from 15.32cm to 48.73cm (Figure 2.5D). These lower correlations and

higher error estimates compared to the $PH_{UAV}$ measurements obtained through our approach show the value in binning and extracting an average to represent height for plots where height variation is present rather than extracting a single value.

***UAV-estimated heights can detect biological variation***

Our goal was to develop a low cost, high-throughput platform for monitoring PH through time that would allow us to look at how genotypes develop and respond to different environmental conditions. A storm with high wind speeds occurred on July 1st of the 2018 growing season in St. Paul, providing a prime opportunity to evaluate the utility of this method to track plant responsiveness to environmental conditions. An example of this responsiveness can be seen in the height profiles for LH82 x DK3IIH6 plots, where plants at high density in the earlier planting date showed a reduction in height 45 days after sowing (Figure 2.6A). Normally, a reduction in height would be unexpected and may reveal issues with the height estimation platform, but this height reduction was due to the lodging that occurred as a result of the storm. We were not able to track the lodging event in the $PH_R$ measurements (Figure 2.6B), as these measurements were not taken until several days after the wind storm and most plots recovered from the lodging prior to this measurement. UAV imagery provides an opportunity to collect data rapidly in response to events such as this storm event and track plants at regular intervals that is much more difficult to do with hand measurements.

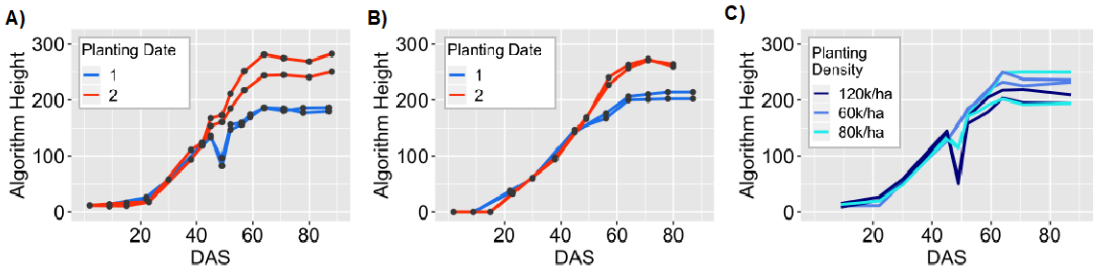


**Figure 2.6.** Height through time for various genotypes and treatments.

*A-B) Height through time as measured by the UAV (A) and hand measurements (B) for two replicate plots of a single genotype (LH82 x DK3IIH6) planted under high density across two planting dates. Dots indicate timepoints of measurement.* ***C)*** *Height through time as measured by the UAV for two replicate plots of a single genotype (LH82 x PHK76) in the early planting date treatment and the three planting densities.*

We expected to note differences in height within genotypes and planting dates based on planting density. Plants grown at higher density tend to grow faster and taller when water and nutrient resources are not limited as they are competing with more plants for sunlight (Tetio-Kagho & Gardner, 1988). Planting density did contribute to differences observed for lodging across genotypes in the early planting date. Plots planted at higher densities experienced a more severe degree of lodging when exposed to strong winds compared to plots planted at a lower density (Figure 2.6C). However, our data suggested that the realized height remained pretty stable across densities and that in many cases, the differences in height due to genotypic variation were reproducible across planting dates and densities (Figure 2.7A-C).

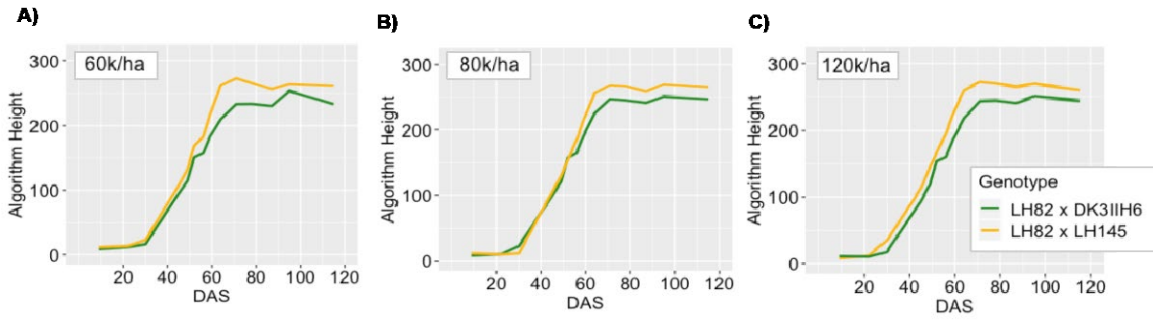


**Figure 2.7.** Height through time for various genotypes and treatments.

*A-C) Height through time as measured by the UAV for plots of two different genotypes (LH82 x DK3IIH6 and LH82 x LH145) in the late planting date treatment and the low (A), medium (B) and high (C) planting densities.*

The $PH_{UAV}$ estimates were also able to document differences in growth rates throughout the growing season between genotypes. For example, LH82 x LH145 planted at high density in the late planting had a faster rate of growth compared to LH82 x DK3IIH6 planted in the same conditions as soon as 20 days after sowing (Figure 2.7C). LH82 x LH145 was able to maintain an advantage in terms of height throughout development and achieve a higher realized height at the end of the season. The ability to track these differences in growth patterns among genotypes that may or may not impact the end of season heights that are typically collected provides additional information to breeders in the process of selecting superior parents and hybrid combinations. Overall, visualization of the plant height profiles for each genotype x condition suggested a fairly robust ability to monitor biological variation for height and responsiveness to environmental conditions under different growth conditions.

***Predicting terminal height from height collected at earlier time points***

Being able to estimate height for any given date is useful for tracking growth; however, being able to predict terminal height using height from earlier time points can allow for the assessment of end-season performance at a time when you can still implement management practices to enhance it. This also can allow breeders to make selections of top-performing plants that meet the desired phenotypic characteristics before making crosses thereby helping maximize their selection efficiency. We wanted to test whether height at early developmental stages could be predictive of terminal height. A previous study by Li et al. (2018) showed low correlations between PH collected for hybrid varieties at early developmental stages to their respective end of season height likely due to differences in the physiological basis for PH at both stages. Including temporal data for height, or rather the rate of change in height through time, could be more informative when predicting terminal height as it captures how different genotypes interact with the environment and how this interaction impacts the trait at hand. Therefore, rather than just using height at specific timepoints (Figure 2.8A) to predict terminal height, we wanted to utilize rate of growth at intervals in time. To do this, a B-spline, or piecewise polynomial function, of 20 degrees was fit to create a smooth curve representative of true growth and the first derivative was then extracted (Figure 2.8B). Timepoints that showed a high contribution to terminal height were used to create a linear regression model to predict terminal height (see methods). The model was derived from ¼ of the data points and tested to predict the other ¾ of the plots. It contained nine timepoints, three of which were in the V2-V4 developmental stages, four in the V5-V7

stages and two in the V8-V10 stages. These timepoints all had biological significance as they fell upon areas of large inflection in the plant growth curve where a weather event or developmental time point caused a dramatic change in height. The first three timepoints which fall upon the V2-V4 developmental stage exhibited a large increase in height characteristic of early plant growth. The second set of three timepoints follow the storm that occurred around the V5-V7 developmental stage which caused a large degree of lodging just prior to their recovery. The last set of timepoints in the V8-V10 stages show a decline in rate of growth followed by a sudden increase. This decrease could be a consequence of weather variables such as temperature and moisture availability whereas the increase could be due to the emergence of tassels. These timepoints were crucial points in plant development where plant growth responded to certain conditions that in turn affected the terminal height obtained.

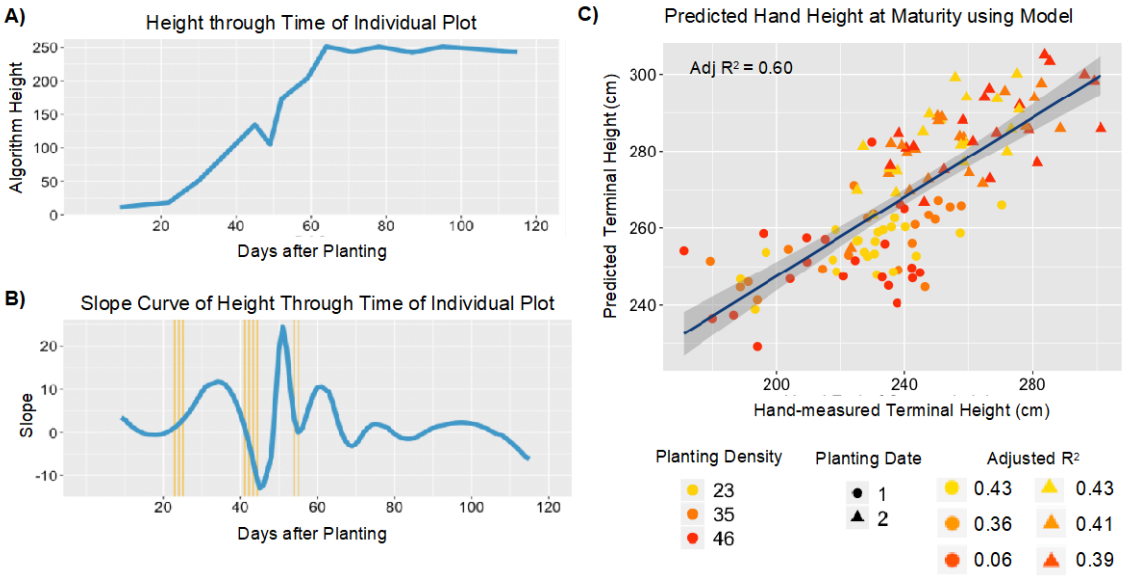


**Figure 2.8.** Predicting terminal height using rate of change in height at certain intervals.

*A) Height through time for an individual plot as recorded by the UAV. B) First derivative of the height through time spline curve in blue and the selected timepoints were the slope contributed most to the prediction of terminal height in yellow. C) Correlation of predicted terminal height on the test dataset utilizing a linear regression model derived from the training dataset based on slope values of selected timepoints and the hand-measured height values at maturity.*

This model had a high ability to predict terminal mean plot $PH_{UAV}$ (adjusted r-squared value of 0.63) and mean plot $PH_R(2)$ (adjusted r-squared value of 0.60; Figure 2.8C). When looking at the different treatments separately, we can see that the ability to predict height across planting dates increases for the late planting treatment and the magnitude of this difference increases with higher planting densities. This is likely due to the challenges in estimating mean plot height for plots that suffered lodging and the higher density treatments in the early planting date experienced the most lodging early in the season. These height prediction results, although specific to this experiment, show the significant correlation that change in height from early season timepoints can have with terminal height and highlight the potential for developing tools to predict terminal height utilizing temporal PH measurements early in development. Maize plants uptake negligible amounts of nutrients such as nitrogen for the first weeks after emergence and then start to exponentially take up more nitrogen until the tasseling stage (Sharma and Bali, 2018). Being able to use height information gathered before the V10 developmental stage to predict terminal height and potentially stress can be a useful tool for guiding nutrient management practices early in development when plants are efficiently absorbing nutrients and can have a high response to fertilization.

## CONCLUSIONS

High-throughput collection of plant height measurements throughout the growing season can allow a better understanding of how different environments influence maize growth and can reveal important factors affecting crop productivity. We have developed a novel approach for extracting plot $PH_{UAV}$ from individual plots that involves estimating the ground height individually for each plot and using that to calculate mean plot height. Overall, $PH_R(2)$ and $PH_{UAV}$ measurements showed a high correlation (adj. r-square value of 0.96); however, correlations within plant height estimates collected on a single date are much lower as they are impacted by the low variability in height expressed on a single date. The reproducibility and quality of $PH_R(2)$ estimates were found to vary throughout development with lower correlations and higher error rates observed in early vegetative stages, and improved correlations and lower error rates observed in later developmental stages. When assessing the error in generalizing mean $PH_R$ for a plot by measuring only a subset of plants in a row, $PH_R$ measurements were found to be greatly variable and impacted by the number and selection of plants sampled. Plot mean $PH_R(2)$ measurements obtained from different sets of plants within a row show a correlation and error across most timepoints comparable to those obtained when correlating plot mean $PH_{UAV}$ measurements to plot mean $PH_R(2)$ measurements.

Implementing this pipeline to visualize height across different genotypes, planting densities and planting date treatments showed a strong ability to monitor biological variation for height across development in response to the environment. Differences in rate of growth between genotypes and planting dates as well as in lodging responses

between planting densities were documented. Moreover, we saw that growth rates generated by PH measurements collected at multiple timepoints early in development can be useful in improving predictions of PH at the end of the season. Together, these findings show the utility of using UAVs for collecting PH data at high temporal resolution to track differences in growth and to predict an end-season trait early in development.

## CODE AVAILABILITY

The scripts and processes used to perform the image analyses and trait extraction are available at https://github.com/SBTirado/UAV_PH.git.

CHAPTER III

## Context Statement

SYNOPSIS

Both stalk and root lodging can cause significant yield losses in maize; however, maize plants are often able to recover from root lodging. There is potential among breeding programs for developing lines that are more tolerant and can more rapidly recover from root lodging. We assessed the incidence of root lodging utilizing end-of-season lodging scores collected among the Genomes 2 Fields (G2F) initiative trials and found a large yet variable incidence of lodging across states, years, and genotypes. Lodging in this dataset was scored manually at the end of the season, and little is known about the drivers of lodging and lodging recovery. We therefore developed an approach for utilizing temporal plant height measurements collected from unmanned aerial vehicles to capture in-season lodging and recovery in a yield trial consisting of 24 maize hybrids planted in replicate under two dates and three planting densities in St Paul, MN in the summers of 2018 and 2019. We found that growth rates during vegetative development as well as the developmental timing of plants when exposed to a storm are predictive of the amount of lodging maize plots will experience. We also found that utilizing temporal height measurements can help in not just estimating lodging and early vegetative growth rates, but that utilizing these estimates can also aid in assessing end of season yield.

## PUBLICATION

Chapter III entitled 'Utilizing Temporal Measurements from UAVs to Assess Root Lodging in Maize and its Impact on Productivity' has been submitted for publication and is currently under review. A preprint of this article has been released:

**Tirado, S. B.**, Hirsch, C. N., & Springer, N. M. (2020). Utilizing Temporal Measurements from UAVs to Assess Root Lodging in Maize and its Impact on Productivity. In *bioRxiv* (p. 2020.05.21.108746). https://doi.org/10.1101/2020.05.21.108746

## CONTRIBUTIONS

During the course of this work, multiple people have made contributions. Nathan Springer and Candice Hirsch helped conceive this experiment and analyze the data and also contributed to writing this paper. Amanda Gilbert and Pete Hermanson provided field technical support. Anna Deneen, Kjell Sandstrom, Shale Demuth, Danielle Sorensen and Jordan Freeman helped me collect and process the UAV data for this experiment. Sara Tirado provided all the protocols and developed the tools for collecting, processing and analyzing this data. Author contact information and acknowledgments have been removed and formatting has been adapted to be consistent throughout this thesis.

CHAPTER III.

# Utilizing Temporal Measurements from UAVs to Assess Root Lodging in Maize and its Impact on Productivity

## INTRODUCTION

Lodging has strong negative impacts on maize yield due to reductions in the photosynthetic capacity of plants, the inability to mechanically harvest lodged plants that did not recover, and the rotting of ears due to being in contact with the ground. Lodging also limits the application of ground-based vehicle navigation through fields by causing the blockage of rows. Lodging occurs primarily through two avenues, one taking place at the plant stalk and the other at the root. Annual yield losses attributable to stalk lodging are estimated to be 5-20%; however, losses for root lodging are not as well documented (Flint-Garcia et al., 2003; Zuber & Kang, 1978). The specific type as well as the severity of the lodging event that occurs can be dependent on many factors including the developmental stage of the crop when experiencing the storm, the severity and patterning of the wind, and a variety of morphological characteristics of the genotype being grown including the stalk strength, root depth and root branching (Ma et al., 2014; Robertson et al., 2014; Sanguineti et al., 1998).

Lodging events that occur at the stalk, referred to as snapping, are most prominent during maize plants' vegetative growth stages when internodes are growing thereby rapidly weakening the cell walls leading to stalk breakage if exposed to strong winds or at the grain-filling stage (Ching et al., 2010). Stalk lodging hinders plant development if

it occurs in vegetative stages and also ear development if it occurs in reproductive stages and plants are unable to recover. Root lodging, however, most often occurs in response to early-season storm events before maize plants have fully developed brace roots (Ennos et al., 1993). At this point, plants have more plasticity and have the ability to recover from the lodging event through a mechanism referred to as 'goose-necking' (Zhang et al., 2011). Even partial recovery to the upright orientation through goose-necking can help minimize yield losses (Dhugga, 2007). This leads to opportunities in breeding pertaining to both root lodging resistance as well as root lodging recovery.

Genotypic resistance to root lodging has been addressed by breeding improved hybrids over the last decades with consistently higher lodging tolerance (Duvick, 2005). However, a large portion of a plant's lodging reaction is dependent on environmental factors as well as interactions between the genotype and the environment making lodging resistance a complex trait to study. Root lodging in particular occurs very irregularly across environments as it is influenced by a multitude of factors such as soil quality and fertility, wind patterns and pest and disease pressures making it challenging to maintain consistent progress in selection (Flint-Garcia et al., 2003; Stamp & Kiel, 1992). To aid in studying root lodging responses, several traits have been utilized to indirectly measure lodging resistance including the horizontal pushing resistance, root pulling resistance, root volume by water replacement, root clump size and weight, and more recently root failure moment (Ennos et al., 1993; Fouéré et al., 1995; Kamara et al., 2003; J. Liu et al., 2011; S. Liu et al., 2012; Thompson, 1968). These however are destructive and labor-intensive measurements. A different approach that has been taken to evaluate lodging

resistance has been to control wind conditions by using a mobile wind machine (Barreiro et al., 2008; Wen et al., 2019). Most studies, however, rely on irregular weather events and subsequently measuring root lodging by visually inspecting and manually annotating the number of plants leaning more than 30 or 45 degrees from vertical. Because this is time-consuming, lodging measurements are typically scored at one timepoint at the end of the season prior to harvest rather than following extreme weather events. These measurements do not capture plants that lodged but were able to fully recover their upright orientation without producing a significant bend in the lower portion of the stalk. Although this is useful in determining genotypes that suffered a higher degree of lodging throughout the season, it gives little insight into how genotypes respond in terms of lodging throughout development and how the timing of the lodging event impacts plant recovery and end-season productivity.

The incidence and severity of lodging responses is exacerbated by the increased incidence of extreme weather events that accompany climate change, and developing tools and knowledge around the drivers of lodging and recovery will allow us to mitigate risk and breed superior germplasm. Assessing the degree of in-season lodging and the rates of recovery require temporal data collection and unmanned aerial vehicles (UAVs) offer a potentially fast and cost-effective way of evaluating fields remotely in an automated fashion. The goals of this study were therefore to develop an approach for measuring lodging responses in a fast and effective manner utilizing UAVs, to use this pipeline to evaluate management and developmental factors that contribute to the severity of lodging responses observed for a set of hybrid lines grown under six different

environment-by-management conditions in MN, and to test the impacts of lodging severity as well as response and rate of recovery on yield at the end of the season.

# RESULTS

## *Root Lodging Incidence Across the US*

The Genomes to Fields (G2F) initiative has generated a publicly available large-scale, multi-year, and multi-state dataset of maize phenotypes. Using this dataset we sought to evaluate the frequency of lodging for varying environments and genotypes ((McFarland et al., 2020)). Environmental and phenotypic data for approximately 74,000 field plots involving more than 2,500 maize hybrid varieties evaluated across twenty states in North America between 2014-2018 has been released (McFarland et al., 2020). Among other traits, the incidence of root lodging, measured as the number of plants per plot where the stalk was 45 degrees or more from vertical as maturity, as well as plot grain yield extrapolated to bushels per acre was collected as part of this experiment. Twenty total states collected phenotypic data throughout the five years; however, there were multiple field sites that did not collect the necessary data for assessing lodging and only 11 out of the 20 states had lodging and stand count data for all five years.

Of the 73,686 G2F plots grown from 2014 to 2018 with lodging data, 10.9% of these suffered from root lodging (based on >5% of all plants within the plot being scored

as lodged) revealing a large incidence of lodging across the US in recent years, with extremely variable quantities across years (Figure 3.1A). An analysis of variance (ANOVA) showed a significant genotypic and environmental contribution to the percentage of plants in a plot that experienced root lodging (Table 3.1). To better assess the variability of lodging responses, we classified plots that lodged into two categories (partial and extreme lodging) based on the percentage of plants per plot that lodged (Figure 3.2, see methods). There is substantial variation in the percentage of plots that experienced root lodging both across states in individual years and across years in individual states (Figure 3.1B). Field sites in some locations, such as Ohio and Texas, experienced very small degrees of root lodging across all years. In contrast, field sites in other states, such as Iowa, experienced large degrees of root lodging throughout all years. There were six states that experienced root lodging in at least one plot across all five years. Other sites, such as Nebraska and Illinois, were very variable and experienced a high degree of lodging some years but no lodging in other years. This variation in lodging responses is likely due to a combination of differences in climatic conditions across states and years as well as in differences in the management practices implemented in different locations, such as the planting date and density.

**Table 3.1**. ANOVA results for the percentage of plants within a plot with root lodging for all plots in the Genomes 2 Fields dataset from 2014 to 2018 without missing data for plants that experienced root lodging, stand counts and yield measurements.

| | Degrees of Freedom | Sum of Squares | Pr(>F) | Significance |
|---|---|---|---|---|
| Genotype | 2444 | 51.5 | <2e-16 | *** |
| State | 17 | 31.1 | <2e-16 | *** |
| Year | 3 | 6.3 | <2e-16 | *** |
| Replicate | 1 | 0 | 0.387 | N.S. |
| State:Year | 28 | 78.5 | <2e-16 | *** |
| Residuals | 34417 | 452.8 | 1.01E-05 | |

'.' significant at 0.1, ' * ' significant at p=0.05; ' ** ' significant at p=0.01; ' *** ' significant at p=0.001; ' N.S. ', not significant.

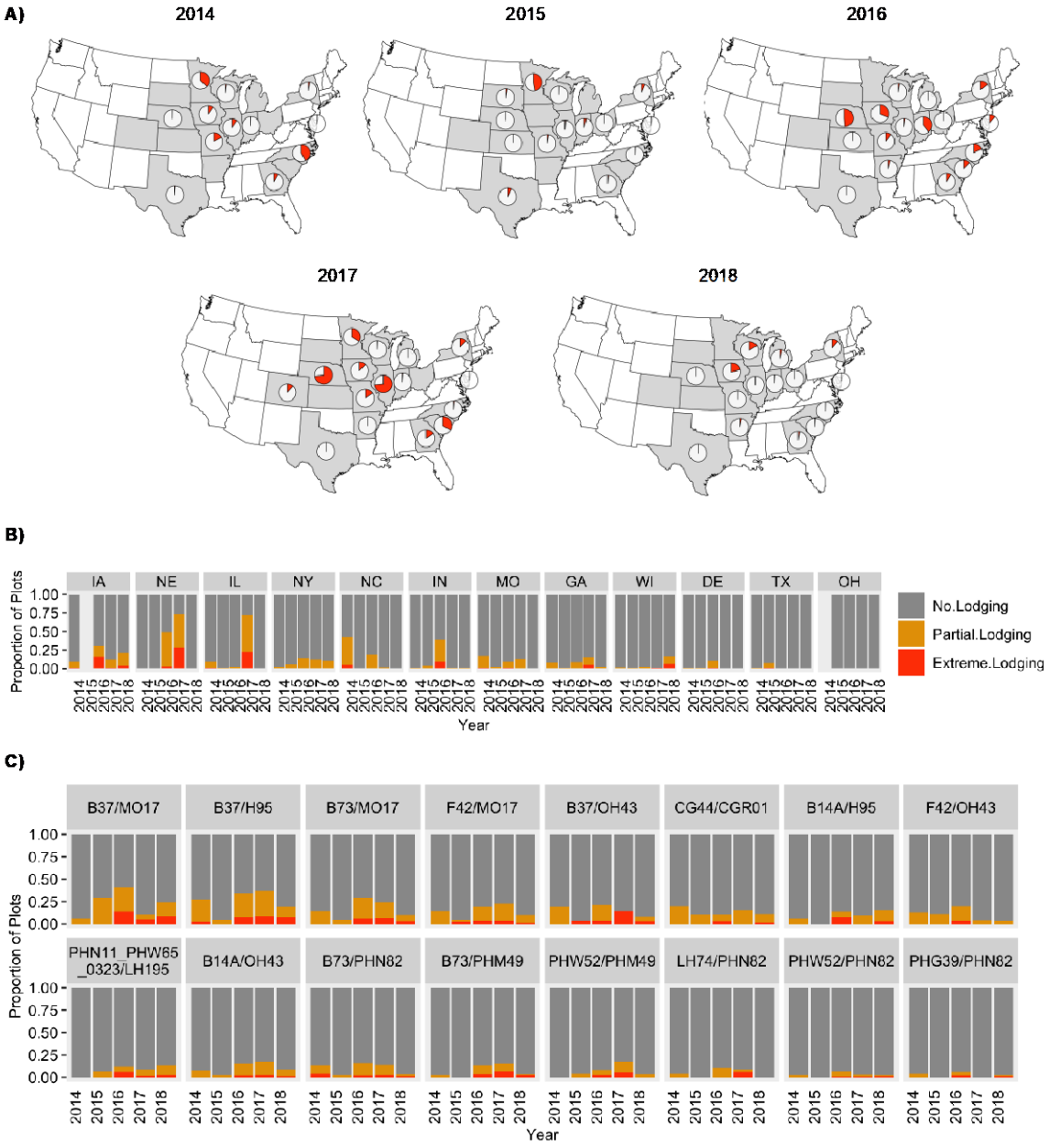


**Figure 3.1.** Lodging severity across the US.

*A) Percent of plots in G2F locations across years with lodging data where more than 5% of plots lodged. B) Percent of plots per state across all years where less than 5% of plants lodged (grey), between 5 and 50% of plants lodged (yellow) and more than 50% of plants lodged (red). C) Percent of plots across all locations and years for the 16 genotypes with lodging data in at least 6 locations all five years where less than 5% of plants lodged (grey), between 5 and 50% of plants lodged (yellow) and more than 50% of plants lodged (red).*

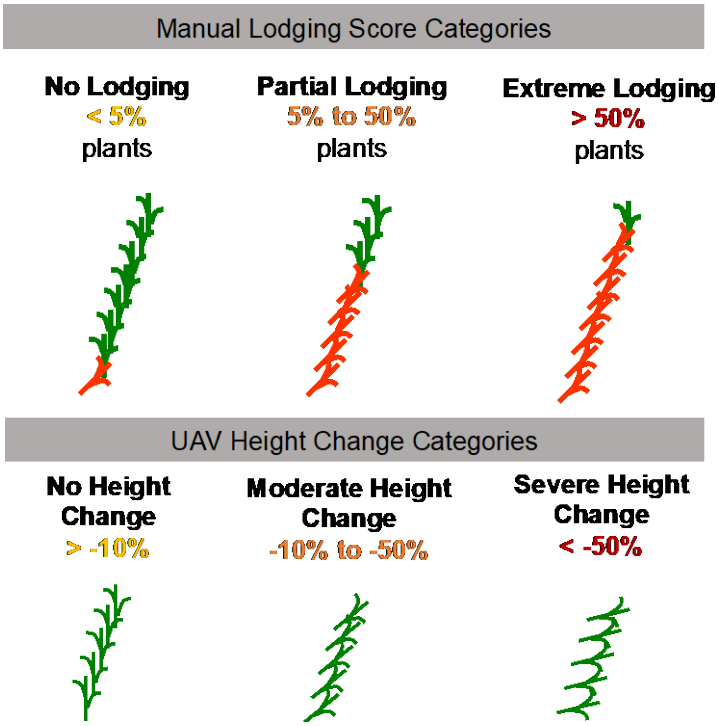


**Figure 3.2**. Categorical scoring system for determining plots that suffered from different lodging severities based on hand measured lodging scores (top) and UAV-derived lodging height change measurements (bottom).

Past studies have found variation in lodging resistance based on genotypic background (Landi et al., 2007; Nelimor et al., 2020). The G2F dataset also provides an opportunity to assess genetic variation for lodging. There was large variability in the amount of genotypes that lodged in at least one environment across the five years ranging from 337 out of 1206 genotypes in 2015 to 714 out of 1161 genotypes in 2018. We focused our analysis on a small subset of genotypes that were planted at many (>6) locations with lodging data available each season (Figure 3.1C). Half of the genotypes experienced lodging in at least one location all five years; however, both the total percentage of plots and the severity of the lodging responses observed varied by genotype

(Figure 3.1C). A subset of the genotypes, such as B37xMo17 or B37xH95, exhibit consistently higher levels of lodging across each year. Other genotypes, such as PHG39xPHN82 or PHW52xPHN82, consistently exhibit very low levels of lodging. The end of season lodging observations within the G2F dataset highlights the prevalence of lodging. However, from this data there is a lack of information about the specific events that trigger lodging or data on the ability of genotypes to recover from these events.

### *Measuring Lodging Responses Using UAVs*

To further our understanding of the factors that contribute to variability in lodging from different events we utilized data from two growing seasons in which naturally occurring weather events provided an opportunity to study variability in lodging as well as the rate and extent of recovery. These experiments consisted of a set of 12 hybrid genotypes grown in replicate 4-row plots with two planting dates (mid May and late May), three planting densities (60k/ha, 90k/ha and 120k/ha) and two years (2018 and 2019) in St Paul, MN. The 2018 dataset consisted of 13 timepoints of UAV data collection, whereas the 2019 dataset consisted of 23 timepoints. In both years, a storm event with strong winds occurred during the vegetative phase of development (July 1st in 2018 and July 15th in 2019) and caused extensive root lodging. Planting densities and sowing dates have been shown to influence end-season root lodging scores across maize genotypes (Li et al., 2015; Sher et al., 2017). The design of these experiments with multiple planting dates and densities enable us to study the impact of developmental

stage, planting density, and genotypic variation on the extent of initial lodging, post-lodging recovery, and impacts on end of season traits including height and yield.

The ability to track lodging and lodging recovery responses requires measurements taken at high temporal resolutions, which is often not feasible with manual observation. UAVs on the other hand provide an efficient means to monitor plant responses to extreme wind events since they can collect data in a fast and efficient manner at high temporal resolutions (Y. Shi et al., 2016). UAV plant height (PH-UAV) measurements were collected at many timepoints throughout development for both of these experiments including the day prior to the wind event and the day following the wind event (Figure 3.3). The UAV-derived digital elevation models (DEMs) of plots on the date prior to the lodging event and the DEMs of the day after were compared and a reduction in height across certain plots in the field was observed (Figure 3.4A-B). This prompted us to develop a method to use PH-UAV measurements to quantify lodging. To develop a lodging severity score from the PH-UAV measurements, the percent change in average plot height extracted from the DEM from the closest timepoint before the storm to the closest timepoint after the storm was calculated (see methods). The severity of the lodging response (no lodging, moderate lodging, or severe lodging) was then determined for each plot based on this percent change in height (Figure 3.2; Figure 3.4B; see methods). The ability to apply this method to determine lodging is influenced by the timepoints of data collected before and after the lodging event. Due to the lower temporal resolution of UAV data collection in the 2018 season, the timepoint closest to the lodging event was 3 days prior, whereas data was collected the day before the lodging event in

the 2019 season (Figure 3.3). For both years, flights were conducted the day following the lodging event. Because this approach involves calculating lodging based on the percent change in plot height before to after the storm event, we highlight the importance of having high temporal resolution in UAV measurements to be able to capture plot height at a date close before a storm occurs.

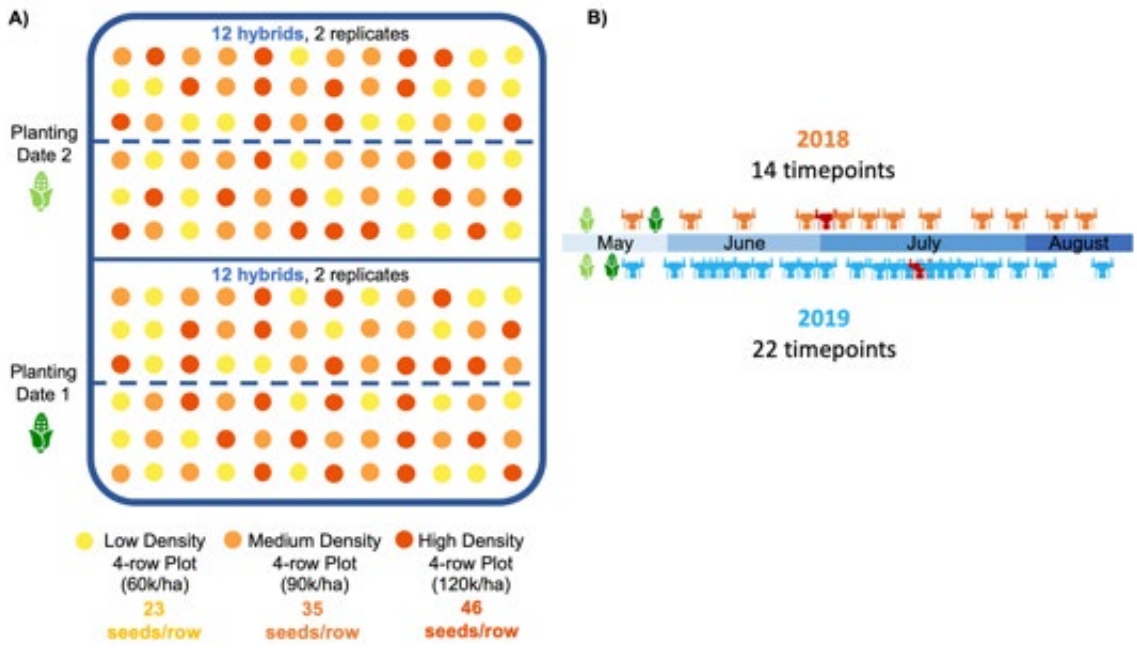


**Figure 3.3.** A) Field experimental layout for 2018 and 2019 biological material. B) Resolution of UAV imagery collection for the 2018 (orange) and 2019 (blue) seasons with the timepoints following the lodging event of each year represented in red.

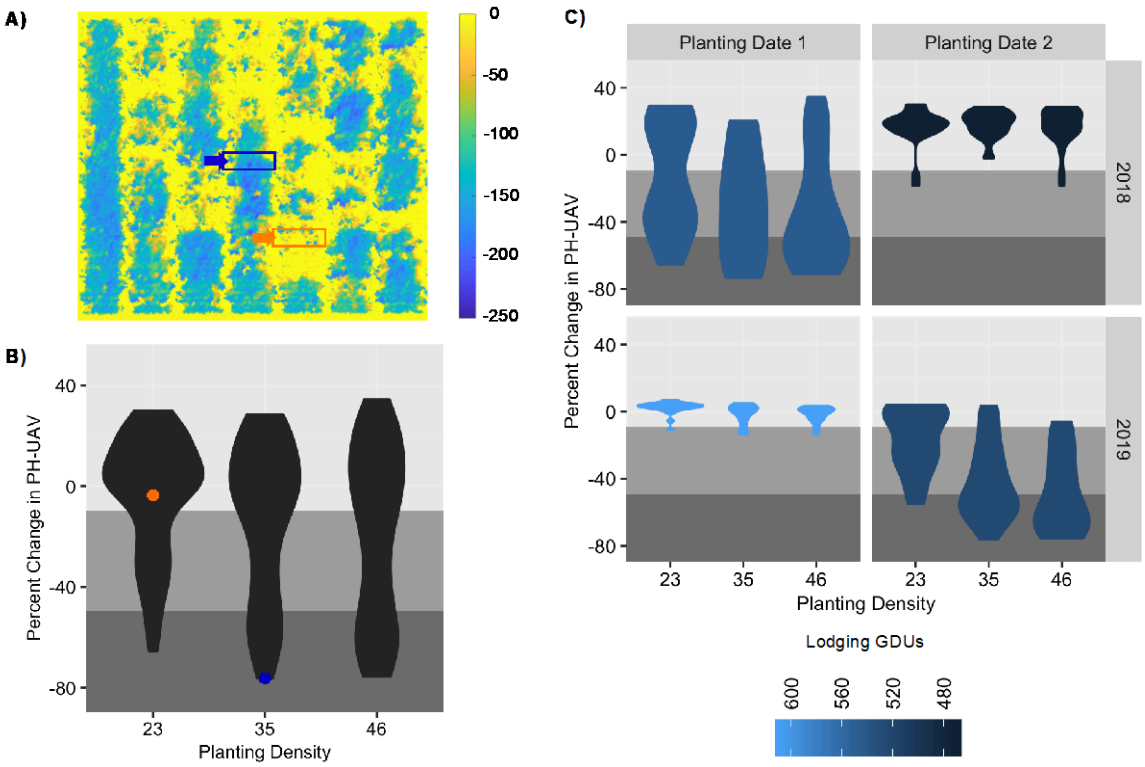


**Figure 3.4.** Utilizing the change in UAV-derived plant height to track plot lodging

*A) Height difference (in cm) for the 2019 late planting date treatment at 7/16/2019 compared to 7/15/2019 following the wind storm that occurred the night of 7/15/2019. Boxes represent plots with low (orange) and high (blue) degrees of lodging. B) Density plot of lodging percent height change for all plots across all treatments in the 2018 and 2019 seasons. The background shading represents the areas where plots where depicted as having no height change (light grey), moderate height change (medium grey), and severe height change (dark grey). Points represent plots marked in panel A with low (orange) and high (blue) degrees of lodging. C) Density plot of lodging percent height change for all plots across individual planting date treatments and years. The color represents the growing degree units (GDUs) of the specific treatment-year combination at the time of the storm event.*

### *Variation in Lodging Responses*

Substantial variability in lodging responses was observed across plots (Figure 3.4A-B). Within environments, there were also major differences in the amount of lodging observed for the two planting dates in each season as well as more subtle

differences based on planting density (Figure 3.4C). The differences in lodging between the two planting dates suggest that plots that were either early in vegetative development or nearing the reproductive stage of development did not experience large amounts of lodging. The early planting had more substantial lodging in 2018 and the later planting had more substantial lodging in 2019; however, these plantings were at similar growing degree units (GDUs) when the lodging event happened (Figure 3.4C). This suggests that maize hybrids are most susceptible to root lodging within a narrow developmental timeframe, and were less impacted in this case when younger than 469 GDUs or older than 590 GDUs.

The developmental timepoint and growing conditions at the time of the storm impacted not just the amount of lodging experienced by certain plots, but also their rates of recovery from the lodging event. For example, LH82 x LH145 grown at high density had a much slower recovery rate when grown in 2018 in the first plating date treatment compared to when grown in 2019 in the second planting date treatment, even though both experienced similar amounts of lodging (Figure 3.5). It took six days for the 2018 plot to get back to the original height it was before the storm event, compared to only 3 days in 2019. The slower recovery rate in the lodged early planting 2018 plot impacted its terminal height achieved and it ended up having a much shorter terminal PH compared to the lodging event that occurred later in development in the 2019 plot (Figure 3.5). The difference between the terminal PH of the lodged plot compared to the non or semi-lodged counterpart grown in the opposite planting date for each year was a lot larger in 2018 compared to 2019 (Figure 3.5). It is also worth noting that the 2019 plot grown in

the first planting date treatment suffered a small amount of lodging and it was able to recover its original height in just one day. This slight lodging and rapid recovery is something we would have missed in 2018 due to having lower temporal resolution of UAV flights.

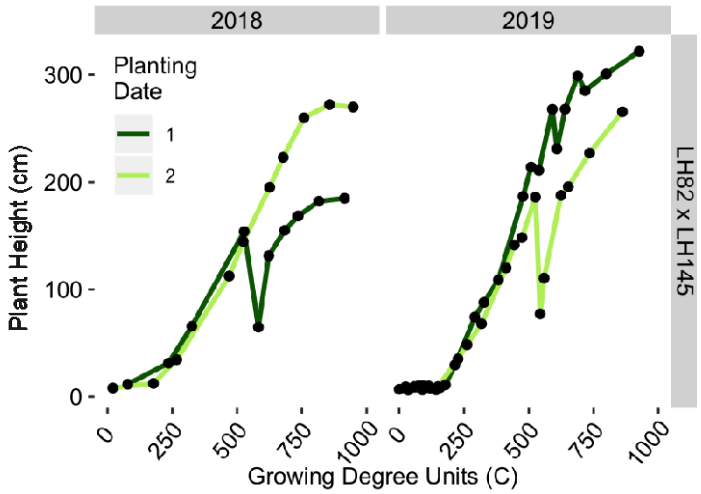


**Figure 3.5.** Utilizing UAVs to track growth and lodging responses through time

*Growth through time for genotype LH82 x LH145 planted at high density across both planting date treatments in the 2018 and 2019 seasons. Points indicate UAV height collection events for each season.*

Our analyses suggest substantial variation in lodging that can be attributed to a variety of factors. The different genotypes, planting dates and densities all appeared to influence the lodging responses observed (Figure 3.6A). An ANOVA was performed to assess the contributions of different factors to explain the change in height observed by UAV measurements (Table 3.2). Multiple factors including the genotype, the planting density, and the plot height prior to the lodging event significantly contributed to the variation in lodging responses observed across both years in the planting date that

suffered high degrees of lodging (Table 3.2). The higher temporal resolution in 2019 allowed us to calculate the slope, or growth rate, across early and mid-season timepoints preceding the lodging event (Figure 3.6B; see methods). These factors were included in the 2019 ANOVA and reveal that mid-season growth rates also significantly contributed to the amount of variation observed for lodging severity (Table 3.2). Our findings suggest that growth rates together with the developmental time point a plot is in at the time of a storm event will largely dictate the severity of the initial lodging event.

**Table 3.2.** ANOVA results for lodging percent height change and yield for plots in the 2018 first planting date treatment and in the 2019 second planting date treatment.

| 2018 P1 | Lodging Height Change | | | | Yield | | | |
|---|---|---|---|---|---|---|---|---|
| Variable | Df | Sum Sq | Pr(>F) | Signif | Df | Sum Sq | Pr(>F) | Signif |
| Genotype | 11 | 19983 | 0.0049 | ** | 11 | 0.12861 | 0.012887 | * |
| Density | 1 | 4199 | 0.0120 | * | 1 | 0.05869 | 7.94E-04 | *** |
| Replicate | 1 | 1552 | 0.1184 | N.S. | 1 | 0.0038 | 3.55E-01 | N.S. |
| EarlyG | NA | NA | NA | | NA | NA | NA | |
| MidG | NA | NA | NA | | NA | NA | NA | |
| PreLodgingPH | 1 | 15147 | 1.01E-05 | *** | 1 | 0.00061 | 0.70994 | N.S. |
| Lodging | NA | NA | NA | | 1 | 0.00631 | 0.235375 | N.S. |
| Recov3 | NA | NA | NA | | 1 | 0.00145 | 0.566106 | N.S. |
| Recov6 | NA | NA | NA | | 1 | 0.00061 | 0.710188 | N.S. |
| TerminalPH | NA | NA | NA | | 1 | 0.0034 | 0.381359 | N.S. |
| Genotype:Density | 11 | 7570 | 0.3662 | N.S. | 11 | 0.09571 | 0.058598 | . |
| Residuals | 45 | 27563 | | | 34 | 0.14706 | | |
| **2019 P2** | **Lodging Height Change** | | | | **Yield** | | | |
| **Variable** | **Df** | **Sum Sq** | **Pr(>F)** | **Signif** | **Df** | **Sum Sq** | **Pr(>F)** | **Signif** |
| Genotype | 11 | 22871 | 5.10E-15 | *** | 11 | 0.029278 | 5.02E-03 | ** |
| Density | 1 | 12022 | 3.34E-15 | *** | 1 | 0.002051 | 0.1277 | N.S. |
| Replicate | 1 | 7 | 0.7686 | N.S. | 1 | 0.000845 | 0.32327 | N.S. |
| EarlyG | 1 | 1 | 0.9012 | N.S. | 1 | 0.000004 | 0.94378 | N.S. |
| MidG | 1 | 5512 | 3.86E-10 | *** | 1 | 0.004187 | 0.03246 | * |
| PreLodgingPH | 1 | 547 | 0.0147 | * | 1 | 0.000313 | 0.54572 | N.S. |
| Lodging | NA | NA | NA | | 1 | 0.001206 | 0.23943 | N.S. |
| Recov3 | NA | NA | NA | | 1 | 0.003828 | 4.03E-02 | N.S. |
| Recov6 | NA | NA | NA | | 1 | 0.000062 | 0.78738 | N.S. |
| TerminalPH | NA | NA | NA | | 1 | 0.01909 | 3.65E-05 | *** |
| Genotype:Density | 11 | 617 | 0.7660 | N.S. | 11 | 0.008398 | 0.54267 | N.S. |
| Residuals | 43 | 3646 | | | 33 | 0.027716 | | |

'.' significant at 0.1, ' * ' significant at p=0.05; ' ** ' significant at p=0.01; ' *** ' significant at p=0.001; ' N.S. ', not significant.

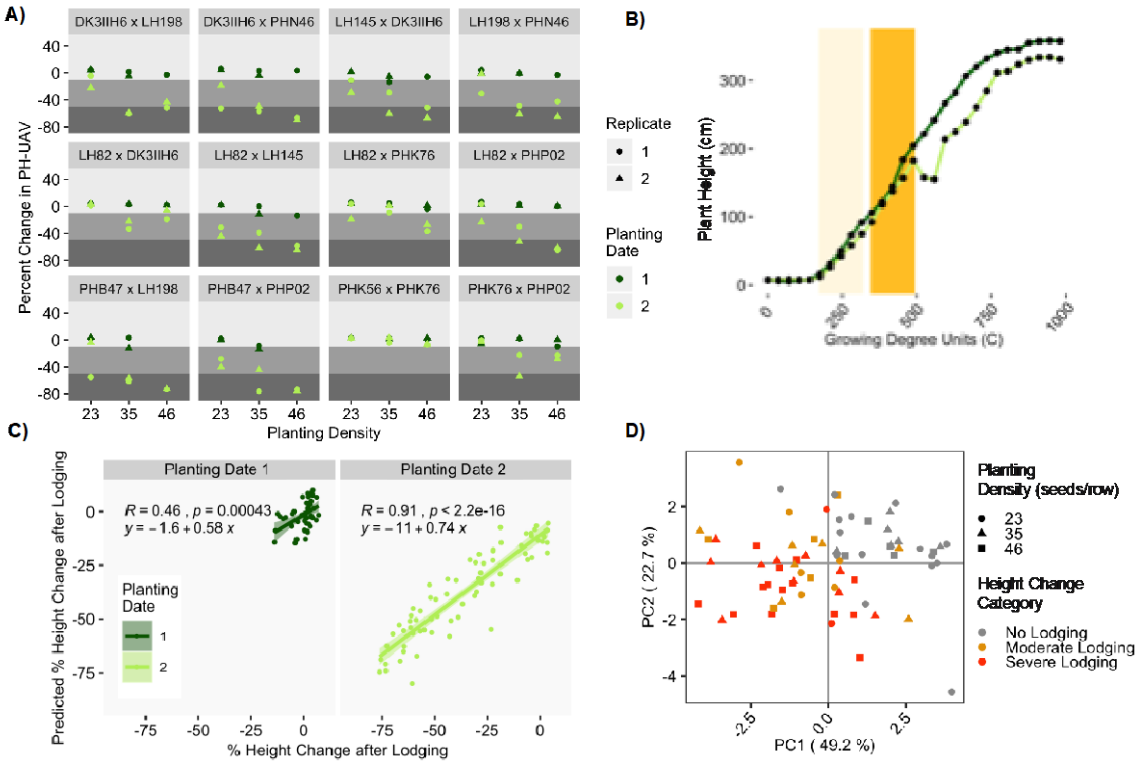


**Figure 3.6.** UAV lodging variation across genotypes and environments and its predictors

*A)Lodging percent height change for replicate plots of each genotype in the 2019 season. The background shading represents the areas where plots were depicted as having no lodging (light grey), moderate lodging (medium grey), and severe lodging (dark grey). B) Height through time for a single replicate of a single genotype (LH145 x DK3IIH6) planted at high density in the first and second planting date treatments. The background shading represents the time ranges selected to calculate the early (light yellow) and mid-season (dark yellow) growth rates. C) Lodging percent height change predictions. The prediction model contained planting density, PH prior to the lodging event, early-season growth rate, and mid-season growth rate as the predictor variables. D) PC1 and PC2 scores from the PCA of the slope between each timepoint within the early and mid-season growth periods shown in panel B of all predicted height values derived from the loess fitted model for all 2019 plots. Points are colored by lodging height change category and shaped by planting density.*

### *Predictors of Lodging Responses*

Genotypic resistance to root lodging has mostly been addressed through indirect selection of morphological traits found to be highly correlated with lodging resistance,

and this has driven efforts to identify QTL linked to these traits (Bruce et al., 2001; Landi et al., 2007; J. Shi et al., 2019). The ability to more efficiently assess in-season root lodging opens new possibilities for identifying new phenotypes linked to lodging resistance that can be selected for and improved. Moreover, identifying correlated phenotypes that can be more easily assessed utilizing UAVs can improve the resolution of genotypic selection efforts by allowing breeders to sample larger panels of genotypes across more locations (Araus & Cairns, 2014; Y. Shi et al., 2016). We sought to determine what factors contribute to the lodging responses observed and whether there are variables that could be strong predictors for lodging. Using the 2019 dataset due to its higher temporal resolution, we ran a stepwise model selection procedure on a linear regression model that incorporated multiple variables (see methods) to predict the lodging percent height change. The selected model contained the planting density, the PH prior to the lodging event, the early-season growth rate, and the mid-season growth rate as the predictor variables. This model, derived from half of the dataset, predicted the lodging height change on the other half of the dataset with very high accuracy (adj R-squared of 0.46 for the first planting date and 0.91 in the second planting date; Figure 3.6C). The lower accuracy in the first planting date was likely due to a small degree of PH change across most plots due to limited amounts of lodging. These results indicate the importance that rates of growth across early vegetative stages as well as height values achieved by plants at the time when they are exposed to storm events have in determining the degree of lodging.

Rates of plant growth can be driven by how genotypes respond to environmental conditions. In this case, the environment encompasses a mixture of management treatments including planting date and planting density together with temperature, precipitation and other climatic factors. Studies have shown that planting density affects plant growth by influencing the ratio of root to shoot growth, the rate and quantity of root biomass accumulation, and the rate of internode elongation thereby affecting both plant and ear height as well as lodging (Hébert et al., 2001; Jiang et al., 2013; Tetio-Kagho & Gardner, 1988; Xue et al., 2016). Because the key drivers we found to be strong indicators of lodging were related to PH and rate of change in PH prior to the lodging event, we hypothesized that these traits were influenced by the response of each genotype to the density treatments they were exposed to. To test this, a loess model was fit across timepoints for each plot in the 2019 season and the plot height across consistent timepoints throughout development for each planting date was extracted with a temporal resolution of 35 GDUs. The slope between each timepoint within the early and mid-season growth rate periods was calculated and used as input into a principal component analysis. The results show that the first two principal components (PC1 and PC2) were able to separate non-lodged from lodged plots as well as planting density with higher planting densities aligning along the axis of higher lodging severities (Figure 3.6D). Slopes across the latest timepoints within the mid-season growing period just prior to the storm event had the largest loadings for PC2 and the slope for timepoints within the transitioning phase between early and mid-season growth had the largest loadings for PC1. Plots also clustered by genotype suggesting that the genotype by density component

had an impact in lodging severity as well by modulating the PH response and rate of growth of individual plots (Figure 3.7).

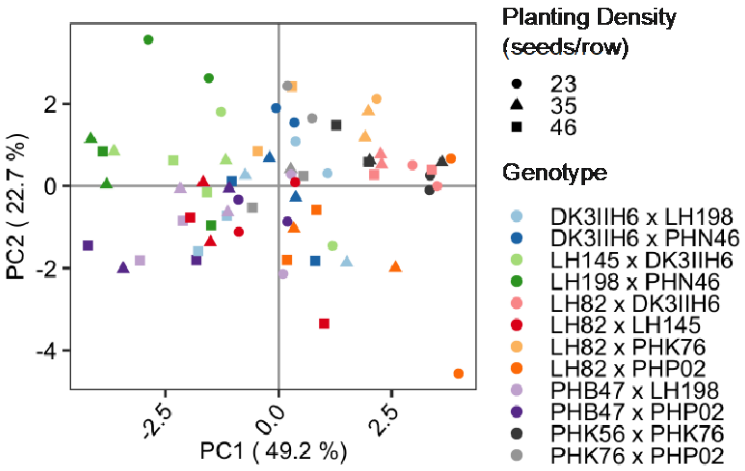


**Figure 3.7.** PC1 and PC2 scores from PCA of all predicted height values derived from the loess fitted model from the slope between each timepoint within the early and mid-season growth periods colored by genotype.

### *Lodging Impact on End-season Productivity*

Seasonal yield predictions have become very important across agricultural stakeholders such as farmers, commodity traders and government officials for making strategic decisions with regards to management and planning. Yield predictions have been done through many methods including surveys, statistical models and process-based models and studies have been executed to more efficiently predict yield across many crops utilizing a multitude of information sources including climatic data, physiological and phenological data as well as remote sensing data (Basso & Liu, 2019). Most studies that have utilized remote sensing data, however, have relied on single-timepoint remote-sensing measurements and haven't investigated the use of temporal measurements in

yield predictions. We therefore wanted to investigate the contribution of different factors obtained through temporal measurements including early-season lodging and factors that contributed to lodging, such as early-season and mid-season growth rates, in predicting final yield. Root lodging has already been shown to contribute to grain yield in maize lines exposed to heat and drought stress treatments and to be useful in identifying lines resistant to abiotic stresses (Nelimor et al., 2020). Scoring in-season lodging and lodging recovery throughout the season therefore shows potential to improve yield predictions and germplasm selection.

We first looked at the G2F plots with end of season lodging information. A strong, significant impact of root lodging and the degree of lodging severity scored by hand at the end of the season on yield was observed (Figure 3.8A). Lodging led to a 12.3 bu/acre yield loss when comparing plots that experienced extreme lodging to those that experienced no lodging. Similarly, lodging percent height change extracted in-season led to significant yield declines in our experimental plots (Figure 3.8B). This yield decline was most prominent in high-density planting treatments compared to lower density treatments (Figure 3.8C).

To better assess which factors were most predictive for yield and to determine the relative impact of lodging on end-season productivity, we again ran a stepwise model selection procedure on a linear regression model that incorporated multiple variables to predict end-season yield for the 2019 dataset (see methods). The variables selected and used to create the yield prediction model were the genotype, the early-season growth rate, the lodging height change, and the terminal PH. This model was able to explain between

55% and 72% of the variation observed for yield across the different lodging severity groups (Figure 3.8D). This indicates the utility of temporal measurements in yield predictions and the potential of incorporating remote-sensing temporal data together with weather and agronomic data for yield prediction model generation. This would, however, require enough temporal resolution to capture unexpected responses such as lodging and storm recovery events.

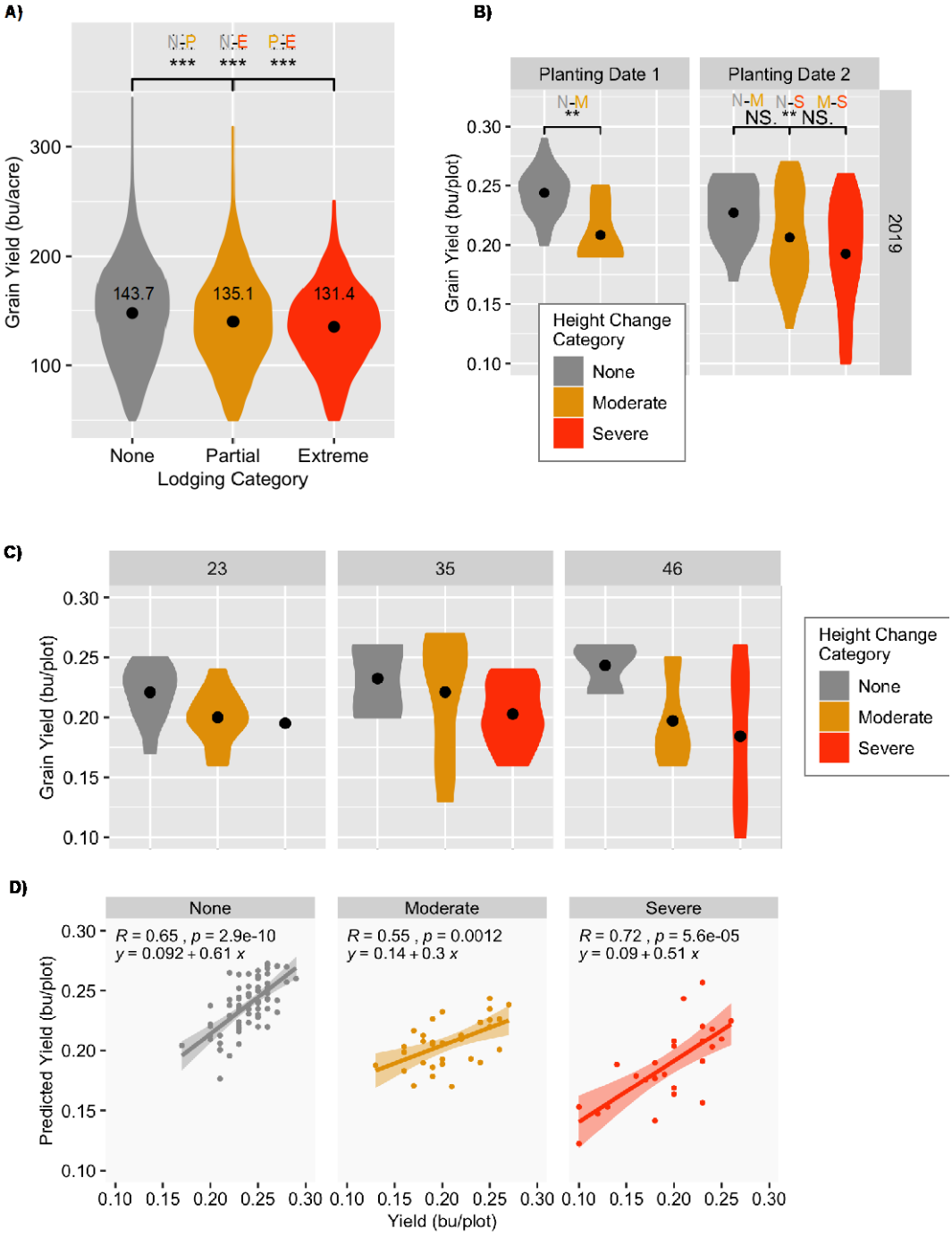


**Figure 3.8.** Impacts of root lodging on yield

***A)*** *Density plot of grain yield (in bushels/acre) for all the Genomes 2 Fields Initiative hybrid plots with lodging data grown across all states and years grouped by lodging score category (none, partial and extreme). Significance values based on t-test comparing different groups are*

*plotted (* significant at p=0.05; ** significant at p=0.01; *** significant at p=0.001; N.S., not significant).* ***B)*** *Density plot of grain yield (in bushels/plot) for all the 2019 experimental plots grouped by height change category (none, moderate and severe) and by planting date. Significance values based on t-test comparing different the groups are plotted (* significant at p=0.05; ** significant at p=0.01; *** significant at p=0.001; NS., not significant).* ***C)*** *Density plot of grain yield (in bushels/plot) for all the 2019 experimental plots in the second planting date treatment grouped by height change category (none, moderate and severe) and by planting density (23, 35, and 46 seeds/row).* ***D)*** *Grain yield predictions split by height change category on 1/2th of all 2019 plots using a model generated with the other 1/2th of the dataset compared to the measured yield values. The model contained genotype, early-season growth rate, lodging height change, and terminal PH as the predictor variables.*

## DISCUSSION

Assessing the degree of in-season root lodging and the rate of recovery is important for better understanding root lodging resistance and for finding suitable lines for environments that are prone to lodging. Evaluating root lodging data collected for thousands of genotypes grown throughout many US locations across multiple years as part of the Genome 2 Fields initiative showed that there are a large number of plots that have lodged across the US in recent years. However, the number and severity are extremely variable across years and states. There is also substantial genetic variation for lodging among the genotypes included in this dataset. For this dataset lodging was only evaluated at the end of the season and therefore does not capture the variable ability of genotypes to recover from mid-season lodging events.

To better track lodging responses, we utilized UAV-derived plant height data collected temporally to assess how different genotypes planted at two timepoints (an early and a late planting) and grown under various planting densities (low, medium and high density treatments) across two years respond to storm events. To measure lodging

and lodging recovery, we developed a metric based on the percent change in height for each plot in response to the storm. Although our metric would capture both root and stalk lodging responses, our plots primarily suffered from root lodging since the storm events occurred across both years during vegetative development when plants are most susceptible to root lodging. If distinguishing between root and stalk lodging was needed, recovery rates could be used to partition both since plants are able to recover to some extent from root lodging but not stalk lodging.

Root lodging responses within our experiment showed that early vegetative growth rates as well as the precise developmental phase of maize plants when exposed to a storm event will determine their response in terms of lodging severity and their rate of recovery. Our maize hybrids were most susceptible to root lodging within a narrow developmental timeframe and plots that were either 469 GDUs or younger or 590 GDUs or older were less impacted and did not experience high degrees of lodging. There was also a genotype by density component modulating early vegetative growth rates which in turn were predictive of lodging responses.

Lodging had a significant, negative yield impact on both the G2F hybrids as well as our experimental plots. Root lodging can cause yield to decrease by reducing the photosynthetic capacity of plants, limiting ear collection from a combine, as well as causing grain mold on ears that were in contact with wet soil. The genotype together with early season growth rates, lodging responses, and terminal height explained a large portion of the variation observed for plot yield. This shows the ability to use temporal measurements derived from UAVs to capture plant responses to weather events to aid in

finding lodging resistant lines and determining field productivity in terms of yield. We also note that the lodging events that were tracked in the experimental sites in Saint Paul as well as many of the G2F sites would preclude the ability to use ground-based phenotyping platforms. In many of these field sites the degree of lodging, at least for some of the plots, was sufficient to block the ability of a ground-based vehicle to move through rows. While UAVs are limited in their ability to monitor traits below the canopy they do provide the ability to survey fields that are no longer navigable by ground.

## METHODS

### *Lodging Score Estimation for the G2F Dataset*

Genome 2 Fields data from 2014 to 2018 was downloaded from https://datacommons.cyverse.org/browse/iplant/home/shared/commons_repo/curated/GenomesToFields_2014_2017_v1 (McFarland et al., 2020). The percentage of plants per plot within the Genome 2 Fields dataset that suffered from lodging was calculated by dividing the number of plants per plot recorded as experiencing root lodging at the end of the season by the total stand counts. These percentages were then assigned a categorical score based on their value (no height change if <5%, moderate height change if between 5% and 50%, and severe height change if >50%; Figure 3.2).

Variation in percent of plants per plot that experienced root lodging was partitioned into genotype, state, year, replicate, and residual. All factors were treated as fixed effects with the linear model $y_{ijkl} = u + g_i + e_j + y_k + r_k + p_{ijk} + (ge)_{i*j} + e_{ijkl}$

where yijk is the phenotype value of the ith genotype in the jth state in the kth year of the lth replication; u is the phenotypic mean across states and years; gi is the ith genotype effect; ej is the jth state effect; yk is the kth year effect; rl is the lth replication effect; (ey)j*k is the interaction effect of the jth state by the kth year; and eijkl is the residual effect. To test the significance of the various effect variables of the linear model on lodging height change, we used the anova function of the R stats package (Team & Others, 2013).

***Experimental Field Design***

Two replicates of 12 maize hybrids were planted in 4-row plots at two dates (early and late planting) and three densities (60k, 90k and 120k plants per hectare) following a Randomized Complete Block Design blocked by planting date and replicate nested within planting date in Saint Paul, MN in the summers of 2018 and 2019 (Figure 3.3A). The hybrids utilized were DK3IIH6 x LH198, DK3IIH6 x PHN46, LH145 x DK3IIH6, LH198 x PHN46, LH82 x LH145, LH82 x PHK76, LH82 x PHP02, PHB47 x LH198, PHB47 x PHP02, LH82 x DK3IIH6, PHK56 x PHK76, and PHK76 x PHP02. Each row was 15ft long center-to-center with 12 ft of plots and 3ft of alleys and 30in spacing between rows. There were a total of 144 four-row plots planted each year. The 12 hybrid genotypes utilized were generated by crossing exPVP lines selected due to their past use in production settings and the availability of seed. This experiment was grown on two acres. Nine 1ft x 1ft ground targets in the form of PCV crosses were distributed around the border and internal alleys of the field for use as ground control points (GCPs) based

on previously developed optimization algorithms (Gómez-Candón et al., 2014); Figure 3.9).

**Figure 3.9**. Ground control point placement throughout field border and internal alleys

***UAV Data Collection and Processing***

UAV data was collected approximately weekly from plant germination to plant physiological maturity. A total of 13 timepoints were collected in 2018 and 23 timepoints in 2019, with 2019 having a much higher temporal resolution during the vegetative growth stages in plant development (Figure 3.3B). UAV data was processed following the procedure established by (Tirado et al., 2020b; Chapter 2) to extract DEMs and average plot plant height values for each date of data collection. The scripts and processes utilized to perform the image analyses and trait extraction are available at https://github.com/SBTirado/UAV_PH.git.

***UAV Lodging Percent Height Change Estimation***

Lodging percent height change ($L_nHC$) for each plot each year was measured utilizing the equation

$$L_nHC = \frac{PH_0 - PH_{-n}}{PH_{-n}}$$

where $PH_0$ is the mean plot plant height extracted from a given plot the day following the storm event and $PH_{-n}$ is the mean plot plant height extracted from a given plot at the closest timepoint (*n* days) of UAV data collection prior to the storm event. The values of n corresponded to three and one day prior to the storm for 2018 and 2019 respectively. The lodging percent height change categories of each plot were then determined based on the $L_nHC$ values (no height change if $L_nHC$ >-10%, moderate height change if -10% < $L_nHC$ > -50%, and severe height change if $L_nHC$ < -50%; Figure 3.2)

***UAV Lodging Recovery Percent Height Change Estimation***

Lodging recovery percent height change ($R_nHC$) for each plot each year was measured utilizing the equation

$$R_nHC = \frac{PH_0 - PH_{+n}}{PH_{+n}}$$

where PH0 is the mean plot plant height extracted from a given plot the day following the storm event and PH+n is the mean plot plant height extracted from a given plot at the closest timepoint (n days) of the lodging data collection event. The values of n corresponded to three and six for the 2018 season and to one, three, four and six in the 2019 season.

### *Weather Data and Growing Degree Days Calculation*

Temperature data from an in-field weather station was gathered. Because the weather station each year was installed a few days after planting, daily min and max temperature data from the University of Minnesota St Paul weather station (Station ID 218450) was extracted for these first days after planting (Minnesota Department of Natural Resources, 2020). Growing Degree Units (GDUs) in were then calculated for each date utilizing the equation

$$GDU(°C) = \frac{T_{max} + T_{min}}{2} - 10$$

where GDU is the growing degree units accumulated for a single day and Tmax and Tmin are the maximum and minimum recorded air temperature values in degrees Celsius for the given date. Temperature values above 30℃ were adjusted to 30℃ and likewise values below 10℃ were adjusted to 10℃ since corn growth rates do not increase or decrease outside the range of these values. A factor of 10℃ was used as the base temperature and subtracted to the temperature difference to calculate the final daily GDUs. The cumulative sum of GDUs for data collection dates was then extracted as the sum of GDUs for all dates between the planting date and the given date.

### *Early-season and Mid-season Growth Rate Extractions*

A loess regression model with a span of 0.3 was fit to the average UAV-derived PH of all time points for each plot in the 2019 season as this model was able to accurately capture lodging responses but reduce noise as to create a growth curve. Height for 35

GDUs within the range of 0 to 1000 were then predicted using the fitted model to obtain height across even time intervals for plots across both planting date treatments. Correlation for height across timepoints prior to the lodging event revealed two groups of correlated timepoints and these were selected to calculate the early-season and mid-season growth rates by taking the change in height from the first to the last GDU within each time period and dividing it by the number of GDUs. The early-season growth rate period ranged from 175 to 315 GDUs and the mid-season growth rate period ranged from 350 to 490 GDUs.

### *Yield Data Collection*

In 2019, grain from the middle two rows of each plot was harvested with a Kinkaid 8XP plot combine equipped with a Harvest Master Single High Capacity GrainGage with Mirus harvest software and total grain weight, test weight, and the percent moisture were collected after all plants had reached physiological maturity. Grain yield per plot was then adjusted to 15.5% grain moisture.

### *Statistics*

Variation in plot lodging percent height change values was partitioned into genotype, density, replicate, pre-lodging PH, and genotype-by-density interaction, and residual. All factors were treated as fixed effects with the linear model $y_{ijk} = u + g_i + e_j + r_k + p_{ijk} + (ge)_{i*j} + e_{ijk}$ where $y_{ijk}$ is the phenotype value of the ith genotype in the jth planting density of the kth replication; u is the phenotypic mean across planting densities;

gi is the ith genotype effect; ej is the jth planting density effect; rk is the kth replication effect; pijk is the effect of PH prior to the lodging event of the ith genotype in the jth planting density of the kth replication; (ge)i*j is the interaction effect of the ith genotype by the jth planting density; and eijk is the residual effect. To test the significance of the various effect variables of the linear model on lodging height change, we used the anova function of the R stats package (Team & Others, 2013).

Variation in plot yield values was partitioned into genotype, density, replicate, early and mid-season growth rates, pre-lodging PH, lodging height change, recovery height change three and six days after the lodging event, terminal PH, genotype-by-density interaction, and residual. All factors were treated as fixed effects with the linear model $y_{ijk} = u + g_i + e_j + r_k + S^e_{ijk} + S^m_{ijk} + p^1_{ijk} + h^3_{ijk} + h^6_{ijk} + p^2_{ijk} + (ge)_{i*j} + e_{ijk}$ where $y_{ijk}$ is the phenotype value of the $i^{th}$ genotype in the $j^{th}$ planting density of the $k^{th}$ replication; u is the phenotypic mean across planting densities; $g_i$ is the $i^{th}$ genotype effect; $e_j$ is the $j^{th}$ planting density effect; $r_k$ is the $k^{th}$ replication effect; $S^e_{ijk}$ is the effect of the early-season growth rates of the $i^{th}$ genotype in the $j^{th}$ planting density of the $k^{th}$ replication; $S^m_{ijk}$ is the effect of the mid-season growth rates of the $i^{th}$ genotype in the $j^{th}$ planting density of the $k^{th}$ replication; $p^1_{ijk}$ is the effect of PH prior to the lodging event of the $i^{th}$ genotype in the $j^{th}$ planting density of the $k^{th}$ replication; $h^3_{ijk}$ is the effect of the recovery height change 3 days after the lodging event of the $i^{th}$ genotype in the $j^{th}$ planting density of the $k^{th}$ replication; $h^6_{ijk}$ is the effect of the recovery height change 6 days after the lodging event of the $i^{th}$ genotype in the $j^{th}$ planting density of the $k^{th}$ replication; $p^1_{ijk}$ is the effect of terminal of the $i^{th}$ genotype in the $j^{th}$ planting density of

the $k^{th}$ replication; $(ge)_{i*j}$ is the interaction effect of the $i^{th}$ genotype by the $j^{th}$ planting density; and $e_{ijk}$ is the residual effect. To test the significance of the various effect variables of the linear model on yield, we used the anova function of the R stats package (Team & Others, 2013).

### *Model Development for Predicting Lodging Severity*

A model was built for using various explanatory variables to predict lodging percent height change values for each plot. An optimal model was selected at each time point based on an original model containing the variables genotype, plating density, pre-lodging PH, lodging GDUs, early-season growth rate, and mid-season growth rate using a stepwise model selection procedure with a 10-fold cross validation step. This was implemented using the train function of the caret R package and selecting the model with the lowest RMSE (Kuhn et al., 2016). These predictor variables were chosen based on their biological foundation as well as their level of significance for predicting lodging percent height change values. The selected model contained the planting density, PH prior to the lodging event, early-season growth rate, and mid-season growth rate as the predictor variables.

### *Model Development for Predicting End-Season Yield*

A model was built for using various explanatory variables to predict yield values for each plot. An optimal model was selected at each time point based on an original model containing the variables genotype, plating density, pre-lodging PH, lodging GDUs,

early-season growth rate, mid-season growth rate, lodging percent height change, reovey height change three and six days after the lodging event, and terminal PH using a stepwise model selection procedure with a 10-fold cross validation step. This was implemented using the train function of the caret R package and selecting the model with the lowest RMSE (Kuhn et al., 2016). These predictor variables were chosen based on their biological foundation as well as their level of significance for predicting lodging percent height change values. The selected model contained the genotype, early-season growth rate, lodging percent height change, and terminal PH as the predictor variables.

## DATA AVAILABILITY

All data including the UAV-derived plot height values, DEMs and plot boundary files for each date of UAV data collection, cumulative GDUs calculated for each date of data collection, and yield data has been made available at the Digital Repository for University of Minnesota under the persistent identifier http://hdl.handle.net/11299/213218.

CHAPTER IV

# Context Statement

## SYNOPSIS

There is significant enthusiasm about the potential for hyperspectral imaging to document variation among plant species, genotypes or growing conditions. However, in many cases the application of hyperspectral imaging is performed in highly controlled situations that focus on a flat portion of a leaf or side-views of plants that would be difficult to obtain in field settings. We were interested in assessing the potential for applying hyperspectral imaging from a top-down view to document variation in genotypes and abiotic stresses. A top-down image of a maize seedling includes a view into the funnel-like whorl at the center of the plant with several leaves radiating outwards. There is substantial variability in the reflectance profile of different portions of this plant. To deal with the variability in reflectance profiles that arises from this morphology we implemented a method that divides the longest leaf into 10 segments from the center to the leaf tip. We show that there is large variability in the hyperspectral profiles across leaf segments which are masked when performing whole-plant averages as tend to be done when analyzing hyperspectral data. We found that using these segments provides improved ability to discriminate different genotypes and abiotic stress conditions (heat, cold or salinity stress) for maize seedlings. We also found substantial

differences in the ability to successfully classify abiotic stress conditions among different inbred genotypes of maize. This provides an approach that can be implemented to help classify genotype and environmental variation for maize seedlings from a top-down view such as that which would be collected in field settings.

## PUBLICATION

Chapter IV entitled 'Utilizing spatial variability from top-down hyperspectral imaging for monitoring genotype and growth conditions in maize plants' has been submitted for publishing and is currently under review. A preprint of this article has been released:

**Tirado, S. B.**, St Dennis, S., Enders, T. A., & Springer, N. M. (2020). Utilizing top-down hyperspectral imaging for monitoring genotype and growth conditions in maize. In *bioRxiv* (p. 2020.01.21.914069). https://doi.org/10.1101/2020.01.21.914069

## CONTRIBUTIONS

During the course of this experiment, other researchers have made contributions to data collection and analysis. The experiment was conceived by Tara A. Enders, Nathan M. Springer and Sara Tirado. Tara A. Enders and Susan St Dennis helped grow the plants and collect the hyperspectral dataset alongside Kjell Sandstrom, Shale Demuth and Danielle Sorensen. Tara A. Enders and Sara Tirado developed the data processing and analysis algorithms and conduct the analyses. Nathan M. Springer helped write this

paper and develop the figures. Author contact information and acknowledgments have been removed and formatting has been adapted to be consistent throughout this thesis.

CHAPTER IV.

# Utilizing spatial variability from top-down hyperspectral imaging for monitoring genotype and growth conditions in maize plants

## INTRODUCTION

Abiotic stresses cause major yield declines across many crops and can limit production by up to 70% (Boyer, 1982). Advances in molecular tools have greatly facilitated breeders in efficiently identifying and selecting germplasm with favorable traits such as tolerance to abiotic stresses; however, breeders still rely on obtaining high quality phenotypic data for developing and implementing these methods (Masuka et al., 2012). Phenotyping has become the main bottleneck in making breeding advances because current methods of phenotyping involve a large amount of time and labor. This limits their applications across breeding programs which typically consist of large populations comprised of thousands of lines grown in replicates across multiple environments (Myles et al., 2009). To effectively breed for tolerance to abiotic stresses, quantifying the severity of the response to a particular stress across different genotypes as well as their ability to recover from the stress is crucial. This would require temporal measurements of phenotypes linked to the stress response which increases the complexity in making progress in breeding for such traits.

The development of high throughput phenotyping tools has taken surge over the last couple of years to obtain phenotype data quickly and at low costs. Most of these methods rely on remote sensing techniques that utilize sensors to capture images of plants and subsequently processing the images to extract meaningful traits. Sensors that measure different ranges of the electromagnetic spectrum have been applied in agriculture. RGB imaging has been widely used to extract morphological traits linked to plant productivity across different crop species in field and indoor settings ( Watanebe et al., 2017; Feng et al., 2018; Varela et al., 2017; Enders et al., 2019). Thermal imaging and near infrared combined with visible imaging have been used to extract information of drought stress across grasses and legume crops (Martynenko et al., 2016; Biju et al., 2018; Benavente et al., 2013; Jin et al., 2017; Zhang et al., 2012).

More recently, with the advent of advanced machine and deep learning algorithms, multispectral and hyperspectral sensors that generate large amounts of data at very high spectral and spatial resolutions have been applied in four key areas in plant phenotyping: identification, classification, quantification, and prediction of a particular stress (Singh et al., 2015). With hyperspectral imaging, the user can take advantage of hundreds of spectral channels to uncover materials and biochemical processes, such as the degradation of pigment molecules and changes in water content, within plant tissues that can differentiate and potentially quantify differences across species, genotypes, and stresses. The degradation of pigments such as chlorophyll alters the amount of reflected, absorbed, and transmitted radiation and can therefore be passively captured using spectral imaging (Blackburn, 2007).

Hyperspectral imaging has been applied for the identification and quantification of several bacterial and fungal infections including fusarium head blight and leaf rust in wheat (Alisaac et al., 2019; Mahlein et al., 2019; Qiu et al., 2019; Ashourloo et al., 2014; Bauriegel et al., 2011), powdery mildew in barley (Thomas et al., 2018), Cercospora leaf spot, powdery mildew and leaf rust in sugarbeet (Mahlein et al., 2012; Rumpf et al., 2010) and Sclerotinia sclerotiorum in oilseed rape plants (Kong et al., 2018). Diseases caused by bacterial or fungal infections tend to have characteristic features such as bacterial pustules with neighboring chlorotic tissue or necrotic lesions that are picked up and easily distinguished using spectral imaging. However, identifying more subtle symptoms such as those caused by abiotic stresses can be challenging. Pandey et al. (2017) found hyperspectral imaging to be useful in quantifying plant leaf chemical properties that could aid in detecting water and nutrient deficiencies among crops and Obeidat et al. (2018) discovered that spectral indices correlated with chlorophyll content could help distinguish between genotypes and cold-stressed plants in indoor settings. Similarly, Behmann et al. (2014) found that hyperspectral imaging can be used to cluster barley plant pixels into different levels of drought-stress based on amount of chlorosis and senescence. Also, Römer et al. (2012) was able to detect drought stress early in development for cereal grains in both indoor and field settings based on a matrix factorization technique that allows for the computation of how similar a plant pixel is to the typical spectrum of a healthy plant. Another way to identify subtle abiotic stress signals using spectral imaging is by correlating reflectance data with other more laborious, time-consuming or costly measurements correlated to the stress response. Feng

et al (2019) made a link between hyperspectral measurements of okra leaves with measurements linked to leaf chlorophyll content and fresh weight traditionally used to assess salt stress across crops.

A common problem when analyzing spectral data of plant surfaces is taking into account uneven light scattering that occurs upon the interaction between incident light and the plant surface being captured (Makdessi et al., 2017). Plant material possesses non-Lambertian reflectance properties and plants themselves contain a large amount of morphological variation causing differences in angle relative to the sensor across leaf segments. Many studies that have evaluated the use of hyperspectral imaging for assessing plant abiotic stresses have utilized indoor setups with uniform, nonreflective backgrounds and have dismissed the effects of plant morphology by securing the plant leaves on a flat background (Obeidat et al., 2018); however, this limits their application in natural settings. Other studies have proposed ways to account for plant architectural variation. Behman et al. (2015) proposed a method to account for differential light scattering by performing geometric calibration of hyperspectral cameras that connects a 3D model with a 2D image and Mohd Asaari et al. (2018) applied a standard normal variate normalization method to correct spectra for uneven illumination effects. Moghimi et al. (2018) circumvented plant architectural differences by identifying endmembers indicative of all plant pixels for a given line in a given treatment and used these to identify salt stress across wheat lines. Feng et al. (2019), on the other hand, was able to develop an instance segmentation model using deep learning to segment individual okra

plant leaves for further evaluation, which is a suitable approach for crops where leaves lie relatively flat horizontally with respect to the sensor.

Variation in plant architecture across different crops species can make finding a single approach for analyzing spectra data challenging; however, it can also be taken advantage of in the context of finding discriminatory patterns within an individual crop. Upon accounting for differences in light scattering of different plant surfaces, the large number of plant pixels representing single or multiple individuals are commonly reduced to a single value such as an endmember (Moghimi et al., 2018) or an average (Mohd Asaari et al., 2018). Looking at all the plant pixels throughout the plant can elucidate biochemical processes in response to certain stimuli that vary spatially throughout a plant. This spatial variation could be useful for identifying more subtle symptoms that may be masked out by reducing the data to a single value per line or treatment or by normalizing the data to account for scattered light due to differences in plant morphology. Moreover, although multiple studies have identified indices that are useful for a particular stress, they have not looked into how these would change due to plant morphology. This study aims to elucidate the effects of morphology and stress on the spatial variation of reflectance values within plant leaves and compare the ability of reflectance data for different regions of the leaf to resolve genetic and environmental factors relative to reflectance data for the entire plant. Currently, this remains unknown and could enlighten new mechanisms for identifying, classifying, quantifying and predicting the onset and recovery of biotic and abiotic stresses where little variation is observed with the naked eye.

## RESULTS AND DISCUSSION

In most field settings, hyperspectral images of cereal crops are collected from above, resulting in a top-down view of the plants. We sought to develop approaches for the analysis of hyperspectral images for maize plants collected from above. We obtained raw intensity data using a top-down approach for wavelengths ranging from approximately 400 to 1000 nm for several controlled-condition experiments. The experiments contained maize seedlings of multiple inbred genotypes subjected to different environmental treatments. Plants were illuminated by halogen lights, which are oriented in two parallel rows of bulbs on either side of the camera and each image contained 3 plants (Figure 4.1). Raw intensity values for the resulting images of plants were converted to reflectance using white and dark references and then normalized by their L2 norm (see methods). For each plant, the NDVI values were utilized to identify pixels containing plant tissue and thresholded to generate a binary image mask to extract the reflectance values at each wavelength for entire plants. The longest leaf for each plant was then identified and broken down into ten segments from the center whorl to the outer leaf tip and reflectance data for each leaf segment was extracted.

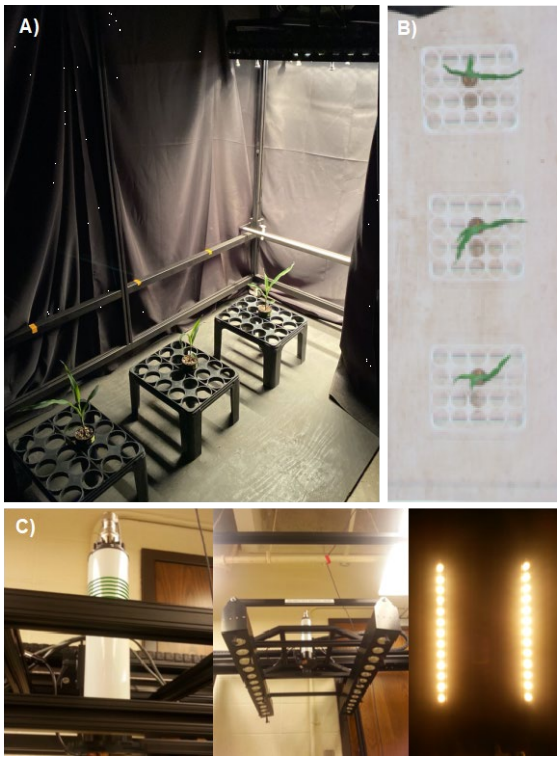


**Figure 4.1.** Hyperspectral imaging setup.

*A) Imaging system utilized. B) RGB representation of staged plants C) Sensor and light configuration.*

Entire plant and leaf segment hyperspectral data was obtained for plants across several different experiments that are summarized in Table 4.1. We sought to address different themes in our analyses of this data. First, different genotypes or environments often result in changes in plant morphology (Enders et al., 2019). Although side-view RGB data is able to capture morphological variation, we evaluated the potential of top-down hyperspectral data to capture these differences by utilizing changes in reflectance for specific regions of a plant. In our analyses, we compared the ability of using whole plant data relative to using specific regions of leaves in the ability to resolve genetic or

environmental factors. Second, hyperspectral imaging provides opportunities to identify genetic or environmental variation. We assessed the relative ability of using hyperspectral imaging data to accurately classify abiotic stress conditions that we have observed induce similar morphological responses within maize seedlings for different genotypes using machine-learning approaches. To achieve these goals, we collected hyperspectral data using the described system for two experiments. The first experiment (E1) consists of three replicates of five genotypes of maize seedlings under four treatment groups (control, cold, salt, and heat) imaged at a single time point. The chosen genotypes were previously demonstrated to differ in morphological responses to cold stress (Enders et al.,2019). The second experiment (E2) consists of two genotypes under four treatment groups (control and three severities of salt stress) imaged at three timepoints (immediately before the stress, 2 days following the stress treatment, and 4 days after following the stress treatment). A total of 540 plant images are represented in the dataset. We have used the dataset to address a series of questions about the ability of hyperspectral imaging to resolve the effects of growth stage, genotype and various abiotic stresses across portions of maize leaves.

**Table 4.1**. Summary of experiments.

| Genotypes | Experiment | Day of Imaging | Treatments | Number of Plants per Genotype-Treatment-Day Combination | Total Number of Imaged plants |
|---|---|---|---|---|---|
| B73<br>Ki11<br>Mo17<br>MS71<br>Ph207 | E1-Rep1 | 13 DAS | Control<br>Cold: 6C day/2C night @ 11-13 DAS<br>Heat: 39C day/29C night @ 11-13 DAS<br>Salt: 50mL 0.75M NaCl @ 11 DAS | 3 | 60 |
| B73<br>Ki11<br>Mo17<br>MS71<br>Ph207 | E1-Rep2 | 13 DAS | Control<br>Cold: 6C day/2C night @ 11-13 DAS<br>Heat: 39C day/29C night @ 11-13 DAS<br>Salt: 50mL 0.75M NaCl @ 11 DAS | 3 | 60 |
| B73<br>Ki11<br>Mo17<br>MS71<br>Ph207 | E1-Rep3 | 13 DAS | Control<br>Cold: 6C day/2C night @ 11-13 DAS<br>Heat: 39C day/29C night @ 11-13 DAS<br>Salt: 50mL 0.75M NaCl @ 11 DAS | 3 | 60 |
| Mo17<br>Ph207 | E2 | 11 DAS<br>13 DAS<br>15 DAS | Control<br>50mL 0.5M NaCl @ 11DAS<br>50mL 0.75M NaCl @ 11 DAS<br>50mL 1M NaCl @ 11 DAS | 15 | 360 |
| | | | | **Total Number of Plant Images** | 540 |

### *Spatial variation in top-down images of seedlings*

The system and approach that was used to generate images of maize seedlings results in a relatively large number of pixels (1,908-13,831) for each plant. These pixels exhibit a range of reflectance values with substantial standard deviation. A top-down image of a maize seedling consists of a central whorl from which leaves extend. The whorl has a funnel-like shape with each leaf extending in an arc (Figure 4.2). Given the variation in reflectance based on the orientation of the plant surface relative to the lights and camera, there is substantial variability in reflectance from the central whorl to the leaf blade tip. In addition, there is biological variation in gene expression and physiological properties of leaves from the base to the tip (Li et al., 2010). We sought to compare the average normalized reflectance values from each plant within zones extracted along the length of a leaf. To classify relatively consistent zones of a plant leaf,

we implemented an approach to divide the longest leaf into ten sections and identify the plant pixels within each section (Figure 4.2, see methods for details). This resulted in a set of 10 segments that were used as a mask for the hyperspectral image cube to extract normalized reflectance values by leaf zone.

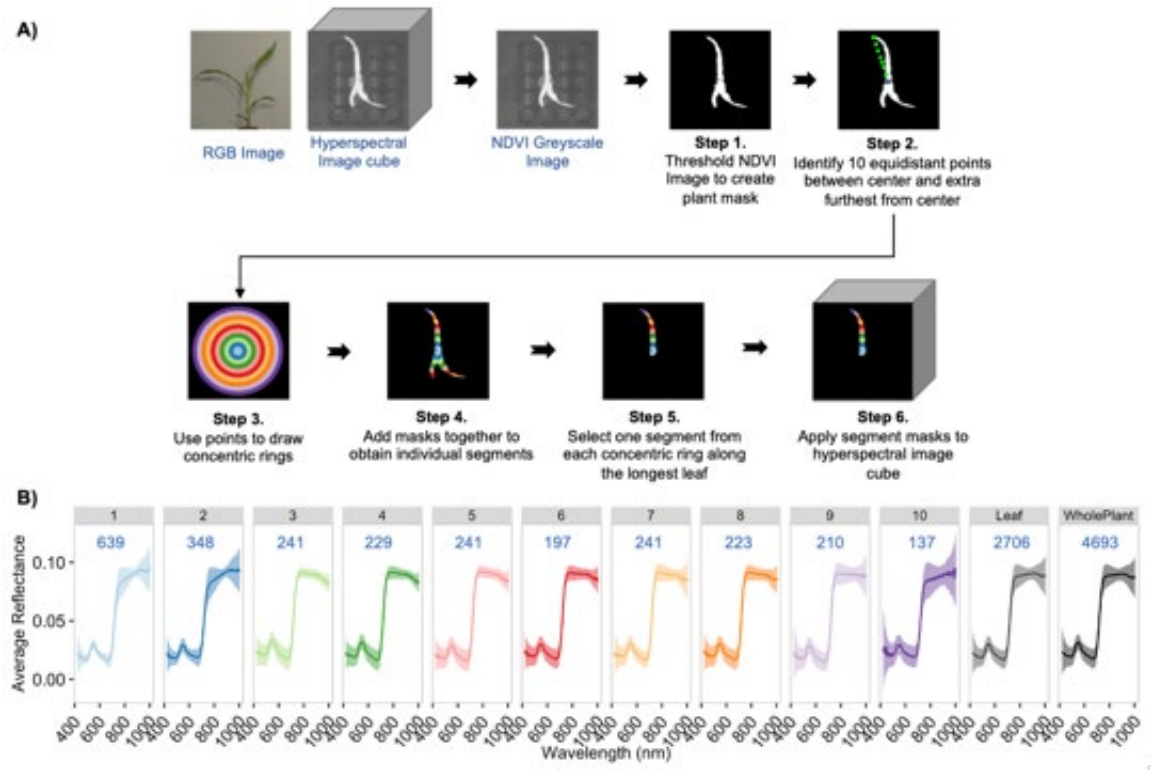


**Figure 4.2.** Evaluating individual leaf segments.

*A) Procedure for extracting hyperspectral data from ten segments across the longest leaf of each plant. B) Mean (dark line) and variance in reflectance of individual leaf segments, the entire longest leaf (all leaf segments combined) and the entire plant of a Mo17 control plant at 13 days after sowing. Pixel counts represented in each panel are indicated by the blue text. Leaf segment is indicated at the top of each panel in black text.*

The average reflectance profiles and variance were compared for the entire leaf relative to each of the ten leaf sections. Substantial variability is observed in pixel counts

across leaf segments due to differences in width across the length of the leaf (Figure 4.2). While the overall pattern of reflectance values is generally similar among plant segments there is substantial variability within and across plant segments for the magnitude of specific patterns. PCA of the reflectance values for each segment of each plant suggests differences in the most outer segments of the leaves relative to more central regions of the leaf (Figure 4.3A). A comparison of the reflectance profiles across leaf segments focused only on the visible range of the spectrum reveals distinct reflectance profiles between leaf segments near the center or leaf tip relative to the middle portion of the leaf in both Mo17 and PH207 (Figure 4.3B).

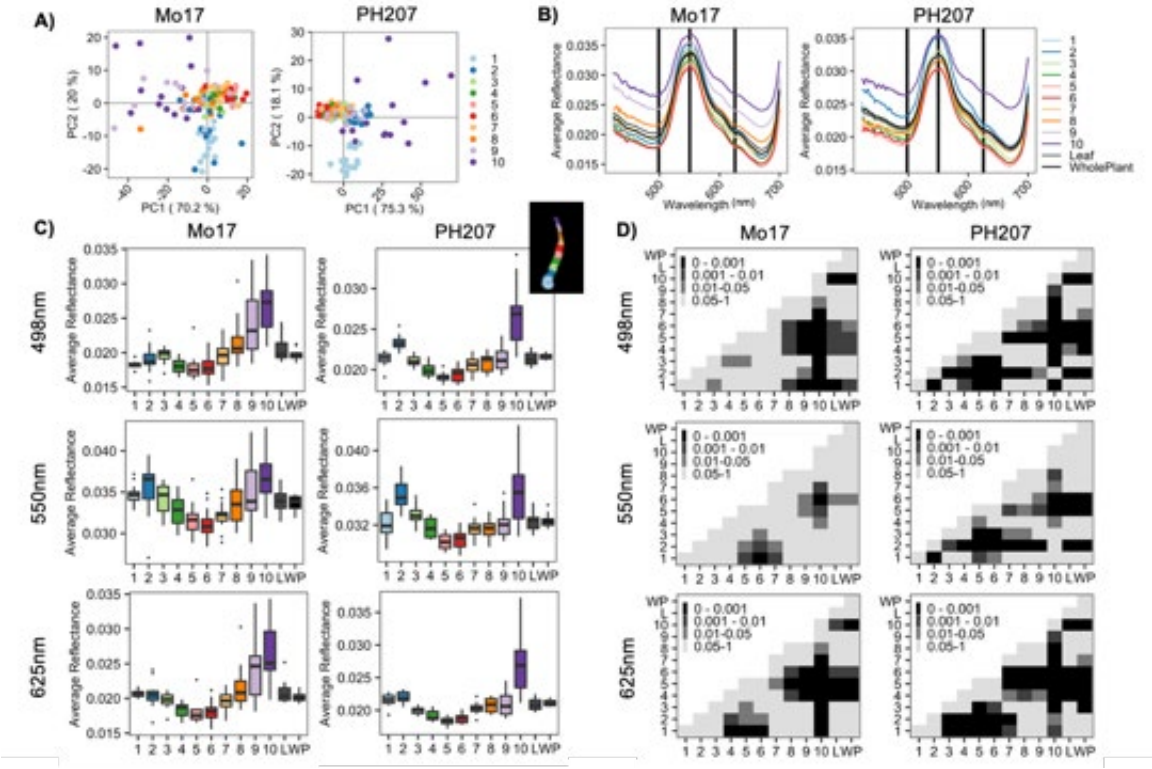


**Figure 4.3**. Reflectance of leaf segments across all Mo17 and PH207 control plants in experiment E2 at 15 days after sowing.

***A)*** *PCA biplots of the mean reflectance across all wavelengths of all 10 leaf segments for individual plants. Each datapoint constitutes an individual leaf segment for a single plant.* ***B)*** *Mean reflectance for the 10 leaf segments, the entire leaf and the entire plant. All plants were utilized to calculate the mean. Vertical black lines indicate wavelengths at 498 nm, 550 nm, and 625 nm.* ***C)*** *Distributions of the average reflectance per plant of leaf segments, the entire leaf, and the entire plant at 498 nm, 550 nm and 625 nm.* ***D)*** *Adjusted p-values from a pairwise wilcox test between pairwise comparisons of leaf segment, entire leaf (L), and whole plant (WP) reflectance, at 498 nm, 550 nm and 625 nm. Results were adjusted for multiple comparisons using the "holm" method. Black color indicates p-value < 0.001.*

We wanted to compare how the average reflectance profiles across different portions of leaf differ from the average reflectance profile of the entire plant. To do this, selected three representative wavelengths in the red, green, and blue range of the light spectrum (625 nm, 550 nm, and 498 nm; Figure 4.3B) and assessed the distribution of average reflectance values for all plants for each of the leaf segments as well as the entire leaf and the entire plant (Figure 4.3C). For several of the segments the reflectance values for these three wavelengths exhibit distributions of values that are significantly different from each other or from the entire plant; however the whole-leaf and whole-plant averages closely align with each other (Figure 4.3C; Figure 4.3D). In general, the patterns are similar for the two genotypes. Relative to the values observed for the entire leaf there are often significant differences in the distribution of values seen from the middle and the tip of the leaf. The tip of the leaf is often distinct from many other zones as well. These observations highlight the variability throughout a single leaf and suggest that using average reflectance values for a plant or leaf will likely obscure spatial variation that may occur due to developmental, genetic or environmental factors.

***Stable patterns of hyperspectral signal for different stages of seedling growth***

The differences in hyperspectral profiles were assessed for PH207 seedlings grown in control conditions that were 11, 13 and 15 days after sowing to document whether there are differences as seedlings mature and whether the differences among leaf segments are consistent over time (Figure 4.4). PCA reveals that differences across leaf segments account for most of the observable variation in reflectance intensity compared to differences observed between days (Figure 4.4A). Across the three time points, average reflectance values cluster into groups corresponding to leaf segments near the leaf tip, leaf segments towards the middle of the leaf, and leaf segments towards the center whorl. No clustering by date was observed even though plant size and morphology changes were observed based on trait data obtained from side-view RGB images (Figure 4.5, see methods). The profiles of reflectance values are slightly different on the three dates (Figure 4.4B) but the distribution patterns for the different leaf segments relative to each other remain consistent. Examination of the distribution of values at three wavelengths reveals similar distributions for plants at the three dates and similar trends among the different leaf segments (Figure 4.4C).

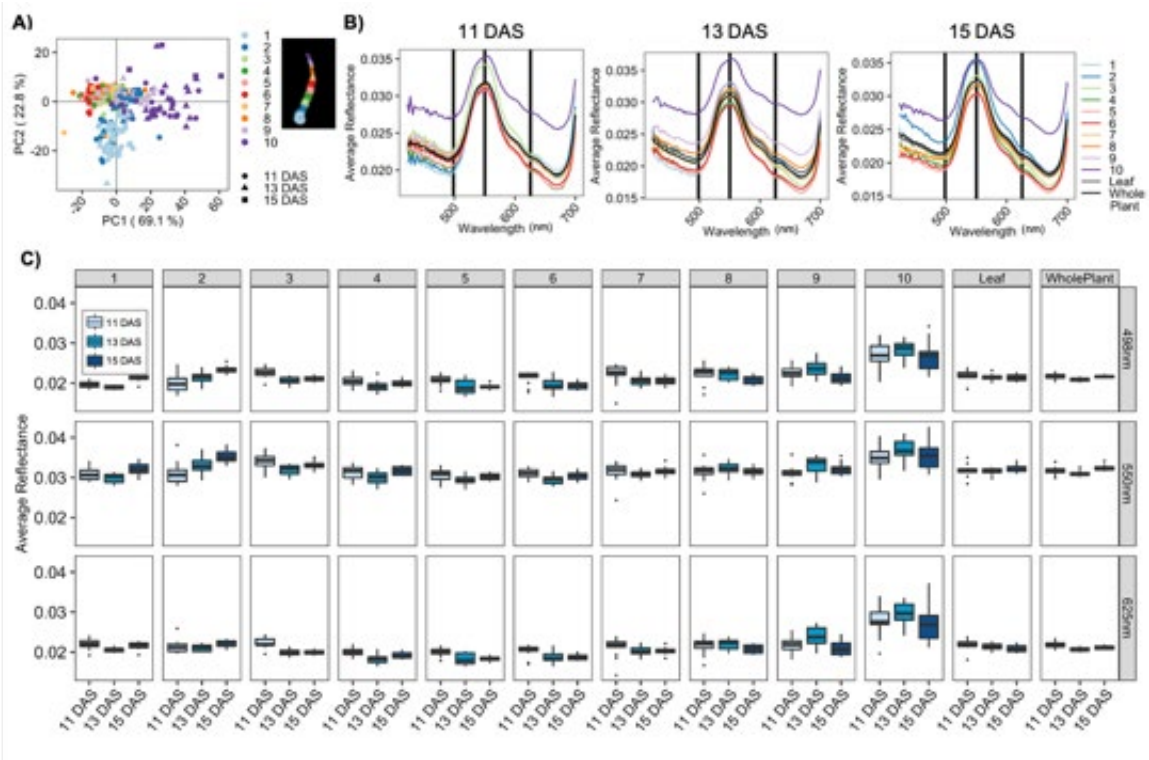


**Figure 4.4.** Reflectance of leaf segments across all PH207 control plants in experiment E2 across 11, 13 and 15 days after sowing.

*A) PCA biplots of the mean reflectance across all wavelengths of all 10 leaf segments for individual plants. Each datapoint constitutes an individual leaf segment for a single plant. B) Mean reflectance for the 10 leaf segments, the entire leaf and the entire plant. All plants were utilized to calculate the mean. Vertical black lines indicate wavelengths at 498 nm, 550 nm, and 625 nm. C) Distributions of the average reflectance per plant of leaf segments, the entire leaf, and the entire plant at 498 nm, 550 nm and 625 nm across the three days of imaging.*

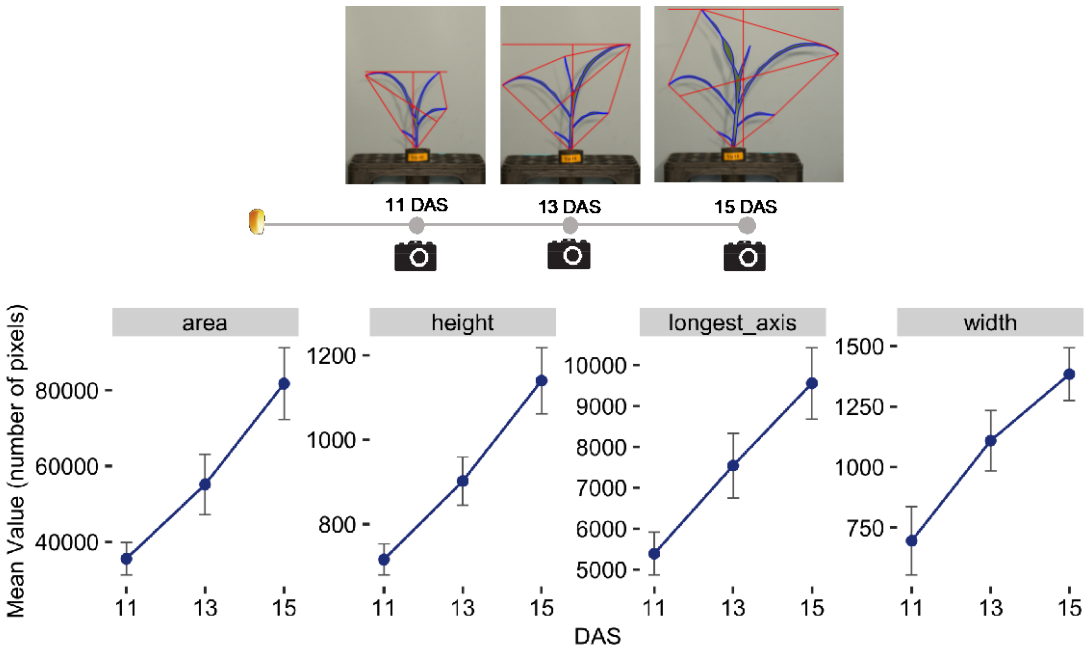


**Figure 4.5.** Mean RGB trait values for all PH207 control plants in experiment E2 across 11, 13 and 15 days after sowing (DAS).

### *Ability to distinguish genotypes using hyperspectral imaging*

Hyperspectral profiling has been widely used for separating different plant species such as weeds (Pantazi, Moshou and Bravo, 2016) and tropical forest trees (Laybros et al., 2019). Fewer studies have used hyperspectral profiling to separate different genotypes or lines of the same species. A study by Obeidat et al. (2018) showed that genotype main effects across short-season maize lines significantly contributed to variation in various spectral reflectance indices as well as spectral reflectance in the visible and near-infrared range when comparing hyperspectral scans of flat leaves. This variation, particularly in the spectral reflectance across the visible range of the spectrum, was likely due to

chlorophyll and carotenoid differences (Obeidat et al., 2018). To assess variation in spectral reflectance among maize genotypes, we applied our leaf segmentation approach to compare the reflectance values across individual leaf segments among the different inbred lines grown in control conditions in experiment E1. Experiment E1 consisted of images from 9 plants for five different genotypes. While the overall average profiles for the entire leaf are relatively similar in the visible range, there are some leaf segments that show more pronounced differences among genotypes (Figure 4.6A). In particular, MS71 shows higher reflectance for wavelengths near 550 nm for central segments of the leaf but lower reflectance compared to other genotypes for wavelengths near 500 nm and 675 nm for segments near the leaf tip. However, these differences are reduced in averages that include all pixels for the entire leaf (Figure 4.6A).

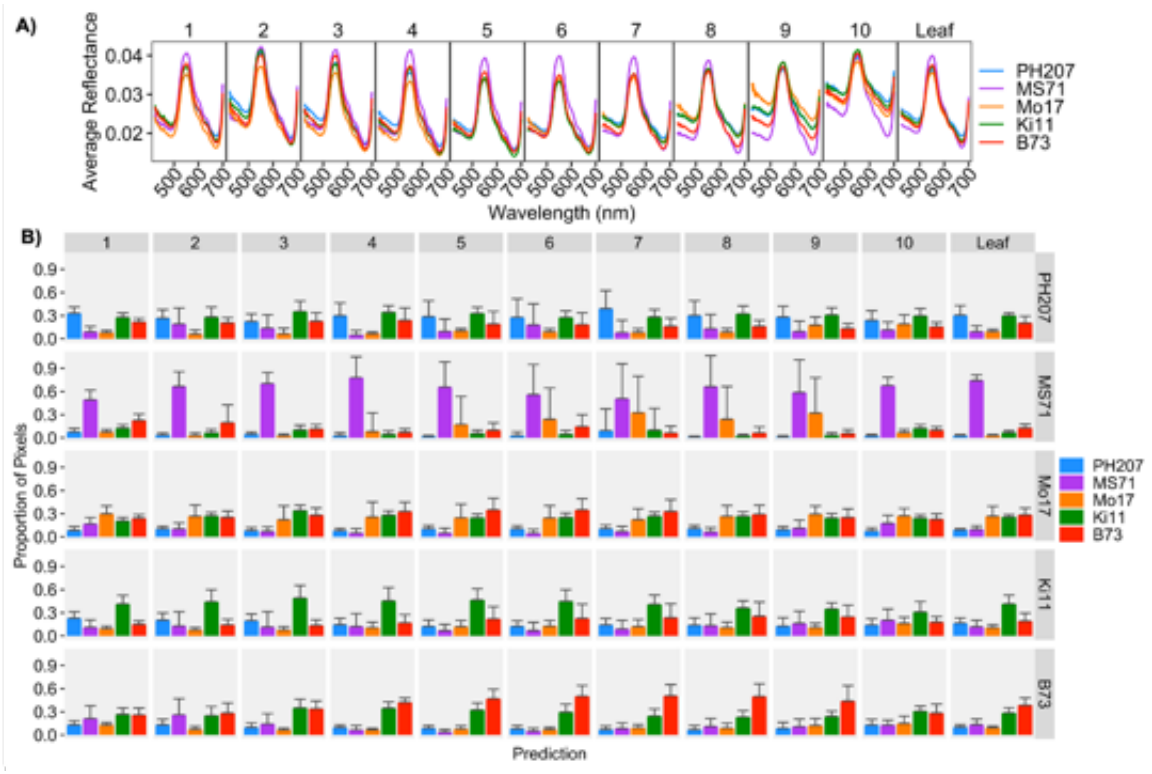


**Figure 4.6.** Genotypic differences in hyperspectral profiles for all control plants of each genotype in Experiment E1.

*A) Average reflectance values across all control plants of each genotype. B) Average proportion of pixels per plant from all plants of a certain genotype (rows) for each leaf segment (columns) predicted to belong to a certain genotypic class. Error bars indicate the standard deviation in pixel values from the mean.*

To further evaluate whether specific leaf segments can be more useful than whole leaves in distinguishing individual genotypes, we developed a cubic support vector machine (SVM) model utilizing ⅙ of all the pixel values from all plants grown in control conditions in experiment E1 to predict the corresponding genotype. The predictor variables included normalized reflectance values for wavelengths in the visible range as well as the leaf segment of the corresponding pixel. We then applied this model to predict

the genotype of the remaining ⅚ pixel values in the dataset. This included pixels from all leaf segments. The proportion of pixels per plant that were classified into each genotype for each of the zones of each maize line was determined (Figure 4.6B). The model is able to correctly identify MS71 pixels in most leaf segments although the accuracy is somewhat lower in the whorl region (Figure 4.6B). The other genotypes are less accurately identified. B73 is most accurately identified for the central leaf segments but is often confused with Ki11 (Figure 4.6B). PH207 and Mo17 generally exhibit relatively low correct prediction accuracies throughout the leaf and are frequently mis-classified as B73 or Ki11 (Figure 4.6B).

***Ability to distinguish and quantify abiotic stresses using hyperspectral imaging***

Two different experiments were performed to investigate the potential to utilize hyperspectral profiling for documenting the effects of abiotic stress on maize seedlings. For experiment E2 we treated two genotypes, Mo17 and PH207, with three different concentrations of salt applied on day 11 immediately after imaging (Figure 4.7A). These plants were then imaged two and four days after the stress application. Two cubic SVM models were developed using ⅙ of all pixels from the control and the medium salt stress treatment groups. In both models, the treatment (Control or 0.75M NaCl) was the response variable. The first model was trained using pixels randomly selected throughout the entire plant; however, the second model only contained pixels randomly selected from the longest leaf. In the first model, the normalized reflectance values for wavelengths in the visible range, the genotype, and the day of imaging represented as

days after sowing (DAS) were set as the predictor variables. In the second model, the corresponding leaf segment was also included as a predictor variable. Moreover, the first model was used to predict all the pixels from entire plants in the E2 dataset from all treatment groups into belonging to the control or salt stressed class (Figure 4.7B). On the other hand, the second model was used to predict all pixels from the longest leaf of all plants (Figure 4.7C).

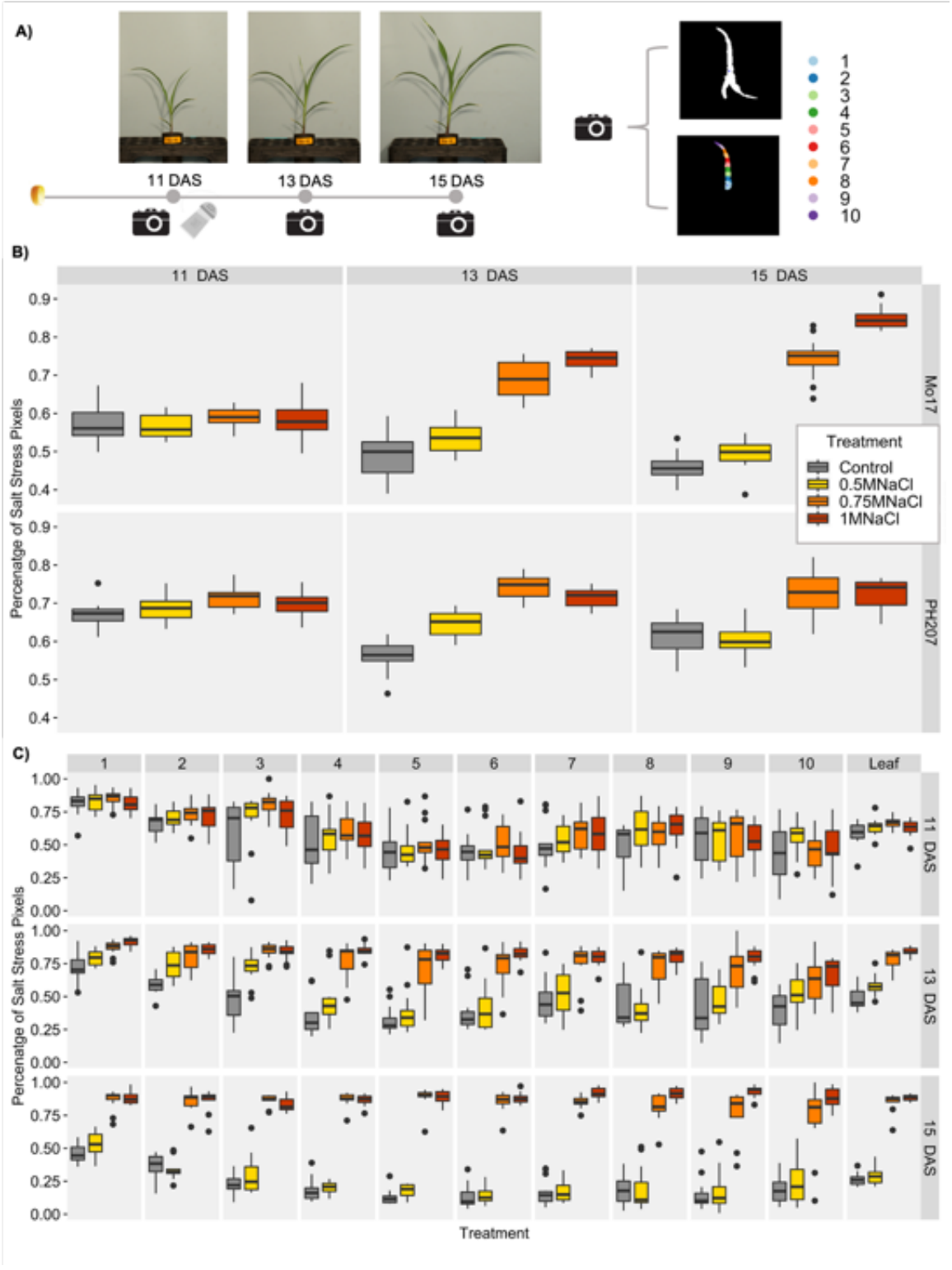
A)
11 DAS
13 DAS
15 DAS
1
2
3
4
5
6
7
8
9
10
B)
11 DAS
13 DAS
15 DAS
Mo17
PH207
Percenatge of Salt Stress Pixels
Treatment
Control
0.5MNaCl
0.75MNaCl
1MNaCl
C)
1
2
3
4
5
6
7
8
9
10
Leaf
11 DAS
13 DAS
15 DAS
Percenatge of Salt Stress Pixels
Treatment

**Figure 4.7**. Proportion of pixels per plant classified as being salt stressed based on cubic SVM model developed from the wavelengths in the visible range of the spectrum and genotype as the predictor variables and using the medium salt stress and control treatments as the response variables.

*A) Three salt treatments were applied after imaging at 11 days after sowing (DAS). Plants were then imaged at 13 and 15 DAS. Reflectance values were calculated for entire plants, entire leaves and individual leaf segments. B) Proportion of total pixels for each plant across treatments in Experiment E2 classified as belonging to the salt stress category for the model developed using pixels across the whole plant. C) Proportion of total pixels for individual leaf segments and the entire leaf per plant for Mo17 classified as belonging to the salt stress category for a model developed using pixels across individual plant segments with segment number as a predictor variable.*

As expected, the proportion of pixels classified as salt-stressed was not different for the control and the treatment groups at day 11 for either model as these images were collected prior to the actual stress treatment application (Figure 4.7B; Figure 4.7C). However, at day 13 and day 15, two and four days after application of salt we see substantial increases in the proportion of pixels classified as salt stressed (Figure 4.7B; Figure 4.7C). When looking at the classifications based on the entire plant using the first model, the proportion of pixels classified as salt stressed increases at higher concentrations of salt treatment and is higher at day 15 than at day 13 (Figure 4.7B). However, there are a high frequency of pixels in control plants classified as salt stressed in this analysis. A comparison of the predictive ability for different leaf segments revealed substantial variation across the leaf. At days 13 and 15 the segments from the middle of the leaf have higher correct prediction accuracy than segments near the leaf tip or whorl (Figure 4.7C). Importantly, these mid-leaf segments also outperform the predictions based on using the entire plant. A relatively small proportion of pixels from

control plants are classified as stressed in these mid-leaf segments while the majority of pixels in plants with 0.75M or 1M NaCl treatment are classified as stressed.

Experiment E1 included five genotypes treated with four conditions including control, heat stress, cold stress and salt stress and plants were imaged after two days of the stress treatment. Visual examination of the plants revealed differences in severity of stress response for the different genotypes (Figure 4.8). This is quantified for cold stress by Enders et al (2019). For example, Ki11 tends to have strong responses, especially to cold and salt stress while Mo17 has minimal visual responses to the stresses (Figure 4.8). The average hyperspectral profiles for the entire leaf reveal limited changes for Mo17 but some differences for Ki11 (Figure 4.9). Although we saw visual differences in responses across genotypes for individual stresses, the symptoms within individual genotypes in response to the various abiotic stresses utilized were very similar (Figure 4.8). We therefore wanted to test the ability for hyperspectral imaging to better differentiate across abiotic stress conditions within genotypes.

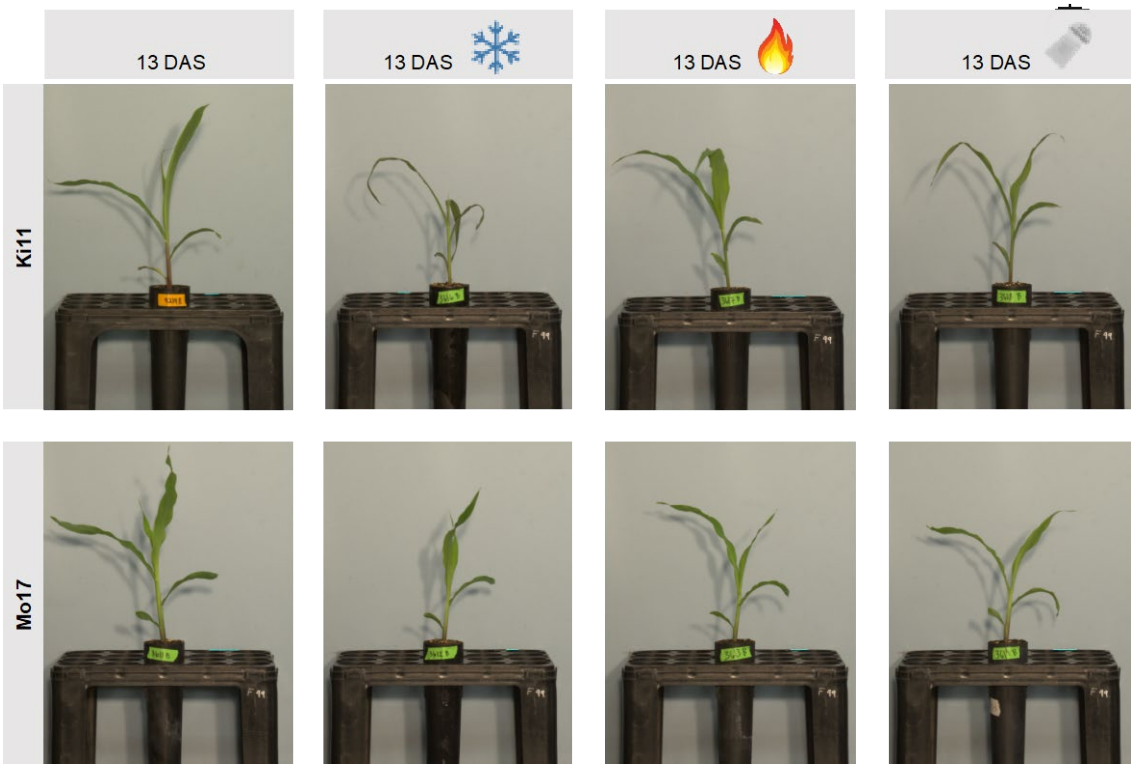


**Figure 4.8.** RGB images for one representative plant in experiment E1 for each treatment for Ki11 and Mo17 genotypes 13 days after sowing.

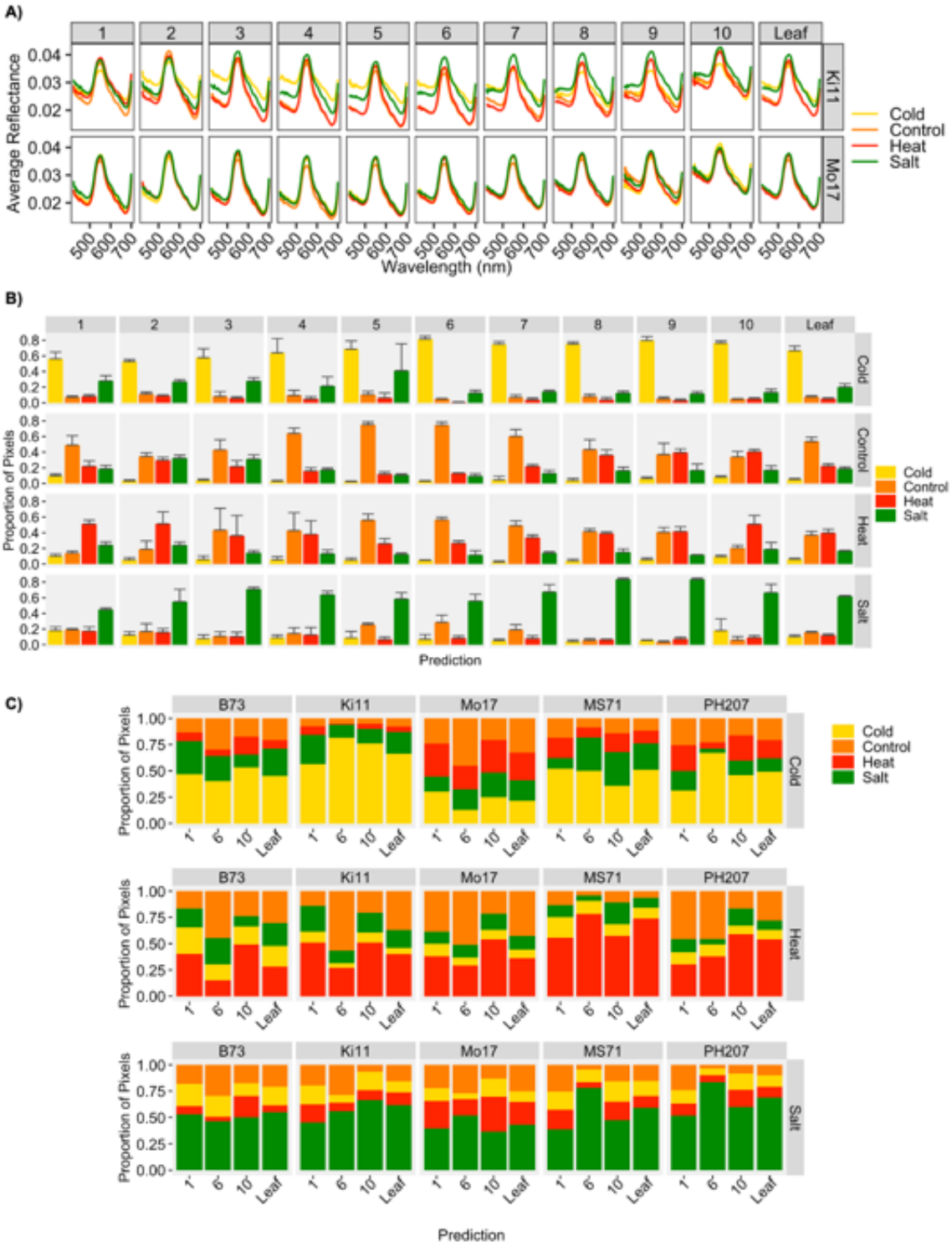
A)
1
2
3
4
5
6
7
8
9
10
Leaf
Ki11
Mo17
Average Reflectance
0.04
0.03
0.02
500
600
700
Wavelength (nm)
Cold
Control
Heat
Salt
B)
Proportion of Pixels
0.8
0.6
0.4
0.2
0.0
Prediction
C)
B73
Ki11
Mo17
MS71
PH207
1'
6'
10'
Leaf
1.00
0.75
0.50
0.25
0.00

**Figure 4.9**. Differences in hyperspectral profiles across treatments for all Ki11 and Mo17 plants in Experiment E1.

***A)*** *Average reflectance values for all plants in the cold, control, heat and salt stress treatments of Ki11 and Mo17 in Experiment E1.* ***B)*** *Average proportion of pixels from all Ki11 plants of a certain treatment (rows) for each leaf segment (columns) predicted to belong to a certain treatment class. Bars represent the mean proportion of all plants per category and error bars represent the standard deviation around the mean.* ***C)*** *Average proportion of pixels from all plants of a certain treatment (rows) for genotypes across selected leaf segments predicted to belong to a certain treatment class. Bars represent the mean proportion of all plants per genotype and treatment class predicted to belong to a certain treatment.*

The differences in hyperspectral profiles for the different treatments were more severe in some leaf segments compared to others (Figure 4.9A). A cubic SVM model was developed to predict the treatment using predictor variables of normalized reflectance values, genotype, and leaf segment. The proportion of pixels classified into each condition is shown for each segment of each actual treatment (Figure 4.9B, C). In general, the SVM model was able to differentiate abiotic stress conditions within individual genotypes. For Ki11 there is a high true prediction accuracy for cold and salt stress across all segments of the plants; however, the prediction accuracy is further improved for segments near the middle of the leaf for cold stress and the tip of the leaf for salt stress (Figure 4.9B). Heat stress is not predicted as accurately with substantial confusion between control and heat stress (Figure 4.9B). This likely reflects minimal phenotypic response to heat stress for Ki11. Similar patterns of enhanced prediction accuracy utilizing middle segments of the leaf compared to the entire leaf across treatments are also observed for the other four genotypes.

If we compare the accuracies of a representative leaf segment in the center whorl, the middle portion of the leaf, the tip of the leaf, and the entire leaf in predicting the abiotic stress response across genotypes, we observe differences in utility of different leaf segments based on the stress being predicted as well as the genotype (Figure 4.9C). Leaf segments in the middle portion of the leaf as well as the leaf tip provided the highest true prediction accuracy overall across treatments and genotypes compared to the center whorl and utilizing all segments form the leaf. Leaf segments towards the middle portion of the leaf (segment 6 in this case) provide a higher prediction accuracy across most genotypes for predicting cold stress and across some genotypes (Mo17, MS71 and PH207) for salt stress; however, the leaf tip was more informative for heat stress and across some genotypes such as Ki11 for salt stress (Figure 4.9C). Overall, most pixels that were misclassified across genotypes and treatments were predicted to belong to the control treatment group rather than alternate stress treatments. This shows the value of hyperspectral imaging in differentiating stress conditions compared to visual inspection or RGB imaging of plants which result in similar responses across treatments.

## CONCLUSIONS

Hyperspectral profiling provides new opportunities for optical analysis of trait variation in crops. Many studies have reported the ability to monitor physiological changes in plants using point profiles of reflectance from a single region of a leaf (Meacham-Hensold et al., 2019; Silva-Perez et al., 2018; Smith et al., 2004; Yendrek et al., 2017). However, there has been less analysis of the ability to separate effects of

genotype or environmental conditions using whole plant images. In this study we highlight the potential for using hyperspectral imaging but also show that using averages of whole plants provides less resolution than focusing on specific regions of plants. The variation in spectral profiles observed from the base of the leaf to the tip of the leaf likely represents a combination of physiological differences as well as variation in the plant shape/leaf angle resulting in differing reflectance. Although there have been studies that have shown variation in biochemical compounds across different sections of plant leaves in response to different growing conditions, the relative ability of hyperspectral data to capture these changes throughout the plant in a non-destructive and high-throughput manner had not previously been looked at. In this study, we have not separated the specific physiological factors but instead have simply relied upon the segmentation of hyperspectral data across the leaf to reduce variance and improve stress discrimination. We have also evaluated which portions of the maize seedling leaves provide higher discriminatory accuracies across treatments and found that these vary by condition and genotype.

There are several limitations to our approach for segmenting the longest leaf and making comparisons of specific leaf segments across dates, genotypes and treatments. In this work, we performed manual detection of the center of the plant and the remainder of the leaf identification and segmentation process was automated. It is likely that spectral properties or plant shape could be used for automated detection of the center of the whorl. Additionally, when comparing leaf segments for varying genotypes or growing conditions the length of the longest leaf may vary as plants exhibit different growth rates

for different stress conditions or among genotypes. This results in differing numbers of pixels for the segments being compared. However, since we are segmenting into 10 equally sized regions the relative segmentation of the leaf should remain consistent. Another potential issue is the variation in the angle of the leaf tip. As a leaf emerges from the whorl it has an upright angle. As the leaf extends the tip will shift from upright to horizontal to having a downward angle. There is biological variation among plants at the same developmental stage for the angle of the leaf tip. This may result in increased variance for segments near the leaf tip, as noted in our PCA plots (Figure 4.3A, Figure 4.4A). However, many stress conditions have visible effects on the leaf margins near the leaf tip and this region provided the best classification for some stresses. One additional potential complication is the presence of mixed pixels that include some plant tissue as well as background. We implemented relatively strict cutoffs to minimize the number of mixed pixels obtained after plant segmentation but there are likely a small number of mixed pixels captured in our plant masks. These may be represented in uneven quantities across leaf segments with more mixed pixels appearing in narrower segments such as the leaf tip relative to the base of leaf.

Our findings highlight the utility of plant segmentation for improved accuracy of genotype or environment predictions using hyperspectral data. It is worthwhile to note that there is not a single region of the leaf with the highest performance. Instead the most accurate regions varied for different stresses or genotypes. We found that there are distinct differences across some leaf segments among genotypes that enable genotypic differentiation. Performing such analysis on large genotypic panels would allow for the

identification of groups of genotypes that are morphologically similar. Finding these groups would be important when evaluating environmental responses as these differences could mask the environmental effects if not taken into account when imaging large genotypic panels.

The use of wider panels of genotypes would likely also result in the classification of genotypic groups with similar stress responses, but in this study we focused on improving the methods for stress detection in a small set of variable genotypes. Our classification prediction rates vary substantially. This is likely due to variation among the genotypes. Some genotypes are more tolerant of certain abiotic stresses and we can observe a higher proportion of pixels misclassified into the control classes for these. In contrast, genotypes that are more sensitive to a certain stress exhibit a larger prediction accuracy for stress prediction for the particular treatment. Although these machine-learning models wouldn't directly transfer to new genotypes, sensor platforms, or environmental conditions such as outdoor field sites, we show that the approach of segmenting leaves for hyperspectral image analysis provides higher discriminatory power for identifying genotypic responses to stress conditions that cannot be accurately assessed utilizing whole-plant averages of spectral profiles or by utilizing other methods that cannot account for morphological differences such as RGB top-down imaging. Extracting and analyzing hyperspectral data across plant segments can likely be conducted for larger scale field experiments and may improve the utility of hyperspectral profiles for documenting genotype, environment and genotype by environment effects.

## METHODS

### *Plant growth*

Two experiments were conducted, E1 and E2 (Table 4.1). For all experiments, seeds were planted approximately 2 inches below the surface in 40 cubic inch D-40 DeePots (Stuewe and Sons, Inc.) containing a 1:1 mix of SunGro (Agawam, MA) horticulture professional growing mix and autoclaved field soil. All plants were grown in Conviron growth chambers with a 16 hr 30°C and 8 hr 20°C day/night cycle and watered every other day.

In experiment E1, five maize genotypes (B73, Mo17, PH207, Ki11, MS71) were subjected to four treatment conditions (control, cold, heat, salt). Plants for all treatments were grown in control conditions until 11 DAS when the stresses were applied for the cold, heat and salt treatments. The cold-stress treatments were implemented using a Thermo Scientific refrigerated incubator programmed with a 16 hr 6°C and 8 hr 2°C day/night cycle and applied for 48 hours. The heat-stress treatments were implemented using a Thermo Scientific refrigerated incubator programmed with a 16 hr 39°C and 8 hr 29°C day/night cycle and applied for 48 hours. The salt stress was a single 50 mL 0.75 M NaCl treatment at Zeitgeber Time 2 (ZT2) at 11 DAS. Plants were imaged with our hyperspectral and RGB imaging systems at the end of the stress treatment at ZT2 at 13 DAS. Three experimental replicates were grown each consisting of three plants per genotype per treatment condition, for a total of 9 plants per genotype per treatment.

Experiment E2 consisted of two maize genotypes (Mo17 and PH207) subjected to four treatment conditions (control, low salt, medium salt and high salt stress). The low, medium and high salt stress treatments were implemented by a single 50 mL 0.5 M NaCl, 0.75 M NaCl or 1 M NaCl treatment, respectively, at ZT2 at 11 DAS. Plants were imaged with our hyperspectral and RGB imaging systems before undergoing stress at ZT2 at 11 DAS, at the end of the stress treatment at ZT2 at 13 DAS and two days after the stress treatment at 15 DAS. The experiment consisted of 15 plants per genotype per treatment.

***Hyperspectral image acquisition***

To capture the hyperspectral images, a custom-built line-scanning system from Middleton Spectral Vision (Madison, WI) was utilized (Figure 4.1). The system contains a Specim V10 spectrograph with a spectral range of 400 to 1000 nm and approximately a 1 nm spectral resolution. The spectrograph was mounted on an Imperx IPX-2M30 camera with 1600x1200 pixel spatial resolution. When acquiring hyperspectral images, a spectral binning of 2x was applied to obtain an average spectral resolution of 2.3nm.

***Hyperspectral Data Pre-processing and Normalization***

Black and white references are gathered by capturing and averaging 10 hyperspectral frames with the camera shutter closed and for a white lambertian reference panel each date of data collection. Intensity values for each pixel at each wavelength are converted to reflectance values by subtracting the dark reference and dividing the result by the difference between the white and dark references (Yoon and Park, 2015). The

resulting reflectance values are then normalized by dividing each spectrum by its L_2 norm, or the square root of the sum of the squares of that signature, following the equation

$$x_{norm} = \frac{x}{\sum_{i=1}^{n}(x_i{}^2)^{1/2}}$$

where $x$ is the full vector of reflectance data in image, $i$ is the response band, $n$ is the total number of measured wavelengths and $x_i$ is the full vector of reflectance data in image for the response band $i$.

***Segmenting Plant Material and Longest Leaf into Individual Segments***

All approaches for identifying, segmenting and extracting data from leaf segments were implemented utilizing custom MATLAB algorithms (MATLAB, 2018a). Plant material was segmented by calculating the NDVI value of each pixel and thresholding to a value of 0.35 or greater to create a binary plant segmentation mask. This threshold was found to balance maintaining the highest percentage of plant pixels while minimizing the number of mixed pixels in the extracted data. Each hyperspectral image contained three plants of the same genotype and treatment in a defined location. Individual plant objects were identified from the plant material mask using the *bwconncomp* function in MATLAB which returns connected components with a connectivity of 8 (MATLAB, 2018b). Objects caused by background noise were then removed by only keeping objects that had a minimum of 1,000 pixels and a maximum of 3,000 pixels and allocated an ID (plant A, B or C) based on their location in the image.

For each plant (plant A, B and C) of each image, the approximate center of the leaf whorl was identified by manually identifying the x-y coordinates of the plant center from an NDVI grayscale representation. This represented the only manual input in the pipeline. Extrema of the plant object were then automatically identified using the *regionprops* function in MATLAB (MATLAB, 2018b). Using the x-y coordinates for each terminal extrema and whorl center, the extrema farthest away from the center was identified for each plant representing the tip of the longest leaf. The distance of the center to the longest leaf tip was then divided into ten equidistant points in linear space and 10 concentric rings were generated utilizing the identified distance between points as the radius (Figure 4.2A). Each ring segment was used as a mask coupled with the plant material segmentation mask to extract leaf segments along the plant (Figure 4.2A). To ensure that only segments belonging to a single, constant leaf were kept, only segments that also overlapped with a straight line that extended from the center of the plant to the longest leaf tip were kept. Each of these ten segments were used as a mask for the hyperspectral image cube, and reflectance data was extracted for wavelengths 420 nm to 1000 nm after trimming off noisy wavelengths. The reflectance values of each pixel in the plant were then normalized by the L2-norm calculated on a whole image basis for each wavelength (see Hyperspectral Data Pre-processing and Normalization methods section). This normalized data was then exported for further analysis.

### *Outlier Detection and Removal*

Individual leaf segments for each plant were visually assessed by looking at the leaf segment binary masks and all data from the given segment excluded in the analysis if the segment encompassed multiple leaves (which happened in cases where part of the given segment was close to the whorl before leaves separated or when leaves overlapped each other), if the leaf segment had less than 25 pixels, or if the segment was not on the primary longest leaf (which occurred in some cases where the leaf curled or overlapped another leaf). A total of 156 plants of the entire 540 had at least one leaf segment excluded (29%); however, the final number of leaf segments excluded was 187 out of the total 5400 (3%). The majority of excluded segments were located adjacent to the whorl in cases where the leaves were short and the second leaf segment encompassed multiple leaves.

### *Prediction Model Development and Implementation*

All cubic support vector machine (SVM) models were developed using the Classification Learner application in MATLAB with specified response and predictor variables (MATLAB, 2018c). Cubic SVM models were selected after testing 13 different machine learning algorithms as these models consistently provided the highest prediction accuracy across the different applications specified in this study. A random subsampling of 1/6th of all pixels from all plants in the target dataset was used as the training dataset to create the model (Figure 4.10). Five-fold cross-validation was utilized to evaluate the performance of the algorithm during model building to prevent model overfitting during

training (Figure 4.10). This involved further randomly partitioning the data into a testing and training set five times. The training sets were used to train the supervised learning algorithm and the testing sets were used to obtain an average cross-validation error estimate to evaluate the algorithm performance. Each trained cubic SVM model was then exported and used to predict response classes for remaining 5/6th of pixels constituting the validation set and obtain prediction accuracy estimates (Figure 4.10).

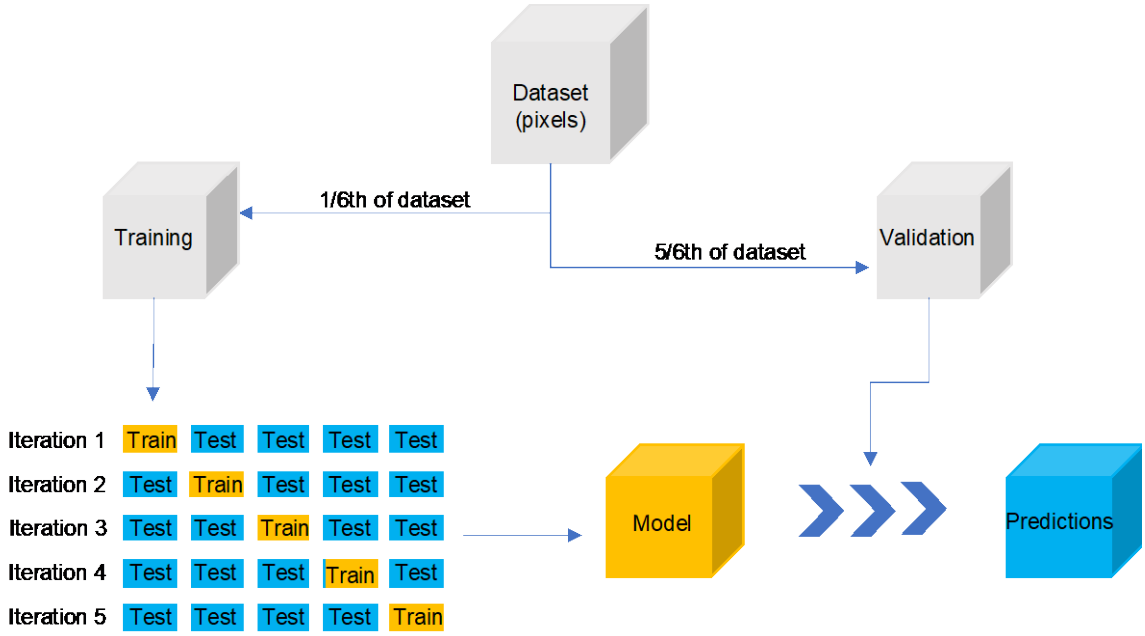


**Figure 4.10.** SVM model training and testing procedure.

### *Statistical Analyses*

The average spectra for each leaf segment of each plant was compared to the average spectra of each other segment as well as the average spectra for the entire leaf and the entire plant to assess which leaf segments significantly differ from each other. The comparisons were made by performing a pairwise Wilcoxon Rank Sum Test between

all pairwise comparisons of leaf segments using the pairwise.wilcox.test function from the R stats package (R Core Team, 2012).

### *RGB Trait Data Acquisition*

RGB side-view images of each set of plants were collected immediately following hyperspectral data collection using the procedures specified in Enders et al. (2019).

## DATA AVAILABILITY

The scripts and processes used to perform the data normalization and leaf segmentation are available at https://github.com/SBTirado/HS_LeafSegmentation.git. The hyperspectral dataset will be made available on Cyverse upon formal publication.

# BIBLIOGRAPHY

Acorsi, M. G., Abati Miranda, F. das D., Martello, M., Smaniotto, D. A., & Sartor, L. R. (2019). Estimating Biomass of Black Oat Using UAV-Based RGB Imaging. *Agronomy-Basel*, *9*(7). https://doi.org/10.3390/agronomy9070344

Afdhalia, F., Supriatna, S., Shidiq, I. P. A., Manessa, M. D. M., & Ristya, Y. (2019). Detection of Rice Varieties Based on Spectral Value Data using UAV-based Images. In Y. Setiawan, L. B. Prasetyo, Y. Murayama, T. D. Pham, G. J. Perez, & P. T. Dat (Eds.), *Sixth International Symposium on Lapan-Ipb Satellite (lisat 2019)* (Vol. 11372). Spie-Int Soc Optical Engineering. https://doi.org/10.1117/12.2541473

Agisoft, L. L. C. (2018). *Agisoft PhotoScan user manual: professional edition* (Version 1.2.6).

Agisoft, L. L. C., & St Petersburg, R. (2019). Agisoft metashape. *Professional Edition*, *7*. https://www.agisoft.com/

*AgiSoft PhotoScan Professional Edition (Version 1.4.4) (Software)*. (2018). https://www.agisoft.com/downloads/installer/

Alisaac, E., Behmann, J., Rathgeb, A., Karlovsky, P., Dehne, H.W., & Mahlein, A.K. (2019). Assessment of Fusarium Infection and Mycotoxin Contamination of Wheat Kernels and Flour Using Hyperspectral Imaging. *Toxins*, *11*(10).

https://doi.org/10.3390/toxins11100556

Al Makdessi, N., Jean, P.-A., Ecarnot, M., Gorretta, N., Rabatel, G., & Roumet, P. (2017). How plant structure impacts the biochemical leaf traits assessment from in-field hyperspectral images: A simulation study based on light propagation modeling in 3D virtual wheat scenes. *Field Crops Research*, *205*, 95–105.

Anderson, S. L., Murray, S. C., Malambo, L., Ratcliff, C., Popescu, S., Cope, D., Chang, A., Jung, J., & Thomasson, J. A. (2019). Prediction of Maize Grain Yield before Maturity Using Improved Temporal Height Estimates of Unmanned Aerial Systems. *The Plant Phenome Journal*, *2*. https://doi.org/10.2135/tppj2019.02.0004

Anthony, D., Elbaum, S., Lorenz, A., & Detweiler, C. (2014). On crop height estimation with UAVs. *2014 IEEE/RSJ International Conference on Intelligent Robots and Systems*, 4805–4812.

Araus, J. L., & Cairns, J. E. (2014). Field high-throughput phenotyping: the new crop breeding frontier. *Trends in Plant Science*, *19*(1), 52–61.

Asaari, M. S. M., Mishra, P., Mertens, S., Dhondt, S., Inzé, D., Wuyts, N., & Scheunders, P. (2018). Close-range hyperspectral image analysis for the early detection of stress responses in individual plants in a high-throughput phenotyping platform. *ISPRS Journal of Photogrammetry and Remote Sensing: Official Publication of the International Society for Photogrammetry and Remote Sensing* , *138*, 121–138.

Ashapure, A., Jung, J., Chang, A., Oh, S., Maeda, M., & Landivar, J. (2019). A

Comparative Study of RGB and Multispectral Sensor-Based Cotton Canopy Cover Modelling Using Multi-Temporal UAS Data. *Remote Sensing*, *11*(23). https://doi.org/10.3390/rs11232757

Ashourloo, D., Mobasheri, M. R., & Huete, A. (2014). Evaluating the Effect of Different Wheat Rust Disease Symptoms on Vegetation Indices Using Hyperspectral Measurements. *Remote Sensing*, *6*(6), 5107–5123.

Barker, J., Zhang, N., Sharon, J., Steeves, R., Wang, X., Wei, Y., & Poland, J. (2016). Development of a field-based high-throughput mobile phenotyping platform. *Computers and Electronics in Agriculture*, *122*, 74–85.

Barot, S., Allard, V., Cantarel, A., Enjalbert, J., Gauffreteau, A., Goldringer, I., Lata, J.-C., Le Roux, X., Niboyet, A., & Porcher, E. (2017). Designing mixtures of varieties for multifunctional agriculture with the help of ecology. A review. *Agronomy for Sustainable Development*, *37*(2), 13.

Barreiro, R., Carrigan, L., Ghaffarzadeh, M., Goldman, D. M., Hartman, M. E., Johnson, D. L., & Steenhoek, L. (2008). Device and method for screening a plant population for wind damage resistance traits (USPTO Patent No. 7412880). In *US Patent* (No. 7412880). https://patentimages.storage.googleapis.com/47/77/61/43f8dec323a37d/US7412880.pdf

Basso, B., & Liu, L. (2019). Chapter Four - Seasonal crop yield forecast: Methods,

applications, and accuracies. In D. L. Sparks (Ed.), *Advances in Agronomy* (Vol. 154, pp. 201–255). Academic Press.

Bauriegel, E., Giebel, A., Geyer, M., Schmidt, U., & Herppich, W. B. (2011). Early detection of Fusarium infection in wheat using hyper-spectral imaging. *Computers and Electronics in Agriculture*, *75*(2), 304–312.

Behmann, J., Mahlein, A.-K., Paulus, S., Kuhlmann, H., Oerke, E.-C., & Plümer, L. (2015). Calibration of hyperspectral close-range pushbroom cameras for plant phenotyping. *ISPRS Journal of Photogrammetry and Remote Sensing: Official Publication of the International Society for Photogrammetry and Remote Sensing* , *106*, 172–182.

Behmann, J., Schmitter, P., Steinrücken, J., & Plümer, L. (2014). Ordinal classification for efficient plant stress prediction in hyperspectral data. *ISPRS - International Archives of the Photogrammetry, Remote Sensing and Spatial Information Sciences*, *XL7*, 29.

Belton, D., Helmholz, P., Long, J., & Zerihun, A. (2019). Crop Height Monitoring Using a Consumer-Grade Camera and UAV Technology. *Pfg-Journal of Photogrammetry Remote Sensing and Geoinformation Science*, *87*(5-6), 249–262.

Benavente, E., García-Toledano, L., Carrillo, J. M., & Quemada, M. (2013). Thermographic Imaging: Assessment of Drought and Heat Tolerance in Spanish Germplasm of Brachypodium Distachyon. *Procedia Environmental Sciences*, *19*,

262–266.

Bendig, J., Bolten, A., & Bareth, G. (2013). UAV-based Imaging for Multi-Temporal, very high Resolution Crop Surface Models to monitor Crop Growth VariabilityMonitoring des Pflanzenwachstums mit Hilfe multitemporaler und hoch auflösender Oberflächenmodelle von Getreidebeständen auf Basis von Bildern aus UAV-Befliegungen. *Photogrammetrie - Fernerkundung - Geoinformation*, *2013*(6), 551–562.

Bendig, J., Bolten, A., Bennertz, S., Broscheit, J., Eichfuss, S., & Bareth, G. (2014). Estimating Biomass of Barley Using Crop Surface Models (CSMs) Derived from UAV-Based RGB Imaging. *Remote Sensing*, *6*(11), 10395–10412.

Bendig, J., Willkomm, M., Tilly, N., Gnyp, M. L., Bennertz, S., Qiang, C., Miao, Y., Lenz-Wiedemann, V. I. S., & Bareth, G. (2013). Very high resolution crop surface models (CSMs) from UAV-based stereo images for rice growth monitoring in Northeast China. *Int. Arch. Photogramm. Remote Sens. Spat. Inf. Sci*, *40*, 45–50.

Biju, S., Fuentes, S., & Gupta, D. (2018). The use of infrared thermal imaging as a non-destructive screening tool for identifying drought-tolerant lentil genotypes. *Plant Physiology and Biochemistry: PPB / Societe Francaise de Physiologie Vegetale*, *127*, 11–24.

Blackburn, G. A. (2007). Hyperspectral remote sensing of plant pigments. *Journal of Experimental Botany*, *58*(4), 855–867.

Board, J. E., & Harville, B. G. (1992). Explanations for Greater Light Interception in Narrow- vs. Wide-Row. *Crop Science*, *32*(1), 198–202.

Boyer, J. S. (1982). Plant productivity and environment. *Science*, *218*(4571), 443–448.

Brocks, S., & Bareth, G. (2018). Estimating Barley Biomass with Crop Surface Models from Oblique RGB Imagery. *Remote Sensing*, *10*(2). https://doi.org/10.3390/rs10020268

Bruce, W., Desbons, P., Crasta, O., & Folkerts, O. (2001). Gene expression profiling of two related maize inbred lines with contrasting root-lodging traits. *Journal of Experimental Botany*, *52*(Spec Issue), 459–468.

Burnette, M., Kooper, R., Maloney, J. D., Rohde, G. S., Terstriep, J. A., Willis, C., Fahlgren, N., Mockler, T., Newcomb, M., Sagan, V., Andrade-Sanchez, P., Shakoor, N., Sidike, P., Ward, R., & LeBauer, D. (2018). TERRA-REF Data Processing Infrastructure. *Proceedings of the Practice and Experience on Advanced Research Computing*, 1–7.

Busemeyer, L., Mentrup, D., Möller, K., Wunder, E., Alheit, K., Hahn, V., Maurer, H. P., Reif, J. C., Würschum, T., Müller, J., & Others. (2013). BreedVision—A multi-sensor platform for non-destructive field-based phenotyping in plant breeding. *Sensors* , *13*(3), 2830–2847.

Campillo, C., Prieto, M. H., Daza, C., Moñino, M. J., & García, M. I. (2008). Using Digital Images to Characterize Canopy Coverage and Light Interception in a

Processing Tomato Crop. *HortScience: A Publication of the American Society for Horticultural Science*, *43*(6), 1780–1786.

Chang, A., Jung, J., Maeda, M. M., & Landivar, J. (2017). Crop height monitoring with digital imagery from Unmanned Aerial System (UAS). *Computers and Electronics in Agriculture*, *141*, 232–237.

Chen, J. M., & Black, T. A. (1992). Defining leaf area index for non-flat leaves. *Plant, Cell & Environment*, *15*(4), 421–429.

Chen, P., Haboudane, D., Tremblay, N., Wang, J., Vigneault, P., & Li, B. (2010). New spectral indicator assessing the efficiency of crop nitrogen treatment in corn and wheat. *Remote Sensing of Environment*, *114*(9), 1987–1997.

Ching, A., Rafalski, J. A., Luck, S., & Butruille, M. G. (2010). Genetic Loci Associated with Mechanical Stalk Strength in Maize (U.S. Patent and Trademark Office. Patent No. 0015623A1). In *Patent* (No. 0015623A1).

Chu, T., Starek, M. J., Brewer, M. J., Murray, S. C., & Pruter, L. S. (2018). Characterizing canopy height with UAS structure-from-motion photogrammetry—results analysis of a maize field trial with respect to multiple factors. *Remote Sensing Letters* , *9*(8), 753–762.

Comar, A., Burger, P., de Solan, B., Baret, F. D. R., Daumard, F., & Hanocq, J.-F. O. (2012). A semi-automatic system for high throughput phenotyping wheat cultivars in-field conditions: description and first results. *Functional Plant Biology: FPB*,

*39*(11), 914–924.

Dammer, K.-H., Thöle, H., Volk, T., & Hau, B. (2009). Variable-rate fungicide spraying in real time by combining a plant cover sensor and a decision support system. *Precision Agriculture*, *10*(5), 431–442.

Dhugga, K. S. (2007). Maize Biomass Yield and Composition for Biofuels. *Crop Science*, *47*, 2211–2227.

Díaz-Varela, R. A., De la Rosa, R., León, L., & Zarco-Tejada, P. J. (2015). High-Resolution Airborne UAV Imagery to Assess Olive Tree Crown Parameters Using 3D Photo Reconstruction: Application in Breeding Trials. *Remote Sensing*, *7*(4), 4213–4232.

*DigitalGlobe | WorldView-3*. (n.d.). Retrieved July 16, 2020, from http://worldview3.digitalglobe.com/

Dobbels, A. A., & Lorenz, A. J. (2019). Soybean iron deficiency chlorosis high throughput phenotyping using an unmanned aircraft system. *Plant Methods*, *15*, 97.

Duan, B., Liu, Y., Gong, Y., Peng, Y., Wu, X., Zhu, R., & Fang, S. (2019). Remote estimation of rice LAI based on Fourier spectrum texture from UAV image. *Plant Methods*, *15*(1), 124.

Duvick, D. N. (2005). Genetic progress in yield of United States maize (Zea mays L.). *Maydica*, *50*(3/4), 193.

Enders, T. A., St Dennis, S., Oakland, J., Callen, S. T., Gehan, M. A., Miller, N. D., Spalding, E. P., Springer, N. M., & Hirsch, C. D. (2019). Classifying cold-stress responses of inbred maize seedlings using RGB imaging. *Plant Direct*, *3*(1), e00104.

Ennos, A. R., Crook, M. J., & Grimshaw, C. (1993). The Anchorage Mechanics of Maize,Zea mays. In *Journal of Experimental Botany* (Vol. 44, Issue 1, pp. 147–153). https://doi.org/10.1093/jxb/44.1.147

FAA. (n.d.). *Unmanned Aircraft Systems (UAS)*. Retrieved July 16, 2020, from https://www.faa.gov/uas/

Fahlgren, N., Gehan, M. A., & Baxter, I. (2015). Lights, camera, action: high-throughput plant phenotyping is ready for a close-up. *Current Opinion in Plant Biology*, *24*, 93–99.

Feng, A., Zhang, M., Sudduth, K. A., Vories, E. D., & Zhou, J. (2019). COTTON YIELD ESTIMATION FROM UAV-BASED PLANT HEIGHT. *Transactions of the Asabe*, *62*(2), 393–403.

Feng, X., Zhan, Y., Wang, Q., Yang, X., Yu, C., Wang, H., Tang, Z., Jiang, D., Peng, C., & He, Y. (2020). Hyperspectral imaging combined with machine learning as a tool to obtain high-throughput plant salt-stress phenotyping. *The Plant Journal: For Cell and Molecular Biology*, *101*(6), 1448–1461.

Flint-Garcia, S. A., Jampatong, C., Darrah, L. L., & McMullen, M. D. (2003). Quantitative trait locus analysis of stalk strength in four maize populations. *Crop*

*Science*, *43*(1), 13–22.

Fouéré, A., Pellerin, S., & Duparque, A. (1995). A Portable Electronic Device for Evaluating Root Lodging Resistance in Maize. *Agronomy Journal*, *87*(5), 1020–1024.

Freeman, K. W., Girma, K., Arnall, D. B., Mullen, R. W., Martin, K. L., Teal, R. K., & Raun, W. R. (2007). By-Plant Prediction of Corn Forage Biomass and Nitrogen Uptake at Various Growth Stages Using Remote Sensing and Plant Height. *Agronomy Journal*, *99*(2), 530–536.

Fukatsu, T., Watanabe, T., Hu, H., Yoichi, H., & Hirafuji, M. (2012). Field monitoring support system for the occurrence of Leptocorisa chinensis Dallas (Hemiptera: Alydidae) using synthetic attractants, Field Servers, and image analysis. *Computers and Electronics in Agriculture*, *80*, 8–16.

Gamon, J. A., Field, C. B., Goulden, M. L., Griffin, K. L., Hartley, A. E., Joel, G., Peñuelas, J., & Valentini, R. (1995). Relationships Between NDVI, Canopy Structure, and Photosynthesis in Three Californian Vegetation Types. *Ecological Applications: A Publication of the Ecological Society of America*, *5*(1), 28–41.

Geipel, J., Link, J., & Claupein, W. (2014). Combined Spectral and Spatial Modeling of Corn Yield Based on Aerial Images and Crop Surface Models Acquired with an Unmanned Aircraft System. *Remote Sensing*, *6*(11), 10335–10355.

Gitelson, A. A., Viña, A., Verma, S. B., Rundquist, D. C., Arkebauer, T. J., Keydan, G.,

Leavitt, B., Ciganda, V., Burba, G. G., & Suyker, A. E. (2006). Relationship between gross primary production and chlorophyll content in crops: Implications for the synoptic monitoring of vegetation productivity. *Journal of Geophysical Research*, *111*(D8), 168.

Gómez-Candón, D., De Castro, A. I., & López-Granados, F. (2014). Assessing the accuracy of mosaics from unmanned aerial vehicle (UAV) imagery for precision agriculture purposes in wheat. *Precision Agriculture*, *15*. https://doi.org/10.1007/s11119-013-9335-4

Grenzdörffer, G. J. (2014). *Crop height determination with UAS point clouds*. *XL-1*, 135–140.

Haboudane, D., Miller, J. R., Tremblay, N., Zarco-Tejada, P. J., & Dextraze, L. (2002). Integrated narrow-band vegetation indices for prediction of crop chlorophyll content for application to precision agriculture. *Remote Sensing of Environment*, *81*(2), 416–426.

Han, L., Yang, G., Dai, H., Xu, B., Yang, H., Feng, H., Li, Z., & Yang, X. (2019). Modeling maize above-ground biomass based on machine learning approaches using UAV remote-sensing data. *Plant Methods*, *15*, 10.

Han, L., Yang, G., Dai, H., Yang, H., Xu, B., Feng, H., Li, Z., & Yang, X. (2019). Fuzzy Clustering of Maize Plant-Height Patterns Using Time Series of UAV Remote-Sensing Images and Variety Traits. *Frontiers in Plant Science*, *10*, 926.

Han, L., Yang, G., Yang, H., Xu, B., Li, Z., & Yang, X. (2018). Clustering Field-Based Maize Phenotyping of Plant-Height Growth and Canopy Spectral Dynamics Using a UAV Remote-Sensing Approach. *Frontiers in Plant Science*, *9*, 1638.

Hasan, U., Sawut, M., & Chen, S. (2019). Estimating the Leaf Area Index of Winter Wheat Based on Unmanned Aerial Vehicle RGB-Image Parameters. *Sustainability: Science Practice and Policy*, *11*(23). https://doi.org/10.3390/su11236829

Hassan, M. A., Yang, M., Fu, L., Rasheed, A., Zheng, B., Xia, X., Xiao, Y., & He, Z. (2019). Accuracy assessment of plant height using an unmanned aerial vehicle for quantitative genomic analysis in bread wheat. *Plant Methods*, *15*, 37.

Hébert, Y., Guingo, E., & Loudet, O. (2001). The Response of Root/Shoot Partitioning and Root Morphology to Light Reduction in Maize Genotypes This research was supported by a grant from Région Poitou-Charentes (no. 94/RPC-R-138). *Crop Science*, *41*, 363–371.

Holman, F. H., Riche, A. B., Michalski, A., Castle, M., Wooster, M. J., & Hawkesford, M. J. (2016). High Throughput Field Phenotyping of Wheat Plant Height and Growth Rate in Field Plot Trials Using UAV Based Remote Sensing. *Remote Sensing*, *8*(12), 1031.

Hu, P., Chapman, S. C., Wang, X., Potgieter, A., Duan, T., Jordan, D., Guo, Y., & Zheng, B. (2018). Estimation of plant height using a high throughput phenotyping platform based on unmanned aerial vehicle and self-calibration: Example for sorghum

breeding. *European Journal of Agronomy: The Journal of the European Society for Agronomy*, *95*, 24–32.

James, M. R., & Robson, S. (2012). Straightforward reconstruction of 3D surfaces and topography with a camera: Accuracy and geoscience application. *Journal of Geophysical Research*, *117*(F3). https://doi.org/10.1029/2011JF002289

Jannink, J.-L., Jordan, N. R., & Orf, J. H. (2001). Feasibility of selection for high weed suppressive ability in soybean: Absence of tradeoffs between rapid initial growth and sustained later growth. *Euphytica/ Netherlands Journal of Plant Breeding*, *120*(2), 291–300.

Jannoura, R., Brinkmann, K., Uteau, D., Bruns, C., & Joergensen, R. G. (2015). Monitoring of crop biomass using true colour aerial photographs taken from a remote controlled hexacopter. *Biosystems Engineering*, *129*, 341–351.

Jiang, W., Wang, K., Wu, Q., Dong, S., Liu, P., & Zhang, J. (2013). Effects of narrow plant spacing on root distribution and physiological nitrogen use efficiency in summer maize. *The Crop Journal*, *1*(1), 77–83.

Jin, X., Shi, C., Yu, C. Y., Yamada, T., & Sacks, E. J. (2017). Determination of Leaf Water Content by Visible and Near-Infrared Spectrometry and Multivariate Calibration in Miscanthus. *Frontiers in Plant Science*, *8*, 721.

Jones, H. G., Stoll, M., Santos, T., de Sousa, C., Chaves, M. M., & Grant, O. M. (2002). Use of infrared thermography for monitoring stomatal closure in the field:

application to grapevine. *Journal of Experimental Botany*, *53*(378), 2249–2260.

Kamara, A. Y., Kling, J. G., Menkir, A., & Ibikunle, O. (2003). Association of Vertical Root-Pulling Resistance with Root Lodging and Grain Yield in Selected S 1 Maize Lines Derived from a Tropical Low-Nitrogen Population. *Journal of Agronomy and Crop Science*, *189*(3), 129–135.

Katsvairo, T. W., Cox, W. J., Van Es, H. M., & Glos, M. (2003). Spatial Yield Response of Two Corn Hybrids at Two Nitrogen Levels. *Agronomy Journal*, *95*(4), 1012–1022.

Kefauver, S. C., Vicente, R., Vergara-Diaz, O., Fernandez-Gallego, J. A., Kerfal, S., Lopez, A., Melichar, J. P. E., Serret Molins, M. D., & Araus, J. L. (2017). Comparative UAV and Field Phenotyping to Assess Yield and Nitrogen Use Efficiency in Hybrid and Conventional Barle. *Frontiers in Plant Science*, *8*. https://doi.org/10.3389/fpls.2017.01733

Kong, W., Zhang, C., Huang, W., Liu, F., & He, Y. (2018). Application of Hyperspectral Imaging to Detect Sclerotinia sclerotiorum on Oilseed Rape Stems. *Sensors* , *18*(1). https://doi.org/10.3390/s18010123

Kuhn, M., Wing, J., Weston, S., Williams, A., Keefer, C., Engelhardt, A., Cooper, T., Mayer, Z., Kenkel, B., & Others. (2016). *Caret: Classification and regression training. R package version 6.0-78*. R Project, https://CRAN. R-project. org/package= caret.

Landi, P., Sanguineti, M. C., Liu, C., Li, Y., Wang, T. Y., Giuliani, S., Bellotti, M., Salvi, S., & Tuberosa, R. (2007). Root-ABA1 QTL affects root lodging, grain yield, and other agronomic traits in maize grown under well-watered and water-stressed conditions. *Journal of Experimental Botany*, *58*(2), 319–326.

Lang, Q., Zhiyong, Z., Longsheng, C., Hong, S., Minzan, L., Li, L., & Junyong, M. (2019). Detection of Chlorophyll Content in Maize Canopy from UAV Imagery. *IFAC-PapersOnLine*, *52*(30), 330–335.

Laybros, A., Schläpfer, D., Féret, J.-B., Descroix, L., Bedeau, C., Lefevre, M.-J., & Vincent, G. (2019). Across Date Species Detection Using Airborne Imaging Spectroscopy. *Remote Sensing*, *11*(7), 789.

Lemaire, G., & Gastal, F. (1997). N Uptake and Distribution in Plant Canopies. In G. Lemaire (Ed.), *Diagnosis of the Nitrogen Status in Crops* (pp. 3–43). Springer Berlin Heidelberg.

Li, L., Zhang, Q., & Huang, D. (2014). A review of imaging techniques for plant phenotyping. *Sensors* , *14*(11), 20078–20111.

Li, P., Ponnala, L., Gandotra, N., Wang, L., Si, Y., Tausta, S. L., Kebrom, T. H., Provart, N., Patel, R., Myers, C. R., Reidel, E. J., Turgeon, R., Liu, P., Sun, Q., Nelson, T., & Brutnell, T. P. (2010). The developmental dynamics of the maize leaf transcriptome. *Nature Genetics*, *42*(12), 1060–1067.

Li, S., Yuan, F., Ata-UI-Karim, S. T., Zheng, H., Cheng, T., Liu, X., Tian, Y., Zhu, Y.,

Cao, W., & Cao, Q. (2019). Combining Color Indices and Textures of UAV-Based Digital Imagery for Rice LAI Estimation. *Remote Sensing*, *11*(15). https://doi.org/10.3390/rs11151763

Li S.-Y., Wang Y.-X., Hu C., & Yan Y. (2015). [Effects of strong wind lodging at pre- and post-tasseling stages on growth and yield of summer maize]. *Ying yong sheng tai xue bao = The journal of applied ecology / Zhongguo sheng tai xue xue hui, Zhongguo ke xue yuan Shenyang ying yong sheng tai yan jiu suo zhu ban*, *26*(8), 2405–2413.

Liu, J., Cai, H., Chu, Q., Chen, X., Chen, F., Yuan, L., Mi, G., & Zhang, F. (2011). Genetic analysis of vertical root pulling resistance (VRPR) in maize using two genetic populations. *Molecular Breeding: New Strategies in Plant Improvement*, *28*(4), 463–474.

Liu, S., Song, F., Liu, F., Zhu, X., & Xu, H. (2012). Effect of Planting Density on Root Lodging Resistance and Its Relationship to Nodal Root Growth Characteristics in Maize (Zea mays L.). *Journal of Agricultural Sciences*, *4*(12), 182–189.

Li, W., Niu, Z., Chen, H., & Li, D. (2017). Characterizing canopy structural complexity for the estimation of maize LAI based on ALS data and UAV stereo images. *International Journal of Remote Sensing*, *38*(8-10), 2106–2116.

Li, W., Niu, Z., Chen, H., Li, D., Wu, M., & Zhao, W. (2016). Remote estimation of canopy height and aboveground biomass of maize using high-resolution stereo

images from a low-cost unmanned aerial vehicle system. *Ecological Indicators*, *67*, 637–648.

Li, W., Niu, Z., Gao, S., Huang, N., & Chen, H. (2014). Correlating the Horizontal and Vertical Distribution of LiDAR Point Clouds with Components of Biomass in a Picea crassifolia Forest. *Forests, Trees and Livelihoods*, *5*(8), 1910–1930.

Li, W., Niu, Z., Huang, N., Wang, C., Gao, S., & Wu, C. (2015). Airborne LiDAR technique for estimating biomass components of maize: A case study in Zhangye City, Northwest China. *Ecological Indicators*, *57*, 486–496.

Li, Z., Coffey, L., Garfin, J., Miller, N. D., White, M. R., Spalding, E. P., de Leon, N., Kaeppler, S. M., Schnable, P. S., Springer, N. M., & Hirsch, C. N. (2018). Genotype-by-environment interactions affecting heterosis in maize. *PloS One*, *13*(1), e0191321.

Lundgren, J. (2019, April 16). *SPLINEFIT - File Exchange - MATLAB Central*. https://www.mathworks.com/matlabcentral/fileexchange/71225-splinefit

Lu, N., Zhou, J., Han, Z., Li, D., Cao, Q., Yao, X., Tian, Y., Zhu, Y., Cao, W., & Cheng, T. (2019). Improved estimation of aboveground biomass in wheat from RGB imagery and point cloud data acquired with a low-cost unmanned aerial vehicle system. *Plant Methods*, *15*, 17.

Madec, S., Baret, F., de Solan, B., Thomas, S., Dutartre, D., Jezequel, S., Hemmerlé, M., Colombeau, G., & Comar, A. (2017). High-Throughput Phenotyping of Plant

Height: Comparing Unmanned Aerial Vehicles and Ground LiDAR Estimates. *Frontiers in Plant Science*, *8*, 2002.

Ma, D., Xie, R., Liu, X., Niu, X., Hou, P., Wang, K., Lu, Y., & Li, S. (2014). Lodging-Related Stalk Characteristics of Maize Varieties in China since the 1950s. *Crop Science*, *54*(6), 2805–2814.

Mahlein, A.-K., Alisaac, E., Al Masri, A., Behmann, J., Dehne, H.-W., & Oerke, E.-C. (2019). Comparison and Combination of Thermal, Fluorescence, and Hyperspectral Imaging for Monitoring Fusarium Head Blight of Wheat on Spikelet Scale. *Sensors* , *19*(10). https://doi.org/10.3390/s19102281

Mahlein, A.-K., Steiner, U., Hillnhütter, C., Dehne, H.-W., & Oerke, E.-C. (2012). Hyperspectral imaging for small-scale analysis of symptoms caused by different sugar beet diseases. *Plant Methods*, *8*(1), 3.

Maimaitijiang, M., Ghulam, A., Sidike, P., Hartling, S., Maimaitiyiming, M., Peterson, K., Shavers, E., Fishman, J., Peterson, J., Kadam, S., Burken, J., & Fritschi, F. (2017). Unmanned Aerial System (UAS)-based phenotyping of soybean using multi-sensor data fusion and extreme learning machine. *ISPRS Journal of Photogrammetry and Remote Sensing: Official Publication of the International Society for Photogrammetry and Remote Sensing* , *134*, 43–58.

Maimaitijiang, M., Sagan, V., Sidike, P., Hartling, S., Esposito, F., & Fritschi, F. B. (2020). Soybean yield prediction from UAV using multimodal data fusion and deep

learning. *Remote Sensing of Environment*, *237*. https://doi.org/10.1016/j.rse.2019.111599

Maimaitijiang, M., Sagan, V., Sidike, P., Maimaitiyiming, M., Hartling, S., Peterson, K. T., Maw, M. J. W., Shakoor, N., Mockler, T., & Fritschi, F. B. (2019). Vegetation Index Weighted Canopy Volume Model (CVMVI) for soybean biomass estimation from Unmanned Aerial System-based RGB imagery. *ISPRS Journal of Photogrammetry and Remote Sensing: Official Publication of the International Society for Photogrammetry and Remote Sensing* , *151*, 27–41.

Makanza, R., Zaman-Allah, M., Cairns, J. E., Magorokosho, C., Tarekegne, A., Olsen, M., & Prasanna, B. M. (2018). High-Throughput Phenotyping of Canopy Cover and Senescence in Maize Field Trials Using Aerial Digital Canopy Imaging. *Remote Sensing*, *10*(2). https://doi.org/10.3390/rs10020330

Malambo, L., Popescu, S. C., Murray, S. C., Putman, E., Pugh, N. A., Horne, D. W., Richardson, G., Sheridan, R., Rooney, W. L., Avant, R., Vidrine, M., McCutchen, B., Baltensperger, D., & Bishop, M. (2018). Multitemporal field-based plant height estimation using 3D point clouds generated from small unmanned aerial systems high-resolution imagery. *International Journal of Applied Earth Observation and Geoinformation*, *64*, 31–42.

Marcial-Pablo, M. de J., Gonzalez-Sanchez, A., Jimenez-Jimenez, S. I., Ontiveros-Capurata, R. E., & Ojeda-Bustamante, W. (2019). Estimation of vegetation fraction using RGB and multispectral images from UAV. *International Journal of Remote*

*Sensing*, *40*(2), 420–438.

Martynenko, A., Shotton, K., Astatkie, T., Petrash, G., Fowler, C., Neily, W., & Critchley, A. T. (2016). Thermal imaging of soybean response to drought stress: the effect of Ascophyllum nodosum seaweed extract. *SpringerPlus*, *5*(1), 1393.

Masuka, B., Araus, J. L., Das, B., Sonder, K., & Cairns, J. E. (2012). Phenotyping for abiotic stress tolerance in maize. *Journal of Integrative Plant Biology*, *54*(4), 238–249.

Matese, A., Toscano, P., Di Gennaro, S. F., Genesio, L., Vaccari, F. P., Primicerio, J., Belli, C., Zaldei, A., Bianconi, R., & Gioli, B. (2015). Intercomparison of UAV, Aircraft and Satellite Remote Sensing Platforms for Precision Viticulture. *Remote Sensing*, *7*(3), 2971–2990.

*MATLAB R2018b* (Version 9.5.0). (2018a). [Computer software]. The MathWorks, Inc.

*MATLAB Image Processing Toolbox Release R2018b*. (2018b). The MathWorks, Inc.

*MATLAB Statistics and Machine Learning Toolbox Release R2018b*. (2018c). The MathWorks, Inc.

Mattupalli, C., Moffet, C. A., Shah, K. N., & Young, C. A. (2018). Supervised Classification of RGB Aerial Imagery to Evaluate the Impact of a Root Rot Disease. *Remote Sensing*, *10*(6). https://doi.org/10.3390/rs10060917

McFarland, B. A., AlKhalifah, N., Bohn, M., Bubert, J., Buckler, E. S., Ciampitti, I., Edwards, J., Ertl, D., Gage, J. L., Falcon, C. M., Flint-Garcia, S., Gore, M. A., Graham, C., Hirsch, C. N., Holland, J. B., Hood, E., Hooker, D., Jarquin, D., Kaeppler, S. M., … de Leon, N. (2020). Maize genomes to fields (G2F): 2014–2017 field seasons: genotype, phenotype, climatic, soil, and inbred ear image datasets. *BMC Research Notes*, *13*(1), 71.

Meacham-Hensold, K., Montes, C. M., Wu, J., Guan, K., Fu, P., Ainsworth, E. A., Pederson, T., Moore, C. E., Brown, K. L., Raines, C., & Bernacchi, C. J. (2019). High-throughput field phenotyping using hyperspectral reflectance and partial least squares regression (PLSR) reveals genetic modifications to photosynthetic capacity. *Remote Sensing of the Environment*, *231*, 111176.

Michalski A, Riche A, Castle M, Holman F, Hawkesford M, Wooster M. (n.d.). *UAS in 3D Crop Modeling for Agricultural Research*. 1314–0604.

Michez, A., Bauwens, S., Brostaux, Y., Hiel, M.-P., Garre, S., Lejeune, P., & Dumont, B. (2018). How Far Can Consumer-Grade UAV RGB Imagery Describe Crop Production? A 3D and Multitemporal Modeling Approach Applied to Zea mays. *Remote Sensing*, *10*(11). https://doi.org/10.3390/rs10111798

Milas, A. S., Romanko, M., Reil, P., Abeysinghe, T., & Marambe, A. (2018). The importance of leaf area index in mapping chlorophyll content of corn under different agricultural treatments using UAV images. *International Journal of Remote Sensing*, *39*(15-16), 5415–5431.

Minnesota Department of Natural Resources. (2020, March 5). *Daily Data: University of MN St Paul Station ID 218450*. The Minnesota Department of Natural Resources Website. https://www.dnr.state.mn.us/climate/historical/daily-data.html?sid=218450&sname=UNIVERSITY%20OF%20MN%20ST.%20PAUL&sdate=por&edate=por

Moghimi, A., Yang, C., Miller, M. E., Kianian, S. F., & Marchetto, P. M. (2018). A Novel Approach to Assess Salt Stress Tolerance in Wheat Using Hyperspectral Imaging. *Frontiers in Plant Science*, *9*, 1182.

Myles, S., Peiffer, J., Brown, P. J., Ersoz, E. S., Zhang, Z., Costich, D. E., & Buckler, E. S. (2009). Association mapping: critical considerations shift from genotyping to experimental design. *The Plant Cell*, *21*(8), 2194–2202.

Na, S.-I., Park, C.-W., So, K.-H., Ahn, H.-Y., & Lee, K. (2018). Development of Biomass Evaluation Model of Winter Crop Using RGB imagery Based on Unmanned Aerial Vehicle. *Korean Journal of Remote Sensing*, *34*(5), 709–720.

Nelimor, C., Badu-Apraku, B., Tetteh, A. Y., Garcia-Oliveira, A. L., & N'guetta, A. S.-P. (2020). Assessing the Potential of Extra-Early Maturing Landraces for Improving Tolerance to Drought, Heat, and Both Combined Stresses in Maize. *Agronomy*, *10*(3), 318.

Nicolas, Virlet, Kasra, Sabermanesh, Pouria, Sadeghi-Tehran, J., M., & Hawkesford. (2017). Field Scanalyzer: An automated robotic field phenotyping platform for

detailed crop monitoring. *Functional Plant Biology: FPB*, *44 (1*. https://doi.org/10.1071/FP16163

Niu, Y., Zhang, L., Zhang, H., Han, W., & Peng, X. (2019). Estimating Above-Ground Biomass of Maize Using Features Derived from UAV-Based RGB Imagery. *Remote Sensing*, *11*(11). https://doi.org/10.3390/rs11111261

Obeidat, W., Avila, L., Earl, H., & Lukens, L. (2018). Leaf Spectral Reflectance of Maize Seedlings and Its Relationship to Cold Tolerance. *Crop Science*, *58*(6), 2569–2580.

Oerke, E.-C., Steiner, U., Dehne, H.-W., & Lindenthal, M. (2006). Thermal imaging of cucumber leaves affected by downy mildew and environmental conditions. *Journal of Experimental Botany*, *57*(9), 2121–2132.

Pandey, P., Ge, Y., Stoerger, V., & Schnable, J. C. (2017). High Throughput In vivo Analysis of Plant Leaf Chemical Properties Using Hyperspectral Imaging. *Frontiers in Plant Science*, *8*, 1348.

Pantazi, X.-E., Dimitrios MoshouauthorAristotle University, School of Agriculture, Agricultural Engineering Laboratory, Thessaloniki 54124, Greece, & Cedric BravoauthorQIPACK BVBA, Milsestraat 101b, 3053 Leuven (Haasrode), Belgium. (2015). *Active learning system for weed species recognition based on hyperspectral sensing*. https://doi.org/10.1016/j.biosystemseng.2016.01.014

Park, B., & Lu, R. (Eds.). (2015). *Hyperspectral Imaging Technology in Food and Agriculture*. Springer, New York, NY.

Paulus, S. (2019). Measuring crops in 3D: using geometry for plant phenotyping. *Plant Methods*, *15*, 103.

Pix4D. (n.d.). *Pix4Dmapper: professional drone mapping and photogrammetry software*. Pix4D. Retrieved July 16, 2020, from https://www.pix4d.com/product/pix4dmapper-photogrammetry-software

*Pix4Dcapture: Free drone flight planning mobile app*. (n.d.). Pix4D. Retrieved July 16, 2020, from https://www.pix4d.com/product/pix4dcapture

Puig, E., Gonzalez, F., Hamilton, G., & Grundy, P. (2015). Assessment of crop insect damage using unmanned aerial systems: A machine learning approach. In T. Weber, M. J. McPhee, & R. S. Anderssen (Eds.), *21st International Congress on Modelling and Simulation (modsim2015)* (pp. 1420–1426). Modelling & Simulation Soc Australia & New Zealand Inc.

Purcell, L. C. (2000). Soybean Canopy Coverage and Light Interception Measurements Using Digital Imagery. *Crop Science*, *40*(3), 834–837.

QGIS Development Team. (2017). *QGIS* (Version 2.18.9) [Computer software]. https://qgis.org/en/site/

Qiu, R., Yang, C., Moghimi, A., Zhang, M., Steffenson, B. J., & Hirsch, C. D. (2019). Detection of Fusarium Head Blight in wheat using a deep neural network and color imaging. *Remote Sensing*, *11*(22), 2658.

R Core Team. (2012). *R: A language and environment for statistical computing*.

http://www.R-project.org/. ISBN 3-900051-07-0.

Ripullone, F., Grassi, G., Lauteri, M., & Borghetti, M. (2003). Photosynthesis-nitrogen relationships: interpretation of different patterns between Pseudotsuga menziesii and Populus x euroamericana in a mini-stand experiment. *Tree Physiology*, *23*(2), 137–144.

Robertson, D., Smith, S., Gardunia, B., & Cook, D. (2014). An Improved Method for Accurate Phenotyping of Corn Stalk Strength. *Crop Science*, *54*(5), 2038–2044.

Römer, C., Wahabzada, M., Ballvora, A., Pinto, F., Rossini, M., Panigada, C., Behmann, J., Léon, J., Thurau, C., Bauckhage, C., Kersting, K., Rascher, U., & Plümer, L. (2012). Early drought stress detection in cereals: simplex volume maximisation for hyperspectral image analysis. *Functional Plant Biology: FPB*, *39*(11), 878–890.

Roth, L., Aasen, H., Walter, A., & Liebisch, F. (2018). Extracting leaf area index using viewing geometry effects-A new perspective on high-resolution unmanned aerial system photography. *ISPRS Journal of Photogrammetry and Remote Sensing: Official Publication of the International Society for Photogrammetry and Remote Sensing* , *141*, 161–175.

Ruckelshausen, A., Biber, P., Dorna, M., Gremmes, H., Klose, R., Linz, A., Rahe, F., Resch, R., Thiel, M., Trautz, D., & Others. (2009). BoniRob--an autonomous field robot platform for individual plant phenotyping. *Precision Agriculture*, *9*(841), 1.

Ruiz, J. J., Diaz-Mas, L., Perez, F., & Viguria, A. (2013). Evaluating the accuracy of

DEM generation algorithms from UAV imagery. *Int. Arch. Photogramm. Remote Sens. Spat. Inf. Sci*, *40*, 333–337.

Rumpf, T., Mahlein, A.-K., Steiner, U., Oerke, E.-C., Dehne, H.-W., & Plümer, L. (2010). Early detection and classification of plant diseases with Support Vector Machines based on hyperspectral reflectance. *Computers and Electronics in Agriculture*, *74*(1), 91–99.

Sanches, G. M., Duft, D. G., Kolln, O. T., dos Santos Luciano, A. C., Quassi De Castro, S. G., Okuno, F. M., & Junqueira Franco, H. C. (2018). The potential for RGB images obtained using unmanned aerial vehicle to assess and predict yield in sugarcane fields. *International Journal of Remote Sensing*, *39*(15-16), 5402–5414.

Sanguineti, M. C., Giuliani, M. M., Govi, G., Tuberosa, R., & Landi, P. (1998). Root and shoot traits of maize inbred lines grown in the field and in hydroponic culture and their relationships with root lodging. *Maydica*, *43*, 211–216.

Schirrmann, M., Giebel, A., Gleiniger, F., Pflanz, M., Lentschke, J., & Dammer, K.-H. (2016). Monitoring Agronomic Parameters of Winter Wheat Crops with Low-Cost UAV Imagery. *Remote Sensing*, *8*(9). https://doi.org/10.3390/rs8090706

Sharma, L., & Bali, S. (2017). A Review of Methods to Improve Nitrogen Use Efficiency in Agriculture. In *Sustainability* (Vol. 10, Issue 2, p. 51). https://doi.org/10.3390/su10010051

Sharma, L. K., & Franzen, D. W. (2014). Use of corn height to improve the relationship

between active optical sensor readings and yield estimates. In *Precision Agriculture* (Vol. 15, Issue 3, pp. 331–345). https://doi.org/10.1007/s11119-013-9330-9

Sher, A., Khan, A., Cai, L. J., Ahmad, M. I., Asharf, U., & Jamoro, S. A. (2017). Response of Maize Grown Under High Plant Density; Performance, Issues and Management - A Critical Review. *Advances in Crop Science and Technology*, *5*(3), 1–8.

Shibles, R. M., & Weber, C. R. (1965). Leaf Area, Solar Radiation Interception and Dry Matter Production by Soybeans 1. *Crop Science*, *5*(6), 575–577.

Shi, J., Drummond, B. J., Habben, J. E., Brugire, N., Weers, B. P., Hakimi, S. M., Lafitte, H. R., Schussler, J. R., Mo, H., Beatty, M., Zastrow-Hayes, G., & O'Neill, D. (2019). Ectopic expression of ARGOS8 reveals a role for ethylene in root-lodging resistance in maize. *The Plant Journal: For Cell and Molecular Biology*, *97*(2), 378–390.

Shimojima K., Ogawa S., Naito H., Valencia M. O., Shimizu Y., Hosoi F., Uga Y., Ishitani M., Selvaraj M. G., & Omasa K. (2017). Comparison between Rice Plant Traits and Color Indices Calculated from UAV Remote Sensing Images. *Eco-Engineering*, *29*(1), 11–16.

Shi, Y., Murray, S. C., Rooney, W. L., Valasek, J., Olsenholler, J., Ace Pugh, N., Henrickson, J., Bowden, E., Zhang, D., & Alex Thomasson, J. (2016). *Corn and sorghum phenotyping using a fixed-wing UAV-based remote sensing system*. *9866*,

98660E.

Shi, Y., Thomasson, J. A., Murray, S. C., Pugh, N. A., Rooney, W. L., Shafian, S., Rajan, N., Rouze, G., Morgan, C. L. S., Neely, H. L., Rana, A., Bagavathiannan, M. V., Henrickson, J., Bowden, E., Valasek, J., Olsenholler, J., Bishop, M. P., Sheridan, R., Putman, E. B., … Yang, C. (2016). Unmanned Aerial Vehicles for High-Throughput Phenotyping and Agronomic Research. *PloS One*, *11*(7), e0159781.

Silva-Perez, V., Molero, G., Serbin, S. P., Condon, A. G., Reynolds, M. P., Furbank, R. T., & Evans, J. R. (2018). Hyperspectral reflectance as a tool to measure biochemical and physiological traits in wheat. *Journal of Experimental Botany*, *69*(3), 483–496.

Singh, A., Ganapathysubramanian, B., Singh, A. K., & Sarkar, S. (2016). Machine Learning for High-Throughput Stress Phenotyping in Plants. *Trends in Plant Science*, *21*(2), 110–124.

Smith, K. L., Steven, & Colls, J. J. (2004). Use of hyperspectral derivative ratios in the red-edge region to identify plant stress responses to gas leaks. *Remote Sensing of Environment*, *92*(2), 207–217.

Snavely, N., Seitz, S. M., & Szeliski, R. (2008). Modeling the World from Internet Photo Collections. *International Journal of Computer Vision*, *80*(2), 189–210.

Song, Y., & Wang, J. (2019). Winter Wheat Canopy Height Extraction from UAV-Based Point Cloud Data with a Moving Cuboid Filter. *Remote Sensing*, *11*(10). https://doi.org/10.3390/rs11101239

Stamp, P., & Kiel, C. (1992). *Seedling traits of maize as indicators of root lodging*. https://hal.archives-ouvertes.fr/hal-00885462/document

Sugiura, R., Tsuda, S., Tamiya, S., Itoh, A., Nishiwaki, K., Murakami, N., Shibuya, Y., Hirafuji, M., & Nuske, S. (2016). Field phenotyping system for the assessment of potato late blight resistance using RGB imagery from an unmanned aerial vehicle. *Biosystems Engineering*, *148*, 1–10.

Su, J., Coombes, M., Liu, C., Zhu, Y., Song, X., Fang, S., Guo, L., & Chen, W.-H. (2020). Machine Learning-Based Crop Drought Mapping System by UAV Remote Sensing RGB Imagery. *Unmanned Systems*, *8*(1), 71–83.

Su, W., Zhang, M., Bian, D., Liu, Z., Huang, J., Wang, W., Wu, J., & Guo, H. (2019). Phenotyping of Corn Plants Using Unmanned Aerial Vehicle (UAV) Images. *Remote Sensing*, *11*(17), 2021.

Svensgaard, J., Roitsch, T., & Christensen, S. (2014). Development of a Mobile Multispectral Imaging Platform for Precise Field Phenotyping. *Agronomy*, *4*(3), 322–336.

Team, R. C., & Others. (2013). *R: A language and environment for statistical computing*. http://finzi.psych.upenn.edu/R/library/dplR/doc/intro-dplR.pdf

Tetio-Kagho, F., & Gardner, F. P. (1988). Responses of Maize to Plant Population Density. I. Canopy Development, Light Relationships, and Vegetative Growth. *Agronomy Journal*, *80*, 930–935.

Thomas, S., Behmann, J., Steier, A., Kraska, T., Muller, O., Rascher, U., & Mahlein, A.-K. (2018). Quantitative assessment of disease severity and rating of barley cultivars based on hyperspectral imaging in a non-invasive, automated phenotyping platform. *Plant Methods*, *14*, 45.

Thompson, A. L., Thorp, K. R., Conley, M. M., Elshikha, D. M., French, A. N., Andrade-Sanchez, P., & Pauli, D. (2019). Comparing Nadir and Multi-Angle View Sensor Technologies for Measuring in-Field Plant Height of Upland Cotton. *Remote Sensing*, *11*(6). https://doi.org/10.3390/rs11060700

Thompson, D. L. (1968). Field Evaluation of Corn Root Clumps 1. *Agronomy Journal*, *60*(2), 170–172.

Tilly, N., Aasen, H., & Bareth, G. (2015). Fusion of Plant Height and Vegetation Indices for the Estimation of Barley Biomass. *Remote Sensing*, *7*(9), 11449–11480.

Tirado, S. B., Hirsch, C. N., & Springer, N. M. (2020a). Utilizing Temporal Measurements from UAVs to Assess Root Lodging in Maize and its Impact on Productivity. In *bioRxiv* (p. 2020.05.21.108746). https://doi.org/10.1101/2020.05.21.108746

Tirado, S. B., Hirsch, C. N., & Springer, N. M. (2020b). UAV-based imaging platform for monitoring maize growth throughout development. *Plant Direct*, *4*(6). https://doi.org/10.1002/pld3.230

Tirado, S. B., St Dennis, S., Enders, T. A., & Springer, N. M. (2020c). Utilizing top-

down hyperspectral imaging for monitoring genotype and growth conditions in maize. In *bioRxiv* (p. 2020.01.21.914069). https://doi.org/10.1101/2020.01.21.914069

Turner, D., Lucieer, A., & Watson, C. (2012). An Automated Technique for Generating Georectified Mosaics from Ultra-High Resolution Unmanned Aerial Vehicle (UAV) Imagery, Based on Structure from Motion (SfM) Point Clouds. *Remote Sensing*, *4*(5), 1392–1410.

Vadez, V., Kholová, J., Hummel, G., Zhokhavets, U., Gupta, S. K., & Hash, C. T. (2015). LeasyScan: a novel concept combining 3D imaging and lysimetry for high-throughput phenotyping of traits controlling plant water budget. *Journal of Experimental Botany*, *66*(18), 5581–5593.

Varela, S., Assefa, Y., Vara Prasad, P. V., Peralta, N. R., Griffin, T. W., Sharda, A., Ferguson, A., & Ciampitti, I. A. (2017). Spatio-temporal evaluation of plant height in corn via unmanned aerial systems. *Journal of Applied Remote Sensing*, *11*(3), 036013.

Varshney, V. (2017). *Supervised and unsupervised learning for plant and crop row detection in precision agriculture* [Kansas State University]. https://core.ac.uk/download/pdf/84312487.pdf

Watanabe, K., Guo, W., Arai, K., Takanashi, H., Kajiya-Kanegae, H., Kobayashi, M., Yano, K., Tokunaga, T., Fujiwara, T., Tsutsumi, N., & Iwata, H. (2017). High-

Throughput Phenotyping of Sorghum Plant Height Using an Unmanned Aerial Vehicle and Its Application to Genomic Prediction Modeling. *Frontiers in Plant Science*, *8*, 421.

Wen, W., Gu, S., Xiao, B., Wang, C., Wang, J., Ma, L., Wang, Y., Lu, X., Yu, Z., Zhang, Y., Du, J., & Guo, X. (2019). In situ evaluation of stalk lodging resistance for different maize (Zea mays L.) cultivars using a mobile wind machine. *Plant Methods*, *15*, 96.

White, J. W., Andrade-Sanchez, P., Gore, M. A., Bronson, K. F., Coffelt, T. A., Conley, M. M., Feldmann, K. A., French, A. N., Heun, J. T., Hunsaker, D. J., Jenks, M. A., Kimball, B. A., Roth, R. L., Strand, R. J., Thorp, K. R., Wall, G. W., & Wang, G. (2012). Field-based phenomics for plant genetics research. *Field Crops Research*, *133*, 101–112.

White, J. W., & Conley, M. M. (2013). A flexible, low-cost cart for proximal sensing. *Crop Science*, *53*(4), 1646–1649.

Xavier, A., Hall, B., Hearst, A. A., Cherkauer, K. A., & Rainey, K. M. (2017). Genetic Architecture of Phenomic-Enabled Canopy Coverage in Glycine max. *Genetics*, *206*(2), 1081–1089.

Xue, J., Zhao, Y., Gou, L., Shi, Z., Yao, M., & Zhang, W. (2016). How High Plant Density of Maize Affects Basal Internode Development and Strength Formation. *Crop Science*, *56*, 3295–3306.

Yang, G., Liu, J., Zhao, C., Li, Z., Huang, Y., Yu, H., Xu, B., Yang, X., Zhu, D., Zhang, X., Zhang, R., Feng, H., Zhao, X., Li, Z., Li, H., & Yang, H. (2017). Unmanned Aerial Vehicle Remote Sensing for Field-Based Crop Phenotyping: Current Status and Perspectives. *Frontiers in Plant Science*, *8*, 1111.

Yang, Q., Shi, L., Han, J., Zha, Y., & Zhu, P. (2019). Deep convolutional neural networks for rice grain yield estimation at the ripening stage using UAV-based remotely sensed images. *Field Crops Research*, *235*, 142–153.

Yang, W., Feng, H., Zhang, X., Zhang, J., Doonan, J. H., Batchelor, W. D., Xiong, L., & Yan, J. (2020). Crop Phenomics and High-Throughput Phenotyping: Past Decades, Current Challenges, and Future Perspectives. *Molecular Plant*, *13*(2), 187–214.

Yendrek, C. R., Tomaz, T., Montes, C. M., Cao, Y., Morse, A. M., Brown, P. J., McIntyre, L. M., Leakey, A. D. B., & Ainsworth, E. A. (2017). High-Throughput Phenotyping of Maize Leaf Physiological and Biochemical Traits Using Hyperspectral Reflectance. *Plant Physiology*, *173*(1), 614–626.

Yin, X., Jaja, N., Angela McClure, M., & Hayes, R. M. (2011). Comparison of Models in Assessing Relationship of Corn Yield with Plant Height Measured during Early- to Mid-Season. *Journal of Agricultural Science*, *3*(3), 14.

Yin, X., McClure, M. A., Jaja, N., Tyler, D. D., & Hayes, R. M. (2011). In-Season Prediction of Corn Yield Using Plant Height under Major Production Systems. *Agronomy Journal*, *103*(3), 923–929.

Young, S. N., Kayacan, E., & Peschel, J. M. (2019). Design and field evaluation of a ground robot for high-throughput phenotyping of energy sorghum. *Precision Agriculture*, *20*(4), 697–722.

Yue, J., Yang, G., Li, C., Li, Z., Wang, Y., Feng, H., & Xu, B. (2017). Estimation of Winter Wheat Above-Ground Biomass Using Unmanned Aerial Vehicle-Based Snapshot Hyperspectral Sensor and Crop Height Improved Models. *Remote Sensing*, *9*(7). https://doi.org/10.3390/rs9070708

Yue, J., Yang, G., Tian, Q., Feng, H., Xu, K., & Zhou, C. (2019). Estimate of winter-wheat above-ground biomass based on UAV ultrahigh-ground-resolution image textures and vegetation indices. *ISPRS Journal of Photogrammetry and Remote Sensing: Official Publication of the International Society for Photogrammetry and Remote Sensing* , *150*, 226–244.

Zermas, D., Morellas, V., Mulla, D., & Papanikolopoulos, N. (2020). 3D model processing for high throughput phenotype extraction - the case of corn. *Computers and Electronics in Agriculture*, *172*. https://doi.org/10.1016/j.compag.2019.105047

Zermas, D., Teng, D., Stanitsas, P., Bazakos, M., Kaiser, D., Morellas, V., Mulla, D., & Papanikolopoulos, N. (2015). Automation Solutions for the Evaluation of Plant Health in Corn Fields. *2015 Ieee/rsj International Conference on Intelligent Robots and Systems (iros)*, 6521–6527.

Zhang, J., Yang, C., Zhao, B., Song, H., Hoffmann, W. C., Shi, Y., Zhang, D., & Zhang,

G. (2017). Crop Classification and LAI Estimation Using Original and Resolution-Reduced Images from Two Consumer-Grade Cameras. *Remote Sensing*, *9*(10). https://doi.org/10.3390/rs9101054

Zhang, Q., Li, Q., & Zhang, G. (2012). Rapid Determination of Leaf Water Content Using VIS/NIR Spectroscopy Analysis with Wavelength Selection. *Spectroscopy Letters; an International Journal for Rapid Communication*, *27*(2), 93–105.

Zhang, Q., Pettolino, F. A., Dhugga, K. S., Rafalski, J. A., Tingey, S., Taylor, J., Shirley, N. J., Hayes, K., Beatty, M., Abrams, S. R., Zaharia, L. I., Burton, R. A., Bacic, A., & Fincher, G. B. (2011). Cell wall modifications in maize pulvini in response to gravitational stress. *Plant Physiology*, *156*(4), 2155–2171.

Zheng, H., Cheng, T., Zhou, M., Li, D., Yao, X., Tian, Y., Cao, W., & Zhu, Y. (2019). Improved estimation of rice aboveground biomass combining textural and spectral analysis of UAV imagery. *Precision Agriculture*, *20*(3), 611–629.

Zhu, W., Sun, Z., Peng, J., Huang, Y., Li, J., Zhang, J., Yang, B., & Liao, X. (2019). Estimating Maize Above-Ground Biomass Using 3D Point Clouds of Multi-Source Unmanned Aerial Vehicle Data at Multi-Spatial Scales. *Remote Sensing*, *11*(22). https://doi.org/10.3390/rs11222678

Zuber, M. S., & Kang, M. S. (1978). Corn lodging slowed by sturdier stalks. *Crops and Soils*, *30*. http://agris.fao.org/agris-search/search.do?recordID=US19780311607